1-1-2013

Modal Updating Cognitive Systems: Behavioral Selection

Gustavo Andres Ospina Idarraga
University of South Carolina

MODEL UPDATING COGNITIVE SYSTEMS:BEHAVIORAL SELECTION

by

Gustavo A. Ospina

Bachelor of Science
Universidad del Valle, 2008

Master of Engineering
University of South Carolina, 2012

Submitted in Partial Fulfillment of the Requirements

For the Degree of Doctor of Philosophy in

Civil Engineering

College of Engineering and Computing

University of South Carolina

2013

Accepted by:

Juan Caicedo, Major Professor

Robert L. Mullen, Committee Member

Dimitris Rizos, Committee Member

Marco Valtorta, Committee Member

Lacy Ford, Vice Provost and Dean of Graduate Studies

ACKNOWLEDGEMENTS

The author would like to express his admiration and gratitude to Dr. Juan Caicedo, for all the guidance and support throughout the course of this research and graduate school. Special thanks to the committee members, Dr. Robert L. Mullen, Dr. Dimitris C. Rizos, and Dr. Marco Valtorta for their valuable time and suggestions.

The author also acknowledges to his family and loved ones the support throughout his study life without which this work would not have been possible.

ABSTRACT

Numerical modeling has been a very effective tool for the simulation of structural systems. Modeling helps engineers and designers to make important predictions about the behavior of the system during simulated loading events. Decisions in structural engineering are most of the time based on the results from numerical simulations, especially during retrofit where numerical modeling is most of the time required. However, numerical idealizations of existing structural systems do not match the actual structure. Several authors acknowledge that the reason behind this mismatch between the behavior of numerical models and the actual systems are due to assumptions in the modeling process and uncertainty in the model parameters. Model updating strategies can be used to reduce the uncertainty in the numerical model, resulting in more meaningful results from structural analysis.

Several researchers report the performance of model updating strategies in terms of the error between numerical and experimental data after the updating strategy has been implemented, but little work has been done in evaluating the physical meaning of the updated parameters and the capabilities of the numerical model to predict the behavior of the structure after the system has been modified (i.e. retrofit analysis). Furthermore, researchers have acknowledged that model updating can lead to non-unique problems, and propose techniques to identify potential solutions to the model updating problem. However, it is not clear how to select the appropriate solution from a family of solutions.

The work described here proposes a methodology for the evaluation of a family of solutions within a probabilistic framework. The methodology proposes a mean for an analyst to incorporate his/her expertise as a probabilistic expression that can be incorporated in the model updating process. Solutions with high probability are more probable to have meaningful parameters. Finally, a benchmark problem is formulated to aid the comparison of model updating techniques that acknowledge the existence of multiple solutions.

TABLE OF CONTENTS

LIST OF TABLES

LIST OF FIGURES

CHAPTER 1. INTRODUCTION

Structural Engineers rely on the power of computers and numerical models for the design of new structures and the retrofit of old structures. Techniques such as finite elements are a standard practice to estimate the behavior of a structure for its design. During the analysis process the engineer makes reasonable assumptions about the strength of the materials, stiffness, geometry, etc. which leads to an economical design. The evaluation of the performance of an existing structure is different. The engineer does not have the freedom to "set" the parameters of the structure. Rather, the engineer should investigate and approximate the values for these parameters based on the actual system.

Numerical modeling is not a trivial task however. In a general sense, every property defining a numerical model such as the cross sectional area of an element, the mass density of a material or the flexural capacity of a beam element is intrinsically computed with a measure of uncertainty. Based on this argument, it can be expected that deterministic numerical models provide a limited representation of a real system. For instance, limitations when modeling real structures arise in the modeling of tapered beams (Bradford and Cuk 1988), curved elements (Brownjohn and Xia 2000), composite sections (Karimi, Tait et al. 2011), or partially restrained conditions (Baeza and Ouyang 2011). Usually, these types of problems require having a very dense numerical model attempting to capture the main characteristics of the system and thus paying an expensive computational cost to improve the accuracy of the results.

In the field of model updating it is common to measure the discrepancies between the system and the numerical model through the error between outputs of a numerical analysis and experimental measurements, such as natural frequencies and/or mode shapes. For instance, (Zhang, Chang et al. 2001) modeled the Kap Shui Mun cable stayed bridge in Hong Kong and reported the discrepancies found as in Table 1.1:

Table 1.1. Selected modes for model updating (Zhang, Chang et al. 2001)

Vibration Mode			Measured (Hz)	Computed (Hz)	Error
1	First vertical bending of deck	V1	0.39	0.41	5.1%
2	Second vertical bending of deck	V2	0.66	0.58	-12.1%
3	Third vertical bending of deck	V3	1.07	0.93	-13.1%
4	Fourth vertical bending of deck	V4	1.54	1.51	-1.9%
5	Fifth vertical bending of deck	V5	1.81	1.74	-3.9%
6	First lateral bending of deck	L1	0.49	0.49	0.0%
7	Second lateral bending of deck	L2	1.25	1.15	-8.0%
8	Third lateral bending of deck	L3	2.12	2.45	15.6%
9	First torsional mode of deck	T1	0.83	0.77	-7.2%
10	Second torsional mode of deck	T2	1.39	1.62	16.5%
11	Third torsional mode of deck	T3	1.9	2.18	14.7%
12	First swaying of Lantau tower	LTS1	0.63	0.57	-9.5%
13	First torsion of Lantau tower	LTT1	1.34	1.48	10.4%
14	First bending of Lantau tower	LTB1	2.2	1.96	-10.9%
15	First torsion of Ma Wan tower	MWT1	1.61	1.89	17.4%
16	First swaying of Ma Wan tower	MWS1	1.78	1.64	-7.9%
17	First bending of Ma Wan tower	MWB1	2.03	2.01	-1.0%

The goal of model updating methodologies is to take a “raw” model and experimental measurements to produce a better representation of the real structure. One of the predominant challenges with structural model updating is that experimental data tends to be a scarce resource, mostly due to economical restrictions. Updated models can be used for a significant number of subsequent analyses such as earthquake response estimation or retrofit analysis. For instance, (Ren, Lin et al. 2007) updated the numerical model of the Qingzhou cable-stayed bridge over the Ming River in China. The updating

variables considered were the tension forces in the cable elements in order to emulate the mid-span static deformation of the structure. Once they achieved the objective, several truck-loading cases were simulated and evaluated on site, reporting the computed stresses in Table 1.2 computed from the composite deck shown in Figure 1.1:

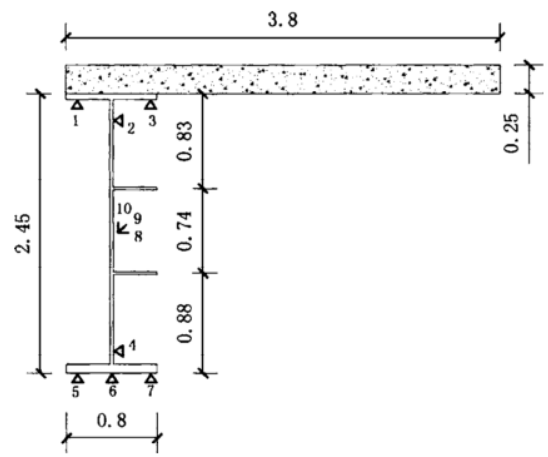

Figure 1.1. Equivalent section of steel-concrete composite deck at mid-span of Qingzhou Cable Stayed Bridge (units in meters)

Table 1.2. Measured and calculated stresses of composite deck (Ren, Lin et al. 2007)

Point #	Position from centroid [m]	Calculated stress [MPa]	Measured stress [MPa]
1	-0.057	-1.28	2.52
2	0.143	3.21	-
3	-0.057	-1.28	3.36
4	2.063	46.30	68.30
5	2.343	52.58	67.40
6	2.343	52.58	66.40
7	2.343	52.58	65.70
8	1.103	24.75	42.80

It can be said then, that model updating is a discipline that doesn't simply look for fitting structural parameters into the available experimental data, but as a disciplines that looks to obtain sets of values for the updating parameters which reduce the uncertainty and thus reduce the uncertainty in the response of the results of numerical analysis.

1.1. Model Updating Methodologies

Model updating methodologies can be classified as deterministic or non-deterministic. Deterministic methodologies do not consider the updating parameters as variables with uncertainty associated but as deterministic values that are not known. These types of methodologies use optimization algorithms to minimize the error between experimental measurements and analytical results. However, most of the time, the experimental information is incomplete, and a limited number of sensors are installed. The error function can only be calculated using experimental data from sensors that match appropriate degrees of freedom in the model.

It has been shown by Udwadia and Sharma (1978) and Udwadia (1985) that the incompleteness of experimental information leads to non-uniqueness on the solution to the minimization problem. Franco et al. (2006) also discuss this point. Furthermore, Zarate and Caicedo (2008) indicate that a local minima can provide a more meaningful representation than the global minima. New model updating approaches have been recently developed acknowledging these challenges (Zarate and Caicedo 2008; Caicedo and Zarate 2011).

1.1.1. Deterministic Methodologies

Deterministic model updating methodologies don not consider uncertainty in the model parameters. The focus of deterministic methodologies is then the minimization of an objective function that typically quantifies the error between experimental and numerical data. Most of these techniques require an optimization methodology or some type of iterations to produce a solution. Other methodologies, called direct

methodologies, use the experimental information and identification algorithms to directly obtain the values for the updating parameters (Tarantola 2002).

Model updating problems in structural engineering are usually complex because of the large number of parameters. It is common to use sensitivity analysis to select significant updating variables and reduce the complexity of the problem. For instance, (Brownjohn and Xia 2000) used sensitivity analysis to correct selected parameters on the Safti Link cable stayed bridge in Singapore (Table 1.3).

Table 1.3. Correlation between updated FEA and EMA (Brownjohn and Xia 2000)

Number (1)	f_{FEA} (Hz) (2)	f_{EMA} (Hz) (3)	D_f (%) (4)	MAC (5)	Mode Shape (6)
1	1.14	1.18	-3.67	97.80	First bending
2	2.62	2.76	-4.89	96.30	Second bending
3	3.29	3.59	-8.36	97.10	First torsion
4	4.18	4.61	-9.36	90.80	Third bending
5	5.86	6.10	-4.00	91.90	Second torsion
6	6.60	7.00	-5.70	84.70	Fourth bending
7	8.70	9.10	-4.38	91.40	Third torsion

Other deterministic methodologies are derived from evolutionary algorithms. These types of methodologies emulate the social behavior of individuals in which portions of the population succeed in a given objective, such as reproduction or identification of promising areas. Example of these are the Genetic Algorithm –GA- (Goldberg 1989) and Particle Swarm Optimization (Eberhart and Kennedy 1995). These evolutionary algorithms have been widely studied, and some authors have specialized them for the search of both global and local minima. For instance, (Zechman and Ranjithan 2004) propose the modification of the GA allowing the branching of the evolutive solutions. Other examples are given by (Venter and Sobieszczanski-Sobieski 2003; Parrott and Xiaodong 2006), who use in favor of the search of local minima, the

jamming that particle swarm methodologies usually present as issue. A typical flowchart of a GA algorithm is shown in Figure 1.2.

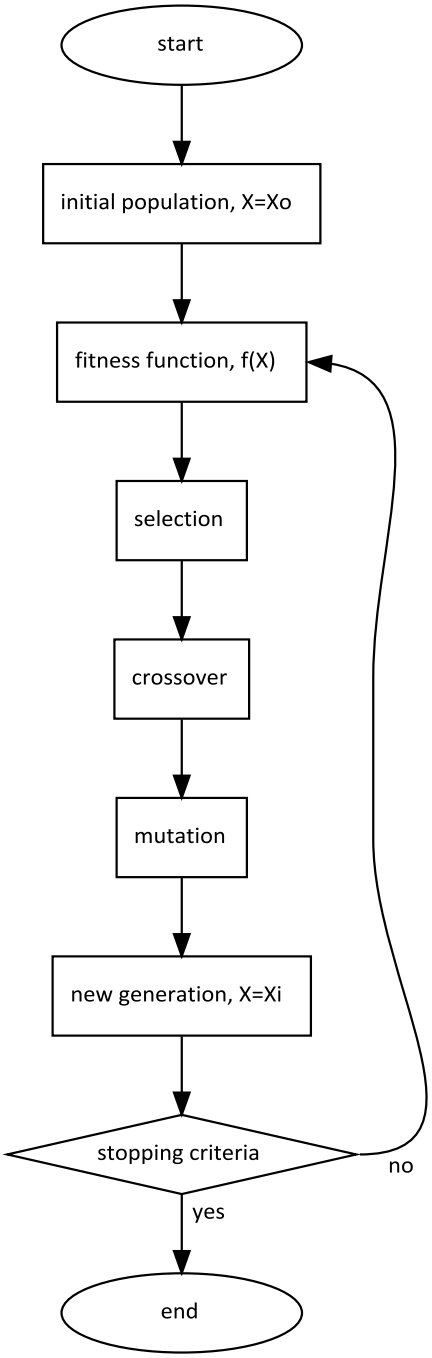

Figure 1.2. Typical GA flowchart

Other types of deterministic methodologies have arisen from decision making activities, where complex models and incomplete information are used. For instance, Modeling to Generate Alternatives –MGA- developed by (Brill, Chang et al. 1982) as a human-machine decision-making system for land use planning. An implementation of MGA is presented by (Zarate and Caicedo 2008), where they proposed the search of other minima by pushing the optimization towards an area perpendicular to the current minima found. The subject of study is the Bill Emerson Memorial cable-stayed bridge in Missouri, USA. They use 6 updating parameters in order to reduce the complexity of the problem, finding 4 alternative solutions (Table 1.4 and Table 1.5), concluding in the need of an analyst expertise for the selection of the "best" solution.

Table 1.4. Model updating alternatives (Zarate and Caicedo 2008)

Solution	Mass %			Inertia %	Stiffness %		f (p)
	Loc 1	Loc 2	Loc 3		Bent	Tower	
Original	0.00	0.00	0.00	0.00	0.00	0.00	0.524
p1	0.00	-5.00	-5.00	5.00	100.00	27.36	0.375
p2	0.00	0.00	0.00	0.00	99.73	0.00	0.451
p3	-4.74	0.00	0.00	0.00	0.00	0.00	0.492
p4	0.00	0.00	0.00	0.00	0.00	100.00	0.495

Table 1.5. Dynamic characteristics of the model updating alternatives (Zarate and Caicedo 2008)

Solution	$\omega 1$ (Hz)	$\omega 2$ (Hz)	$\omega 3$ (Hz)	$\omega 4$ (Hz)	100*(1-MAC)			
					$(\phi_{id,1},\phi_{fe,1})$	$(\phi_{id,2},\phi_{fe,2})$	$(\phi_{id,3},\phi_{fe,3})$	$(\phi_{id,4},\phi_{fe,4})$
Exp.	0.32	0.41	0.63	0.71	-	-	-	-
Original	0.29	0.39	0.60	0.63	4.9	5.4	3.1	10.4
1	0.31	0.41	0.61	0.63	4.3	5.9	4.1	7.5
2	0.31	0.4	0.61	0.63	4.3	6.1	3.9	10.8
3	0.3	0.4	0.62	0.63	4.4	6	5.1	14.6
4	0.3	0.4	0.61	0.63	4.7	5.6	3.5	10.1

The challenges associated with objective functions with multiple solutions are not limited to the computational cost. Finding multiple alternatives to update a model leaves the engineer with the task to decide what model (or models) to use in subsequent analysis, especially because modeling errors, low sensor density and other aspects could indicate that local minima of the error function might have a better physical representation than the global minima (Zarate and Caicedo 2008; Zarate 2009; Caicedo and Zarate 2011). For example, which of the models presented in Table 1.4 and Table 1.5 should be used for an earthquake retrofit analysis?

1.1.2. Non-Deterministic Model Updating Methodologies

Non-deterministic model updating considers uncertainty in the parameters. Some approaches describe the uncertainty in probabilistic terms (Beck and Katafygiotis 1998), others describe it through interval arithmetic (Madarshahian, Caicedo et al. 2013), and others use statistical measures of dispersion to describe the variability of the updating parameters. The description of this variability is very useful when compared to deterministic methodologies, given that it provides a mean for the evaluation of the uncertainty of the results.

Non-deterministic methodologies following a probabilistic approach are mostly based on Bayes' inference. Formally, this methodology uses conditional probabilities to express the frequency on which a given event occurs. In model updating, the probability of a given parameter is seen as a degree of belief based on prior information instead. This means that an analyst can express his/hers degree of believe about a given model parameter in terms of a probability distribution. The Bayes' theorem provides the mean to update this prior belief when new evidence is obtained. This probabilistic approach has

gained a lot of popularity due its capacity to handle uncertainty in ill-conditioned, non-unique problems. The seminal papers by (Beck and Katafygiotis 1998) provide the foundation for the implementation of this type of approaches.

Examples of Bayesian model updating can be found in (Vanik, Beck et al. 2000; Beck and Au 2002; Marwala and Sibisi 2005; Cheung and Beck 2009). For example, Marwala *et al.* (2005) updated the elastic modulus of a simply supported (25.4mm x 13.4mm x 1.0m) aluminum beam. The reported results from the implementation of the Bayesian updating are shown in Table 1.6:

Table 1.6. Experimental and numerical natural frequencies in Marwala et al. (2005)

Mode	Experimental fn (Hz)	Initial FEM fn (Hz)	Average updated FEM fn (Hz)	Standard Deviation (Hz)
1	64	70	67	2.8
2	184	193	183	7.6
3	389	379	360	16.1
4	599	628	590	28.7
5	898	942	893	76.4

The robustness of this methodology is examined by (Vanik, Beck et al. 2000; Beck and Au 2002; Cheung and Beck 2009). In the work of Cheung and Beck (2009), a 10-story building is simulated subject to earthquake excitation where the acceleration records are contaminated with noise. As shown in Table 1.7, a great level of confidence in the identification of the modal characteristics of the simulated system was achieved.

Low sensor density has also an effect in Bayesian based techniques. Caicedo and Zarate (2011) showed that the posterior PDF of the stiffness of a 2 DOF structure could result in two areas of high probability (Figure 1.3a). A combination of MGA (Brill, Chang et al. 1982) and GA was used to automatically find these areas.

Table 1.7. Experimental and Numerical modal parameters (Cheung and Beck 2009)

Mode	Experimental Data		Updated Model	
	Natural frequency (Hz)	Damping ratio (%)	Natural frequency (Hz) and Covariance	Damping ratio (%) and Covariance
1	0.735	0.92	0.734 (0.2%)	0.85 (8.0%)
2	2.158	2.71	2.149 (0.3%)	2.60 (7.1%)
3	3.562	4.45	3.600 (0.7%)	4.03 (9.5%)
4	4.891	6.03	4.878 (0.8%)	5.83 (8.6%)
5	6.047	7.65	6.022 (1.8%)	7.33 (8.8%)
6	7.106	9.11	7.214 (2.3%)	8.42 (10.1%)
7	8.049	10.13	7.990 (2.4%)	9.17 (11.5%)
8	8.62	11.11	8.828 (2.7%)	9.56 (13.1%)
9	9.306	11.58	9.661 (3.2%)	9.60 (13.5%)
10	9.631	11.92	10.519 (4.5%)	9.26 (15.5%)

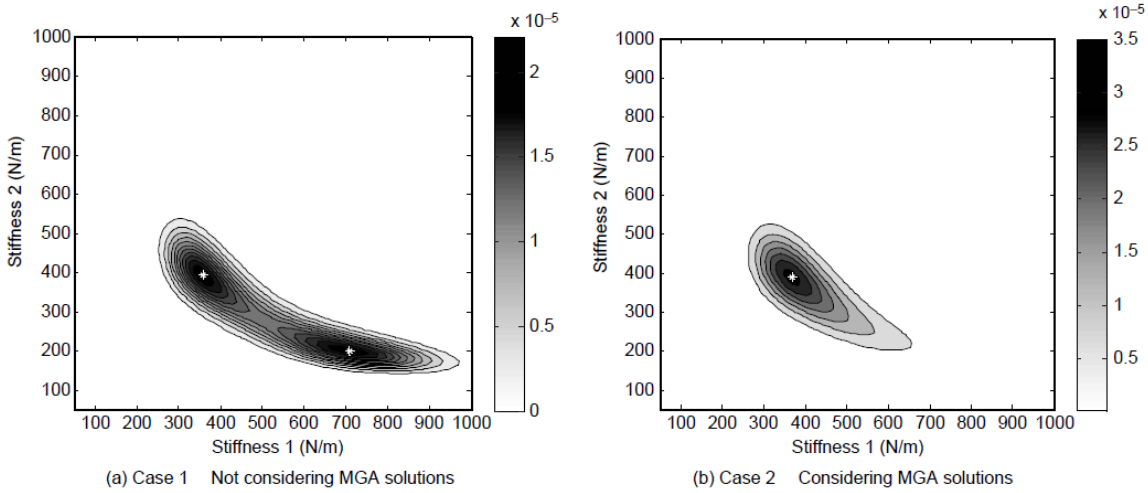

Figure 1.3. Posterior PDF with 4 experimental records (Caicedo and Zarate 2011)

The paper also discusses that the analyst can learn from knowing the existence of these areas of high probability and better define the prior PDF. Figure 1.3b shows the result of the updating after the analyst has considered the two areas of high probability.

Finally, other non-deterministic approaches are the Maximum Entropy (Adhikari and Friswell 2004), Bootstrapping (Goller, Pradlwarter et al. 2009) interval methods, fuzzy logic and random fields (Fonseca 2005).

1.2. Model Performance Evaluation Methodologies

One question of interest for structural engineers is: "What model should I use for a particular analysis?" There is no methodology widely accepted to measure the performance of numerical models in structural engineering. The purpose of model updating methodologies is to reduce the uncertainty in the numerical model in order to have a greater confidence on analytical results used for design, retrofit and other purposes. Model updating can have limited success if experimental data does not fully describe the system. The reason behind this issue can be explained partially, because a successful evaluation of the performance of numerical models would require an expensive experimental program where structural systems are tested a number of times. However, it is the best that can be done given the available data. When data is cheap to be collected is easier to evaluate numerical models, as it happens with areas such as water resources (e.g. precipitation records), who appear to have matured faster than structural engineering on the evaluation of model performance.

Methodologies for model performance evaluation developed in the water resources area involve statistical measures (Fox 1981; Willmott 1982) and other criteria based on statistical information for the quantification of the discrepancies between numerical and experimental output (Baranyi, Pin et al. 1999; Moriasi, Arnold et al. 2007). Responses of the numerical models are also compared to experimental data using least squares algorithm, a typical methodology used in model fitting. As presented by Matott, Babendreier et al. (2009), Table 1.8 summarizes typical methodologies used for model evaluation by water resources engineers.

Table 1.8. Quantitative methods for model evaluation

Method	Purpose of method	Subclassifications
Data Analysis (DA)	to evaluate or summarize input, response, or model output data	time series, population, geospatial
Identifiability Analysis (IA)	to expose inadequacies in the data or suggest improvements in the model structure	temporal, behavioral, spatial
Parameter Estimation (PE)	to quantify uncertain model parameters using model simulations and available response data	single solution, multiple solution
Uncertainty Analysis (UA)	to quantify output uncertainty by propagating sources of uncertainty through the model	sampling methods, approximation methods
Sensitivity Analysis	to determine which inputs are most significant	screening, local, global
Multimodel Analysis (MMA)	to evaluate model uncertainty or generate ensemble predictions via consideration of multiple plausible models	quantitative, qualitative
Bayesian Networks	to combine prior distributions of uncertainty with	hierarchical Bayesian,

Arguably, only UA and MMA truly evaluate the performance of a model, while other methods are used for model updating. For instance, UA propagates uncertainty in numerical models and characterizes the uncertainty distribution in the response of the system. Such characterization is usually performed in terms of a probability distribution or in by statistical means (Tsai 1987; Tsai and Franceschini 2005; Helton, Johnson et al. 2006). In structural engineering, such methodology is used instead to perform model updating (Muhanna, Zhang et al. 2007). Similarly, MMA is a methodology used to evaluate problems that can be modeled using different types of approaches. The methodology basically assigns scores to the evaluated models given a specific scenario, where the scoring gives a ranking to the models (Burnham and Anderson 2002). (Link and Weiland 2009) use this methodology to evaluate damage detection in structures, where different stages of damage require a different model and thus, a boundary defining such stages is obtained through MMA.

Model updating presents a different approach to determine if a model is appropriate. Model comparison using Bayes' inference (Box and Tiao 2011) provides a

method to contrast the probability of two or more models. One of the advantages of using Bayes is that the technique considers overfitting. Models with many parameters usually have a lower probability than those with many parameters, unless the experimental data fits well a model with several parameters.

1.3. Challenges in Model Updating

Several are the challenges for any model updating methodology. Remarkable advances made in computational power and modeling techniques have motivated researcher in all type of areas to enhance models to improve the representation of physical systems. Nonetheless, model updating problems are still very complex, and some deficiencies still need further research, such as the visualization of systems with multiple parameters. Several of these challenges are the motivation for this research.

1.3.1. Uncertainty and Modeling errors

The development of numerical methods for the discrete representation of physical systems, usually represented by differential equations, is a first step in the modeling of a physical system such as a structure. Every physical quantity can be measured with a degree of uncertainty. This variability in the updating parameters of a model updating problem can't be avoided, and under estimations of such variability can lead to an inaccurate representation of the system behavior (Lam 1998; Sanayei, Wadia-Fascetti et al. 2001).

In structural engineering in particular, the representation of the connections between elements and/or supporting conditions is a source of modeling errors. For instance, in a structural analysis it is common to represent foundations systems as rigid bodies, when reality shows that foundations might have small deformations and/or

rotations, depending on the type of foundation and its conditions. Other example is the consideration of lateral-bracing elements in buildings as axial (truss) elements, while such perfect condition is hardly found in real structures.

Modeling errors can also arise from a poor spatial characterization of the real structure. Most of times, numerical models are developed from structural drawings. This type of modeling error, for example, affects the effective length of elements and thus, their mechanical properties. Similarly, curved and/or tapered structural elements also contribute to the challenge of creating a good numerical representation of the real system.

Other common modeling error is the lack of knowledge about the stress state of structural elements once they are in static equilibrium. Pre-stressed beams, cracked concrete sections, tensioned cables, and concentration of stresses due to irregularities during construction and assemblage of the structure are also factors playing an important role and usually they are not considered (and almost impossible to determine) before a numerical model is developed.

1.3.2. Low Sensor Density

Good experimental data is crucial to perform model updating in a real structure. However, it becomes difficult to achieve this objective, given that most of the time the structure of interest is very complex. For instance, an analyst can be interested in performing a reliability analysis on an existing bridge. A numerical model for such structure will easily have a large amount of degrees of freedom. The resources required to perform a full instrumentation and experimentally measure all the degrees of freedom can make it an impractical procedure. For these reasons, only key locations are instrumented and data from these locations is used later to interpolate the behavior at non-instrumented

locations. This low-sensor density is a common denominator in projects involving analysis of existing structures. Just in very few cases of modern structures, the project considers an extensive instrumentation of the structure for a continuous monitoring of several phenomena of interest, such as the Tsing Ma Bridge in Hong Kong (Wong 2007) with a total of 1723 sensors (Figure 1.4).

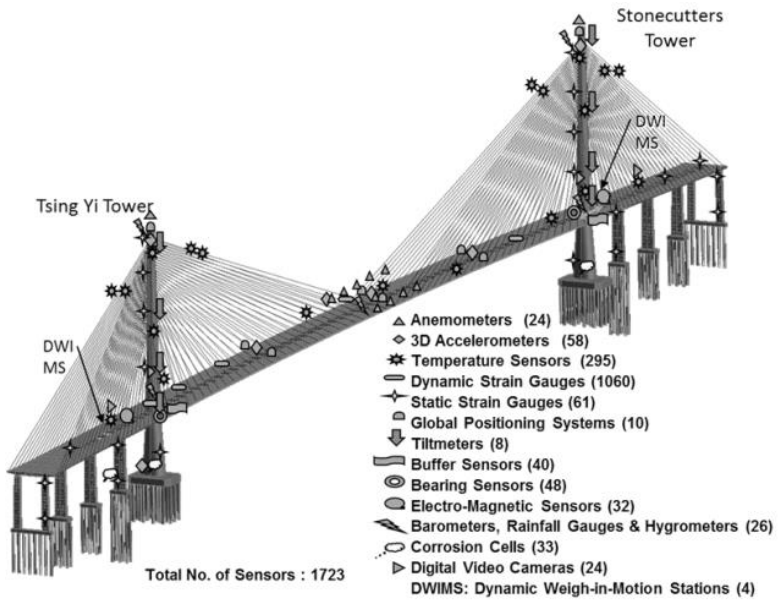

Figure 1.4. Layout of sensory system on Tsing Ma Bridge (Wong 2007)

1.3.3. MULTIVARIATE PROBLEMS

Model updating of structural systems are usually complex problems due to the large amount of degrees of freedom and model variables. Numerical simulation of real structures requires numerical models with physical meaning to be considered useful for studies such as retrofit analysis. Consider for instance the representation of a 2-story shear building as depicted in Figure 1.5:

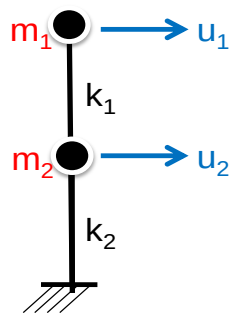

Figure 1.5. Conceptual representation of a 2-story shear building

The model to be updated typically consists of four random variables (two masses and two stiffness). The problem can get even more complicated, if the analyst decides to replace the constrained support by a spring system, whose stiffness values would increase the number of variables. The analyst can also consider damping, potentially increasing the number of variables by two. The situation depicted before shows that a simple model updating problem usually will be a computationally expensive multivariate problem.

1.3.4. Visualization

In the same way a model updating problem becomes complex as the number of variables increase, other challenge arises from this multivariate condition. This is, the visualization of the feasible space or variables for a solution or group of solutions. Regular visualization techniques offer great visualization tools when dealing with 1 or 2 variables. Dealing with more than 2 variables is a complex task, and usually the methodologies used to provide an insight of these problems condense the information, making it difficult to interpret. For instance, Figure 1.6 below depicts a hypercube in 4 dimensions, printed on a 2-dimensional space. An analyst should be trained in how to interpret these graphs and make conclusions based on the results of model updating problems.

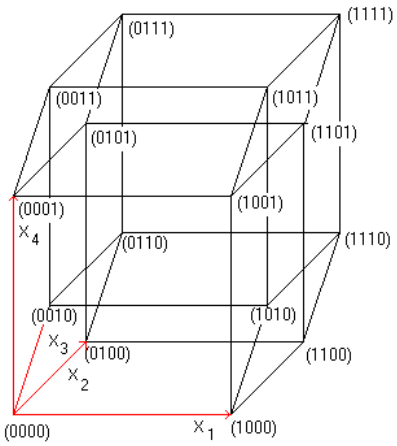

Figure 1.6. Conceptual representation of a hyper-cube (4D)

1.4. Model Updating Cognitive Systems: MUCogS

Caicedo and Zarate (2011) proposed MUCogS based on the need of creating models of existing structures with physically meaningful parameters. MUCogS states that due to the uncertainty associated with numerical models and low spatial sensor density, local minima found in a model updating process can provide a more accurate physical meaning than the global minimum. In a probabilistic sense this means that some areas of the solution space can provide more physically meaningful parameters than other areas with higher probability.

MUCogS has been thought as a framework with a computational core that makes use of computational resources and with a human/computer interface that allows experienced users to incorporate their knowledge in the analysis. These capabilities allow MUCogS to consider problems with many updating variables that are computationally demanding.

So far, MUCogS has incorporated several techniques that have been modified to make possible the search for local minima in optimization problems, such as GA and MGA. The goal of MUCogS is to develop a framework for a cooperative human-

computer model updating system, increasing and developing critical thinking skills in analysts in the search for updated models with physical meaning, and obtaining meaningful models. However, MUCogS is still under development, and lacks of a methodology that incorporates the analyst expertise into the model selection task. This research focuses in this particular area.

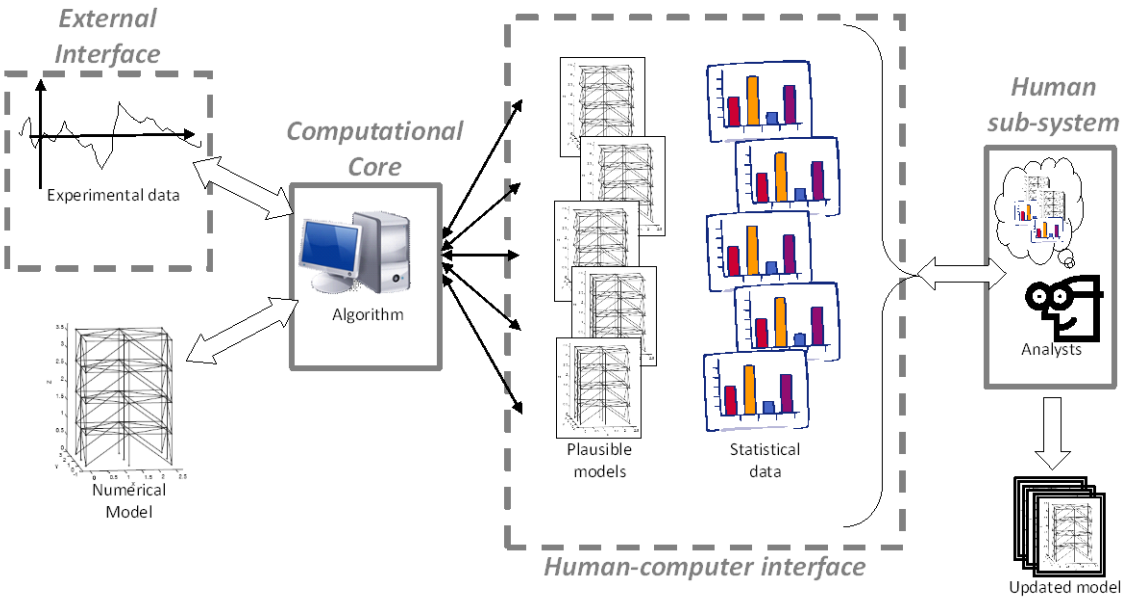

Figure 1.7. MUCogS (Model Updating Cognitive Systems) conceptual scheme

1.5. Research Contribution

The contribution of the proposed research is to offer a technique to select appropriate solutions and models based on the analyst knowledge about the behavior of the structure. To this end, the contribution of this research can be described in the following items:

- Develop a methodology to select solutions based on the analyst knowledge about the behavior of the structure.

- Develop a methodology to select models from a family of models, using the analyst knowledge about the behavior of the structure.
- Implement the technique within the MUCogS framework

The technique is based on Bayes' inference but unlike prior work on this area, the analyst expresses their knowledge in terms of the behavior of the structure in addition to the value of the parameters.

CHAPTER 2. VISUALIZATION TOOLS

The graphical representation of data sets has always been a mean to help interpret any kind of phenomena from a statistical point of view. For instance, the collection of data points relating the applied force and the resulting deformation of a linear mass-spring system allows engineers to estimate the constants that characterize such linear system by applying correlation techniques derived from statistical tools. The inclusion of a graphical representation of the data points and their statistical properties is a common –almost mandatory- requirement for a valid scientific documentation of such type of experimentation (orthographic x-y representation in this case) for a better understanding of the phenomena under analysis.

From an engineering point of view the use of graphical representations is critical, especially during the recent years when the computational power has dramatically increased, providing engineers with powerful resources for data collection and data analysis. An example where graphical representations are required in engineering is found in the mechanics of materials, where a uniaxial deformation test on a given material requires the collection of applied force and deformation data, and the Cartesian representation (Figure 2.1) of these data points help in the characterization of the material given loading conditions.

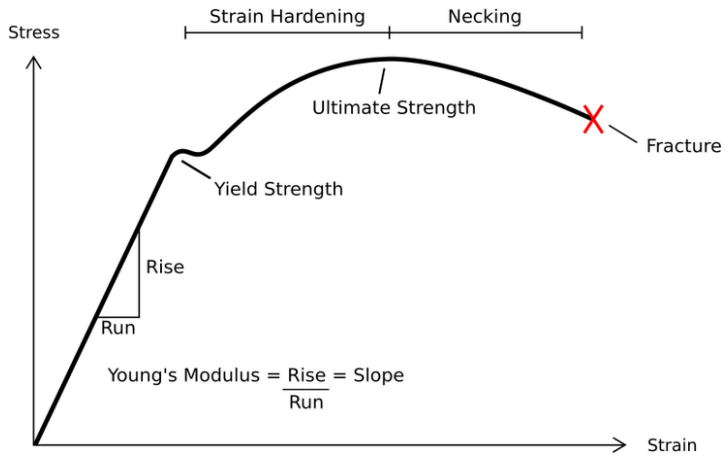

Figure 2.1. Typical stress-strain curve in ductile materials
(https://en.wikipedia.org/wiki/Deformation_(engineering))

However, Cartesian X-Y representations are limited tools for engineering areas dealing with multiple parameters. It is common to have multivariate problems in most of engineering areas, such as Water Resources, Operation Research or Structural Engineering, where several parameters are subject of optimization and/or analysis. The interpretation of data in such cases becomes very abstract as the degree of complexity increases, and the visual representation of the data becomes a challenging task.

The challenges presented by multivariate problems have been boarded by several authors who have proposed tools for the synthesis of multivariate data (Wong and Bergeron 1997; Estrada 2011). The proposed tools attempt to extract important features, helping the analyst with the recognition of patterns and/or giving the analyst information about the behavior of the used variables. The capability of the visualization tool for synthetizing important data is key in order to provide a good insight into the multivariate data.

2.1. Short Review of Multivariate Visualization Techniques

The following sections provide an overview of different methods for multivariate visualization. These tools are used in later chapters to provide a graphical representation of the updated models.

2.1.1. Parallel coordinates

One of the common tools for multivariate visualization is the parallel coordinates technique (Inselberg and Dimsdale 1991). Parallel coordinates "map" an N-Dimensional set of points into an X-Y plane by replicating the Y-axis N times, each one labeled accordingly (commonly, each axis is labeled as $x_1, x_2, \ldots, x_N$) all perpendicular to and equidistant along the X-axis. A point C with coordinates $(c_1, c_2, \ldots, c_N)$ is represented by the polygonal line intersecting the replicated axis $x_1, x_2, \ldots, x_N$. This technique is very powerful, in the sense that theoretically, the number of dimensions that can be mapped into the X-Y plane is infinite. Figure 2.2 displays the parallel coordinates plot of 20 random numbers in a 10-dimensional space.

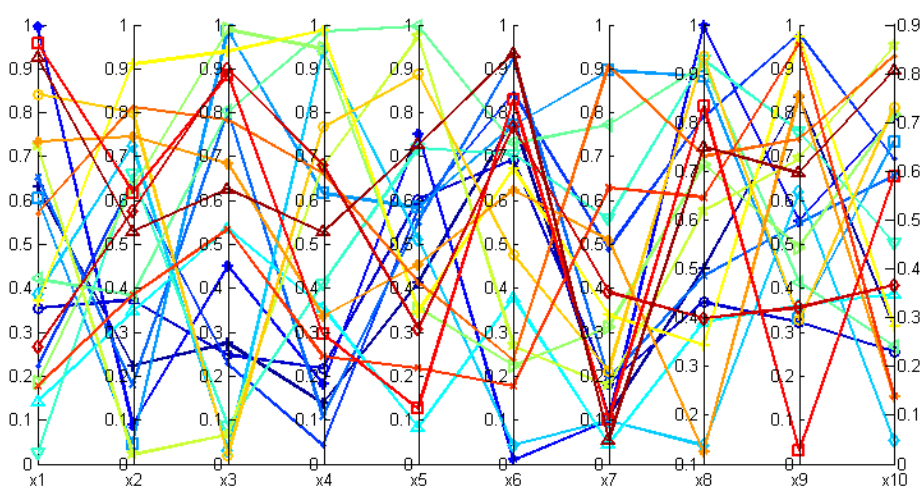

Figure 2.2. Parallel coordinates plot

2.1.2. SCATTERPLOT MATRIX

The scatterplot methodology is a visualization technique used to inspect samples taken from a multivariate function. The technique creates a matrix pairing all variables (x_1 *vs.* x_2, x_1 *vs.* x_3, …, x_{n-1} *vs.* x_n) allowing the identification of patterns within each variable's data distribution. This tool is useful when using sampling methods such as the Markov Chains, where it is important to track the distribution of the samples. The methodology is also useful in the identification of data clustering. An example of this technique is shown in Figure 2.3, where samples from a function with 3 variables are plotted, showing minima at $[x_1\ x_2\ x_3] = [0\ 0\ 0]$ and $[x_1\ x_2\ x_3] = [1\ 1\ 1]$.

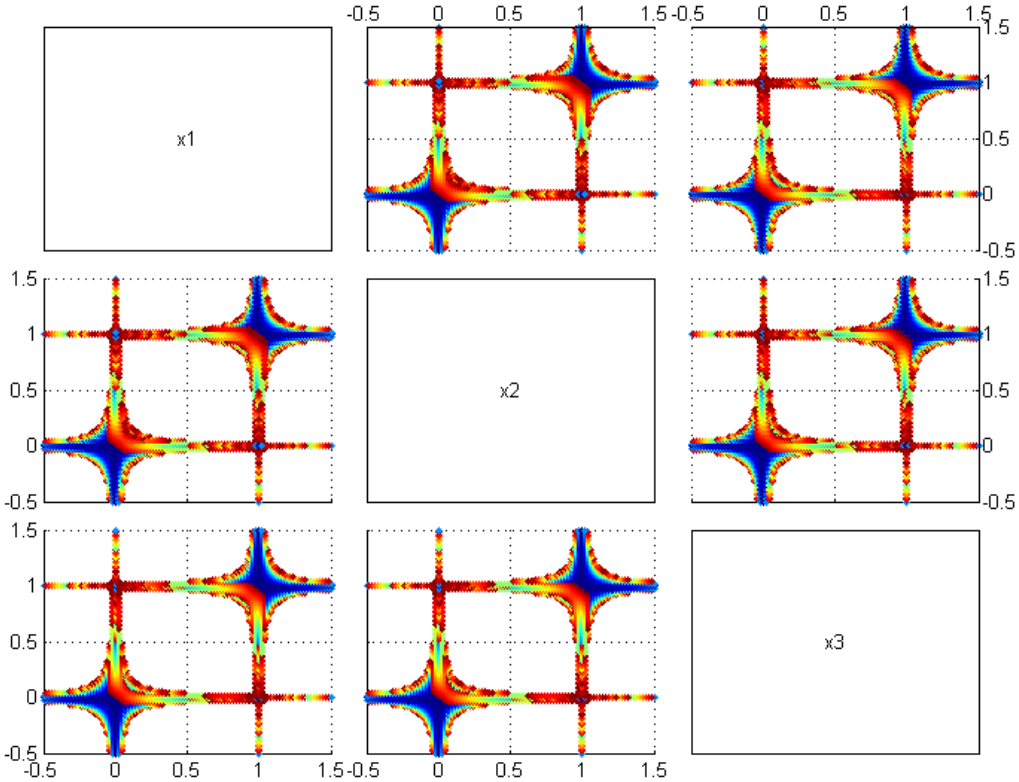

Figure 2.3. Scatterplot matrix

2.1.3. Radial Visualization: Radviz

Radviz uses the Euclidean X-Y-Z space, eliminating the orthogonality of the X-Y plane to fit as many dimensions as needed (Sharko, Grinstein et al. 2008), and using the Z-axis to represent values of f(x). Formally, Radviz converts to X-Y coordinates any N-dimensional array:

$$x_i = \frac{(\Sigma_{j=1,\ldots,d}\, a_{i,j}\cos\theta_j)}{\Sigma_{j=1,\ldots,d}\, a_{i,j}} \qquad y_i = \frac{(\Sigma_{j=1,\ldots,d}\, a_{i,j}\sin\theta_j)}{\Sigma_{j=1,\ldots,d}\, a_{i,j}} \qquad i=1,\ldots,N$$

This type of representation is useful for the visual exploration of local minima of a function, if a vicinity of points is plotted simultaneously. However, the radial visualization forces to several points to share the same X-Y space, as it would happen with the points [0,0,…,0] and [1,1,…,1] which will share the same X-Y point. Figure 2.4 uses Radviz to represent the point [2 3 4 6 3]:

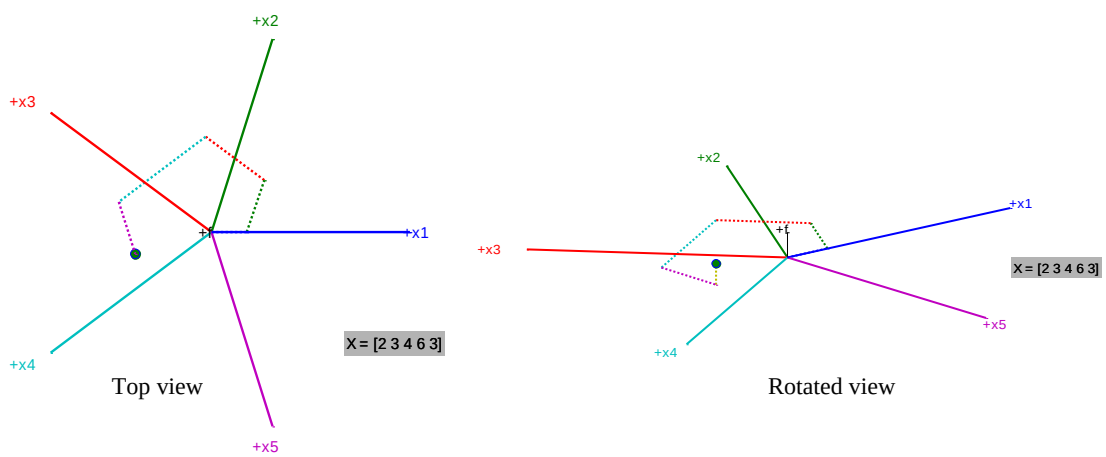

Figure 2.4. Radviz representation of X = [2 3 4 6 3]

2.1.4. Multivariate section cut

The multivariate section cut concept is derived from the idea of a straight line crossing a 2D or 3D space. This idea can be extended to an N-D space, clarifying the

shape of the function f(X) along the points defined by the hyper-line. This technique is useful in optimization processes, where the peaks of the function are of interest, as it happens with model updating methodologies. The hyper-line defining the section cut uses the vector addition rule, as

$$R_x = R_o + \Delta * u_{12}$$

Where Ro denotes the position of the starting point, u_{12} is a unitary vector defining the position of the ending point relative to the starting point, and Δ represents the desired spacing between connecting points. The plotting of the values R_x vs. f(X) generates the multivariate section cut. Figure 2.5 describes the Radviz representation of a 4-dimensional problem. Figure 2.6 uses multivariate section cuts between selected points in Figure 2.5 for the identification of local minima.

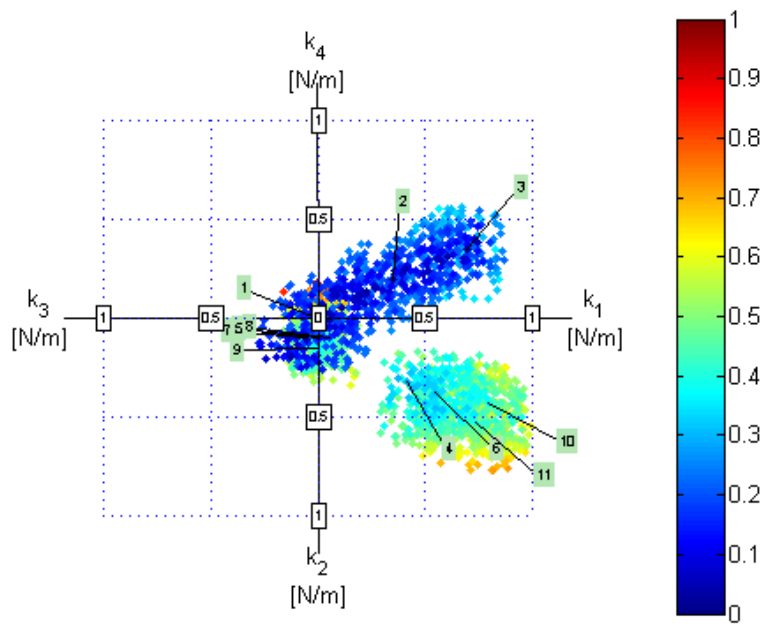

Figure 2.5. Selected Radviz points from 4D optimization problem

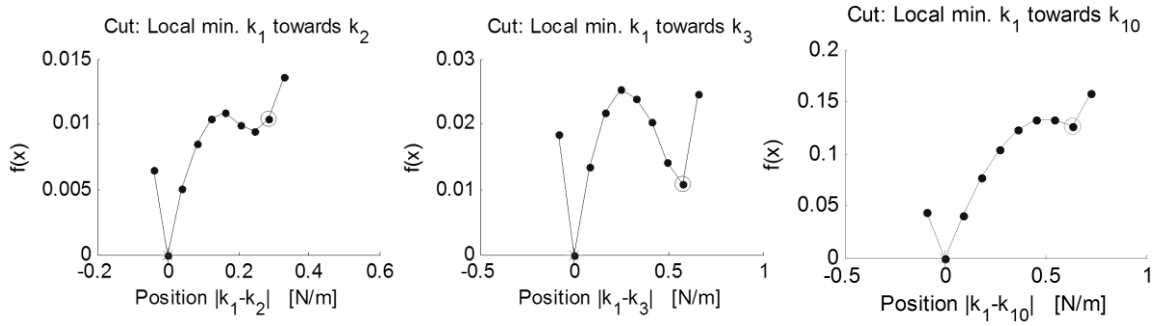

Figure 2.6. Multivariate section cut between selected points from 4D problem

The previous figures illustrate the usefulness of the Radviz and Multivariate section cut for optimization problems, where inspection of local minima is needed.

CHAPTER 3. BEHAVIORAL SELECTION TECHNIQUE

The main contribution of this research is to offer a technique that allows an analyst to incorporate his/her expertise into the model updating process. In traditional Bayes' model updating this is performed by specifying a prior PDF of the parameters. However, the analyst knowledge of the structure is arguably on its behavior and not the value of the parameters. For example, a bridge engineer might not have prior knowledge about the equivalent stiffness of a bridge temperature join for a 20 years old bridge and joints partially filled with debris. However, the engineer might be able to estimate the deflection for a particular load based on prior experience with load/deflection tests performed in similar bridges. This is even more important if we acknowledged the fact that model updating problems can lead to several solutions. An analyst can evaluate which solution is more probable, and the incorporation of his/her expertise can substantially change the results of the analysis. For example, in Zarate and Caicedo (2008) a numerical model of the Bill Emerson Memorial Bridge is updated. The problem considered 6 updating parameters, which represented the mass of the deck, the rotational stiffness of the deck-tower connection, and the moment of inertia of the spine beam. The model updating procedure obtained four solutions (Table 1.4), each one physically different. The first solution reduces 5% the mass at 2 locations and increases the moment of inertia of the deck by 5%, the second solution increases 99.73% the stiffness at the deck's bent, the third solution reduces the mass by 4.74% at location 1, and the fourth solution doubles the stiffness at the tower. The question at hand is: which of these

solutions an analyst should use for subsequent analysis? and: how can we enable the analyst to use their prior knowledge?

The success of MUCogS as a framework for model updating highly depends on its abilities to guide the analyst in the search of solutions in the updating process. However, identifying which model is more appropriate representation of the structure has not been studied in detail. Given that prior information about particular parameters of the model could be difficult to identify, the proposed technique uses the behavior of the structure to help the analyst identify appropriate models. A suitable way to incorporate the expertise criterion can be as follows:

- The analyst defines a test from which a virtual response can be expressed. The analyst should have enough expertise to select an appropriate test for the structure in consideration. For example load tests on bridges if the person has prior experience with these procedures.
- The analyst expresses the expected behavior of the structure to the given test as a "virtual" response (i.e., no test is actually run)
- The probability of each model and solution is calculated given the expected behavior of the structure.
- Plausible solutions are sorted based on their calculated probabilities.

Structural engineers can accumulate knowledge from the repetitive process of structural testing. This cumulated knowledge let them *"feel"* the structure behavior, and most of times, let them successfully anticipate the response of a structural system to a given loading situation. For instance, modern seismic design codes require structures to not to exceed a determined amount of lateral deformation, usually expressed as a lateral drift ratio. Experienced engineers can make estimations about such parameters on a given

structural system by using visual inspections only. Depending on the type of structural system, this specific situation may be different. For instance, it makes sense to consider lateral drifts in buildings and mid-span deflections in bridges. This concept is illustrated in Figure 3.1.

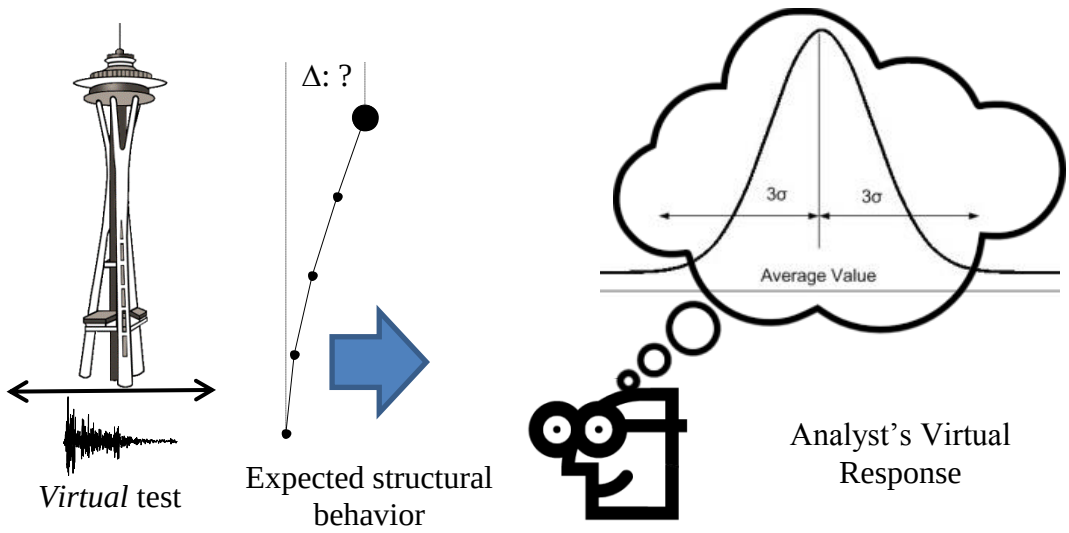

Figure 3.1. Analyst's Expertise

3.1. EXPECTED STRUCTURAL BEHAVIOR

The analyst expertise can be expressed in three different ways: i) a deterministic number, ii) a probability density function (PDF), and iii) an interval. A deterministic number might not be suitable because it does not allow expressing uncertainty. For example, consider inter-story drift in a multistory building. In this work it does not make sense to express the expected inter-story drift as 1/100 but as a value with uncertainty. The inter-story drift can be expressed as a normal distribution with mean 1/100 and standard deviation of 1/500 for example. It could also be expressed as an interval, for instance as [1/90 1/110] of the floor's height. The same can be done with a wide variety of parameters. In the case of earthquake excitation the analyst can express for example,

base shear force, maximum roof displacement, etc. This work focuses in the case when prior knowledge is specified as a PDF.

For instance, consider the 2 DOF model discussed in Caicedo and Zarate (2011) (Figure 3.2). The 2-story steel structure has a total height of 980mm and a floor area of 305x108 mm^2. The mass of each floor was measured as 710g and 860g for the first and second floor respectively. The reported average natural frequencies are 2.08Hz and 5.82Hz. Caicedo and Zarate (2011) considered the stiffness of both floors as parameters for updating. These two parameters were updated using the MUCogS framework. In the paper, Caicedo and Zarate reported two solutions from the updated PDF corresponding to peaks of maximum posterior located at $[k_1\ k_2]$= [358 390] N/m and $[k_1\ k_2]$ = [714 196] N/m (Figure 3.2). The probability of each solution can be approximated by analyzing the surrounding area of every peak of maximum probability.

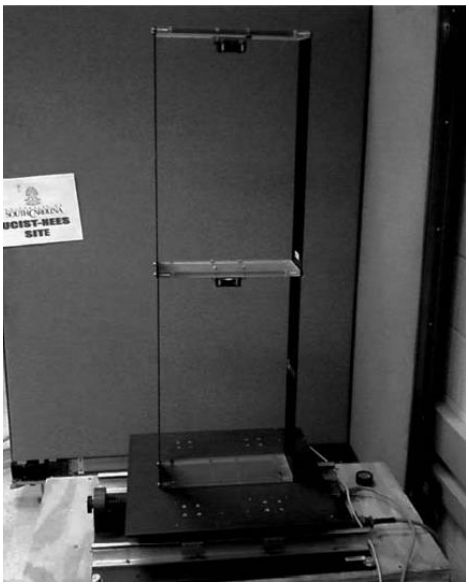

a. Actual system

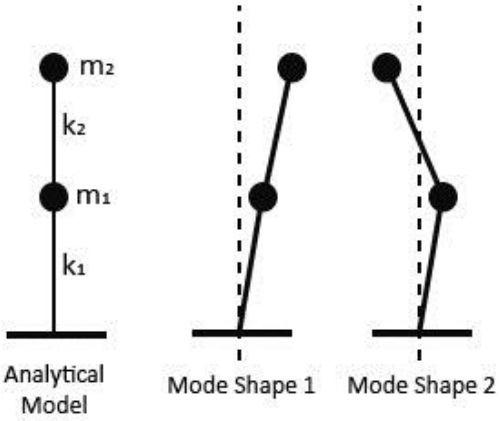

b. System idealization

Figure 3.2. 2-DOF system (Caicedo and Zarate 2011)

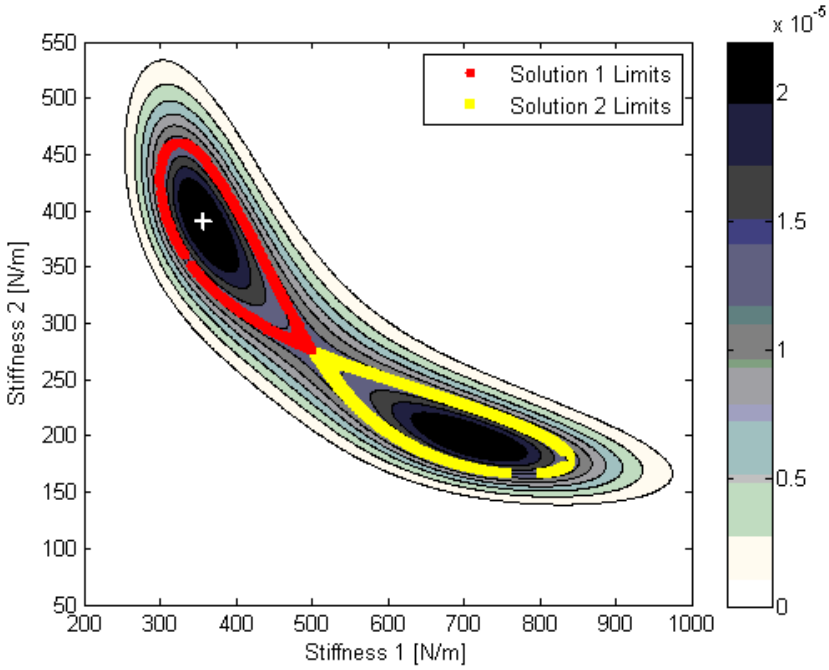

Figure 3.3. Reported solutions and their approximated area of influence (Caicedo and Zarate 2011)

In Figure 3.3 the two solutions seem to have similar probabilities, but a closer look to the structure (Figure 3.2a) indicates that one of them is more likely than the other because the floors appear to have similar stiffness (the two floors look the same). An analyst can use this information and decide to use one of the areas of high probability for their model. However, model selection is more complicated in larger systems, where the structure might not be easy to inspect and many parameters are updated. Therefore, a systematic way of evaluating these solutions is needed.

For example, the expertise of an undergraduate student with no knowledge about this research was used to estimate the displacement of the structure under a hypothetical loading case of 1.57 N (0.36 lb.) and 3.82 N (0.86 lb.) located at the first and second floors of the structure shown in Figure 3.2. The undergrad has worked with the structure before and has a reasonable experience about the behavior of the system, estimating the

relative displacement range as [3.6 25.7] mm for the first floor, and [3.6 25.7] mm for the second floor. A uniform interval was assumed between the provided interval (Figure 3.4a). Figure 3.4b shows the probability of the stiffness given the expressed behavior.

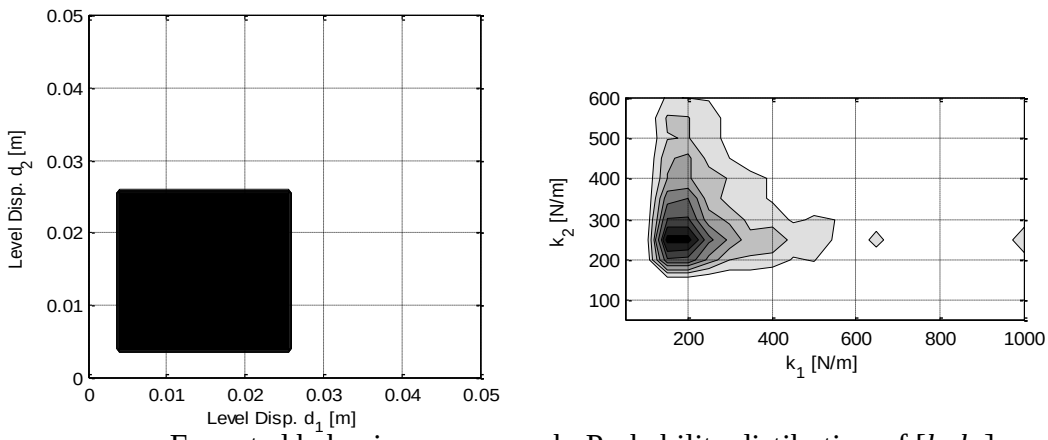

a. Expected behavior b. Probability distibution of [k_1 k_2]

Figure 3.4. Expertise virtual response for 2D structure

3.2. Probability of Solutions Given Expected Behavior

The techniques to describe the probability distribution of the updating parameters in a numerical model have been widely studied. The work by (Beck and Katafygiotis 1998) provide the foundation for the implementation of this Bayesian approach. Other researchers have further developed these ideas to include them in areas such as Structural Health Monitoring (SHM) (Vanik, Beck et al. 2000), Structural Reliability (Papadimitriou, Beck et al. 2001) or Damage Detection (Yuen 2010). Bayes' theorem is (Ang, Tang et al. 2007):

$$P(E_i|A) = \frac{P(A|E_i)P(E_i)}{P(A)}$$

where E_i represents any given event with associated probability P(E_i) (prior knowledge of E_i). Conceptually, Bayes' Theorem can be seen as a mean to update this

probability when another event A provides new evidence about event E_i. P(E_i|A) is the probability of event E_i given the new evidence A (posterior knowledge of E_i), and the quotient P(A|E_i)/P(A) represents the support of event A provided for event E_i. Given that event E_i can have multiple states (true or false for instance), the total probability theorem can be used to represent P(A) as a normalization constant letting the Bayes' theorem to be re-written as

$$P(E_i|A) = \frac{P(A|E_i)P(E_i)}{\sum P(A|E_i)P(E_i)}$$

In a model updating context, the prior knowledge of structural parameters (θ) can be represented using probability distributions. When new evidence (D) about the structural parameters of the system is available, the Bayes' theorem updates this prior knowledge, and a posterior probability distribution of the structural parameters is obtained. The Bayes' theorem is usually expressed using the following equation (Vanik, Beck et al. 2000):

$$P(\theta|D) = c * P(D|\theta)P(\theta)$$

where

$$c^{-1} = \int P(D|\theta)P(\theta)\mathrm{d}\theta$$

Figure 3.5 describes the Bayes' concept:

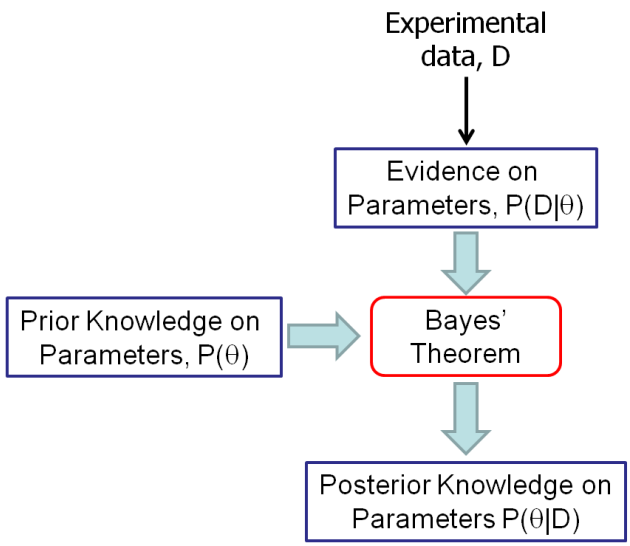

Figure 3.5. Conceptual representation of Bayes' theorem

3.2.1. PRIOR DISTRIBUTION: P(θ)

The prior distribution P(θ) is the degree of belief on the parameters θ. When an initial estimation on the distribution of θ is difficult to establish, it is valid to consider a uniform probability distribution g(θ), within a parameter range. This uniform distribution expresses vague or general information about θ, and it is commonly called a non-informative prior. The selection of non-informative priors is common practice in Bayesian methodologies (Kass and Wasserman 1996) and can be expressed as

$$g(\theta) = \mathrm{p}_o = \frac{1}{\prod(\theta_{upper} - \theta_{lower})} \qquad \theta_{lower} < \theta < \theta_{upper}$$

$$g(\theta) = 0 \qquad \text{otherwise}$$

where $g(\theta)$ is determined by the lower and upper boundaries of the parameters, θ_{lower} is the lower bound of the parameters and θ_{upper} is upper bound of the parameters.

3.2.2. LIKELIHOOD DISTRIBUTION: P(D|θ)

Likelihood distributions in Bayesian Model Updating express the probability of experimentally obtained data D given a set of parameters θ. Commonly, the likelihood is defined as a Normal distribution:

$$f(\theta, D) = \frac{1}{\sqrt{2\pi|\Sigma(\varepsilon)|}} * \exp\left(-\frac{1}{2}\left|\frac{\varepsilon(\theta, D)}{\sigma(\varepsilon)}\right|^2\right)$$

In the previous expression, $\varepsilon(\theta, D)$ denotes the error between the experimental parameters θ and the experimental measurements of such parameters, *D*, and $\sigma(\varepsilon)$ denotes the standard deviation of such error. According to the maximum entropy principle, a Gaussian distribution imposes the minimal structural constraint within the specified moments (μ,σ) and thus, has maximum entropy among all distributions with specified mean μ and standard deviation σ. One practical way of expressing $\varepsilon(\theta, D)$ using modal parameters is

$$f(\theta, D) = \frac{1}{c_1} * \exp\left(-\frac{1}{2}\sum_{j=1}^{n}\left|\frac{\omega_j^{id} - \omega_j^{fe}(\theta)}{\sigma_j^{\omega error}}\right|^2 - \frac{1}{2}\sum_{j=1}^{n}\sum_{i=1}^{m}\left|\frac{\phi_{j,i}^{id} - \phi_{j,i}^{fe}(\theta)}{\sigma_{j,i}^{\phi error}}\right|^2\right)$$

Where, *n* is the number of identified modes of vibration, *m* is the number of modal coordinates, ω_j^{id} is the *j*-th identified natural frequency, $\omega_j^{fe}(\theta)$ is the *j*-th natural frequency of the finite element model, $\phi_{j,i}^{id}$ is the *i*-th modal coordinate of the *j*-th identified mode shape, $\phi_{j,i}^{fe}(\theta)$ is the *i*-th modal coordinate of the *j*-th mode shape of the finite element, $\sigma_j^{\omega error}$ is the standard deviation of the error of the *j*-th identified natural frequency and $\sigma_{j,i}^{\phi error}$ is the standard deviation of the error of the *i*-th modal coordinate

that corresponds to the *j*-th identified mode shape. The PDF is normalized with the constant c_1 which yields to

$$c_1 = \int_{\theta_{lower}}^{\theta_{upper}} \exp\left(-\frac{1}{2}\sum_{j=1}^{n}\left|\frac{\omega_j^{id} - \omega_j^{fe}(\theta)}{\sigma_j^{\omega error}}\right|^2 - \frac{1}{2}\sum_{j=1}^{n}\sum_{i=1}^{m}\left|\frac{\phi_{j,i}^{id} - \phi_{j,i}^{fe}(\theta)}{\sigma_{j,i}^{\phi error}}\right|^2 \right) d\theta$$

3.2.3. POSTERIOR DISTRIBUTION: P(θ|D)

The posterior distribution P(θ|D) represents the updated probability distribution of the structural parameters θ given the experimental data D. The general expression for it has been defined as

$$P(\theta|D) = c * P(D|\theta)P(\theta)$$

The research documented in this Dissertation considers the prior knowledge of parameters θ as a non-informative prior as described in 3.2.1, and the distribution of the supporting evidence D as described in 3.2.2. Under these assumptions, P(θ|D) can be written as

$$P(\theta, D) = c * \mathrm{p}_o * \mathrm{c}_1 * \exp\left(-\frac{1}{2}\sum_{j=1}^{n}\left|\frac{\omega_j^{id} - \omega_j^{fe}(\theta)}{\sigma_j^{\omega error}}\right|^2 - \frac{1}{2}\sum_{j=1}^{n}\sum_{i=1}^{m}\left|\frac{\phi_{j,i}^{id} - \phi_{j,i}^{fe}(\theta)}{\sigma_{j,i}^{\phi error}}\right|^2 \right)$$

$$\theta_{lower} < \theta < \theta_{upper}$$

$$P(\theta|D) = 0 \quad \text{otherwise}$$

Here, similar to the previous expression P(D|θ), the PDF requires a normalization constant *c* equivalent to the integral of P(θ|D) over the domain of θ. After simplifications, they yield to

$$P(\theta|D) = \mathrm{c} * \exp\left(-\frac{1}{2}\sum_{j=1}^{n}\left|\frac{\omega_j^{id} - \omega_j^{fe}(\theta)}{\sigma_j^{\omega error}}\right|^2 - \frac{1}{2}\sum_{j=1}^{n}\sum_{i=1}^{m}\left|\frac{\phi_{j,i}^{id} - \phi_{j,i}^{fe}(\theta)}{\sigma_{j,i}^{\phi error}}\right|^2\right)$$

$$c^{-1} = \int_{\theta_{lower}}^{\theta_{upper}} \exp\left(-\frac{1}{2}\sum_{j=1}^{n}\left|\frac{\omega_j^{id} - \omega_j^{fe}(\theta)}{\sigma_j^{\omega error}}\right|^2 - \frac{1}{2}\sum_{j=1}^{n}\sum_{i=1}^{m}\left|\frac{\phi_{j,i}^{id} - \phi_{j,i}^{fe}(\theta)}{\sigma_{j,i}^{\phi error}}\right|^2\right) d\theta$$

3.3. Model Probability

Consider that the structural parameters θ belong to a class of models $\boldsymbol{M}$, and that a subset of parameters θ belong to some region $S_i(\theta)$ defining a particular optimal model M_i representing the physical system (Beck and Katafygiotis 1998). Then the optimal regions S_i can be called solutions of the model updating problem with an associated posterior probability $P(S_i|D)$, and can be compared, under the assumed correctness of $\boldsymbol{M}$ (Jaynes 2003):

$$P(S_i|D, \boldsymbol{M}) = \frac{P(D|S_i\,, \boldsymbol{M})}{P(D|\boldsymbol{M})} P(S_i|\,\boldsymbol{M}) = \frac{P(D|S_i\,, \boldsymbol{M})}{\int P(D|S\,, \boldsymbol{M}) P(S|\,\boldsymbol{M})\mathrm{d}\theta} P(S_i|\,\boldsymbol{M})$$

Given that a single model class $\boldsymbol{M}$ exists, the probabilities of each model M_i defined by the region $S_i(\theta)$ can be calculated without the need to compute the normalization constant of $P(\theta|D)$. For instance, the probability of the model M_k can be chosen as reference, and odd ratios can be used to compare models:

$$\frac{P(M_i|D, \boldsymbol{M})}{P(M_k|D, \boldsymbol{M})} = \frac{\frac{P(D|M_i\,, \boldsymbol{M})}{P(D|\boldsymbol{M})} P(M_i|\,\boldsymbol{M})}{\frac{P(D|M_k\,, \boldsymbol{M})}{P(D|\boldsymbol{M})} P(M_k|\,\boldsymbol{M})} = \frac{P(D|M_i\,, \boldsymbol{M}) P(M_i|\,\boldsymbol{M})}{P(D|M_k\,, \boldsymbol{M}) P(M_k|\,\boldsymbol{M})}$$

The same expression applies for different model classes $\boldsymbol{M} = \{\boldsymbol{M}_1, \boldsymbol{M}_2, \ldots, \boldsymbol{M}_k\}$.

3.4. Expertise Criterion: "Virtual Response"

The virtual response expressing the analyst's experience ($\boldsymbol{V_R}$) can be included in the Bayesian analysis as shown in Figure 3.6:

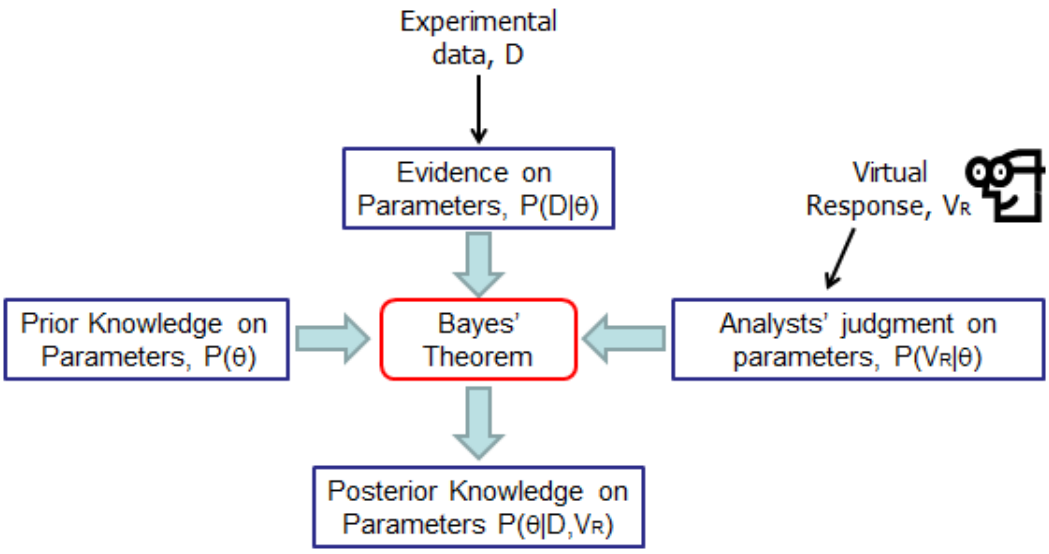

Figure 3.6. Conceptual representation of Bayes' theorem for 3 events

The probability of three events A, B and C is commutable. This is (Ang, Tang et al. 2007),

$$P(ABC) = P(CBA)$$

From conditional probability properties, the probability of the intersected events is computed as

$$P(BC) = P(B|C)P(C)$$

Then, the probability of the intersection of three events can be written as

$$P(A|BC)P(B|C)P(C) = P(C|BA)P(B|A)P(A)$$

$$P(A|BC) = P(C|BA)\frac{P(B|A)P(A)}{P(B|C)P(C)}$$

The expression to the right of $P(C|BA)$ can be reordered:

$$P(A|BC) = P(C|BA)\frac{P(BA)}{P(BC)}$$

The intersected events are commuted one more time:

$$P(A|BC) = P(C|BA)\frac{P(AB)}{P(CB)}$$

Finally, the intersected events are expressed in terms of the conditional probability:

$$P(A|BC) = P(C|BA)\frac{P(A|B)P(B)}{P(C|B)P(B)} = P(C|BA)\frac{P(A|B)}{P(C|B)}$$

Then the Bayes' Theorem for three events A, B and C can be written as

$$P(A|BC) = \frac{P(C|BA)P(A|B)}{P(C|B)}$$

By analogy, the expression in terms of θ, D and V_R is

$$P(\theta|DV_R) = \frac{P(V_R|D\theta)P(\theta|D)}{P(D|V_R)}$$

where P(θ|D) is the posterior distribution of the parameters θ. This expression is expanded in terms of the likelihood and prior distribution as

$$P(\theta|DV_R) = \frac{P(V_R|D\theta)P(D|\theta)P(\theta)}{P(D|V_R)P(V_R)}$$

Finally, assuming that the events V_R and D are independent, given that the analysts can provide V_R before experimental data is obtained,

$$P(\theta|DV_R) = \frac{P(V_R|\theta)P(D|\theta)P(\theta)}{P(D)P(V_R)}$$

Given that the denominator serves as normalization constant, the Bayes' Theorem including virtual responses can be written as follows:

$$P(\theta|DV_R) = c * P(V_R|\theta)P(D|\theta)P(\theta)$$

This expression can be used to calculate the odds ratios between the probability of models:

$$P(M_i|D, V_R, \boldsymbol{M}) = \frac{P(V_R|M_i, \boldsymbol{M})P(D|M_i, \boldsymbol{M})P(M_i|\boldsymbol{M})}{P(D|\boldsymbol{M})P(V_R|\boldsymbol{M})}$$

$$\frac{P(M_i|D, V_R, \boldsymbol{M})}{P\left(M_j\middle|D, V_R, \boldsymbol{M}\right)} = \frac{P(V_R|\, M_i, \boldsymbol{M})P(D|\, M_i, \boldsymbol{M})P(M_i|\boldsymbol{M})}{P\left(V_R\middle|\, M_j, \boldsymbol{M}\right)P\left(D\middle|\, M_j, \boldsymbol{M}\right)P\left(M_j\middle|\boldsymbol{M}\right)}$$

CHAPTER 4. BENCHMARK STRUCTURE

The Model Updating Cognitive Systems (MUCogS) has been designed as a framework for the implementation of model updating methodologies, in order to provide the analyst with updated models capable of representing a real system with physically meaningful parameters. Since MUCogS is a framework and not a particular methodology, it is expected that many techniques can be used within the framework. For example (Caicedo and Yun 2010) proposed an evolutionary approach to identify multiple solutions in a deterministic model updating context. Zarate and Caicedo (2007) proposed a methodology based in Modeling to Generate Alternatives (MGA) to obtain plausible solutions in the updating of complex numerical models. It is difficult to compare the performance of these techniques if they are applied to different structures. One alternative is to use the ASCE benchmark problem, but this benchmark was not designed to address the problem of multiple solutions. The modal data from the ASCE problem is very standard for a shear building and the models are relatively simple, not leading to the existence of multiple solutions in the updating problem.

This chapter proposes to develop a benchmark problem that can be used to compare methodologies that deal with the selection of multiple solutions. The Structural Dynamics and Intelligent Infrastructure (SDII) research group at the University of South Carolina designed and constructed a modular test structure, whose simplicity for modeling, instrumentation and characterization serves for the formulation of the benchmark problem (Figure 4.1).

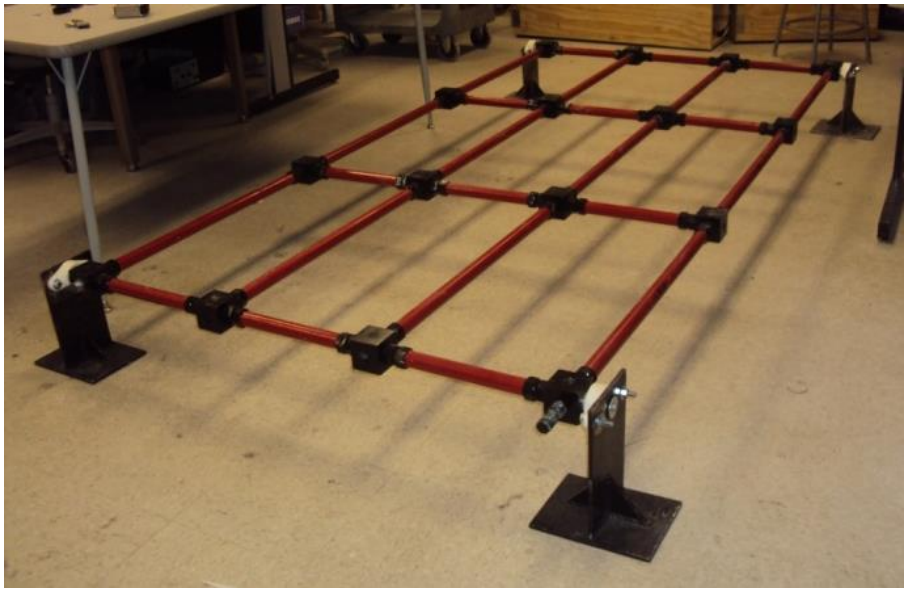

Figure 4.1. SDII test structure

Experimental information of the test structure is made available through the characterization of its dynamic properties. Modal identification is performed by acquiring input force/output acceleration data from impact tests. The identification is repeated after modifying the system by adding a mass of 8.68Kg to one of the nodes. The proposed metrics for the comparison of methodologies use the modal properties of the modified system, emulating a "structural retrofit" situation, useful to evaluate the quality of the predicted behavior of the selected models.

Finally, it is expected that the benchmark problem encourages other researchers to recognize multiple alternatives in model updating, helping in the development of methodologies for the integration of the human expertise.

4.1. Test Structure Description

The test structure is a 4x4 grid (x-y plane) of beam elements supported at the corners. The supports are made of 5/16" thick plates with mounted bearings allowing rotation in the x-direction only. The structure is 2.49m long (y-direction) and 1.21m wide

(x-direction). The grid consists of cold rolled steel tubes (DOM 1.25”x0.188”) interconnected with 2.5”x2.5x2.5” 1018 cold-rolled steel cubes, internally threaded and connected with 1" threaded rods. A plan drawing is shown in Figure 4.2, and information about geometrical and material properties is presented in Table 4.1.

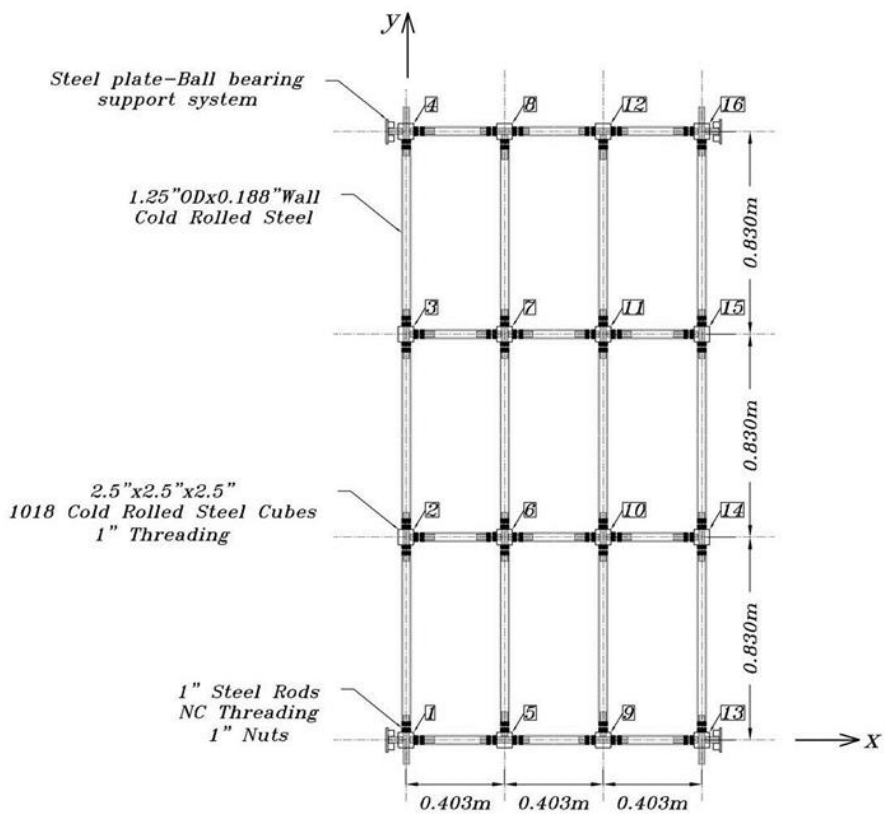

Figure 4.2. Test structure plan drawing

Table 4.1. Test structure properties

Node Coordinates		
#	X [m]	Y [m]
1	0.000	0.000
2	0.000	0.830
3	0.000	1.660
4	0.000	2.490
5	0.403	0.000
6	0.403	0.830
7	0.403	1.660
8	0.403	2.490

Node Coordinates		
#	X [m]	Y [m]
9	0.806	0.000
10	0.806	0.830
11	0.806	1.660
12	0.806	2.490
13	1.209	0.000
14	1.209	0.830
15	1.209	1.660
16	1.209	2.490

Beam Elements	
Section	DOM 1.25x0.188
Area	406 mm^2
Ixx	3864 mm^4
Iyy	3864 mm^4
J	7729 mm^4
Material	Cold rolled steel
E	199.9 Gpa
r	7890 kg/m^3
ν	0.3 -

Additional Mass	
Nodes	**Lumped Mass**
1,4,13,16	2.98 kg
2,3,14,15	3.13 kg
5,8,9,12	3.13 kg
6,7,10,11	3.59 kg

4.2. EXPERIMENTAL TESTING

The acquisition of experimental data from the test structure consists of input force/output accelerations using one impact hammer and 8 accelerometers. Two different test configurations are used to obtain modal information from all 16 nodes of the structure. Accelerometers were attached to nodes 3, 4, 7, 8, 11, 12, 15 and 16 for the first type of test and attached to nodes 1, 2, 5, 6, 9, 10, 13 and 14 for the second type of test. Complete modal data is obtained by combining both types of test. Data files are collected using three National Instruments NI-9234 acquisition moduli mounted on a NI cDAQ 9174 chassis with a predefined internal sampling frequency of 1652 Hz. Details about the accelerometers and DAQ are presented in Table 4.2 and Table 4.3.

Time responses are recorded from all channels with duration of 20 seconds. A total of 10 records from impacts at nodes 6, 9 and 11 are collected. Every record consists of three equally spaced impacts at the same location. Figure 4.3 shows a representative response from all channels due to impact at node #6.

Table 4.2. Sensor data

Ch.	Sensor Type	Model	S/N	Sensitivity	Range (1)	Range (2)	Resonant Freq.
1	Accelerometer	PCB 333B50	LW51385	1019 mV/g	±0.5g pk	0.5 to 3000 Hz	³ 20kHz
2	Accelerometer	PCB 333B50	39381	1019 mV/g	±0.5g pk	0.5 to 3000 Hz	³ 20kHz
3	Accelerometer	PCB 333B50	LW51250	1019 mV/g	±0.5g pk	0.5 to 3000 Hz	³ 20kHz
4	Accelerometer	PCB 333B50	LW51384	995 mV/g	±0.5g pk	0.5 to 3000 Hz	³ 20kHz
5	Accelerometer	PCB 333B50	40787	1035 mV/g	±0.5g pk	0.5 to 3000 Hz	³ 20kHz
6	Accelerometer	PCB 333B50	LW51249	982 mV/g	±0.5g pk	0.5 to 3000 Hz	³ 20kHz
7	Accelerometer	PCB 333B50	40789	1054 mV/g	±0.5g pk	0.5 to 3000 Hz	³ 20kHz
8	Accelerometer	PCB 333B50	40790	1062 mV/g	±0.5g pk	0.5 to 3000 Hz	³ 20kHz
9	Impact Hammer	PCB 086C03	23410	2.33 mV/N	±2224N pk	-	³ 22kHz

Table 4.3. DAQ configuration

Acquisition Module	Module Type	Model	S/N	Channels	Nodes	
					Test 1	Test 2
1	Analog signal acquisition, 4 input channels, ±5 V, 51.2 kS/s per Channel, 24-Bit IEPE	NI-9234	1822140	1 2 3 4	3 4 7 8	2 1 6 5
2	Analog signal acquisition, 4 input channels, ±5 V, 51.2 kS/s per Channel, 24-Bit IEPE	NI-9234	1822138	5 6 7 8	11 12 15 16	10 9 14 13
3	Analog signal acquisition, 4 input channels, ±5 V, 51.2 kS/s per Channel, 24-Bit IEPE	NI-9234	14626CF	9	6,9,11	6,9,11

4.3. MODAL IDENTIFICATION

Given that both input and output experimental data is available, the transfer function between force and acceleration is estimated using Matlab. The transfer functions are calculated using default values estimated by Matlab (8192 points in the Fourier transform, overlap of 3670 points and a total of 7 windows for this case). The Eigensystem Realization Algorithm (ERA) is used to perform modal identification (Juang and Pappa 1985). ERA requires Impulse Response Functions (IRF), which can be obtained as the inverse Fourier Transform (ifft) of the averaged transfer functions (Bendat and Piersol 2000). The estimated IRFs have a sampling rate of 1652Hz and are down-sampled to 200Hz prior to identification. Resampling focuses modal identification to modes under 100 Hz. Figure 4.3 and Figure 4.4 are representative figures of the procedure used for the identification of IRFs. A full set of used data is found in Appendix A.

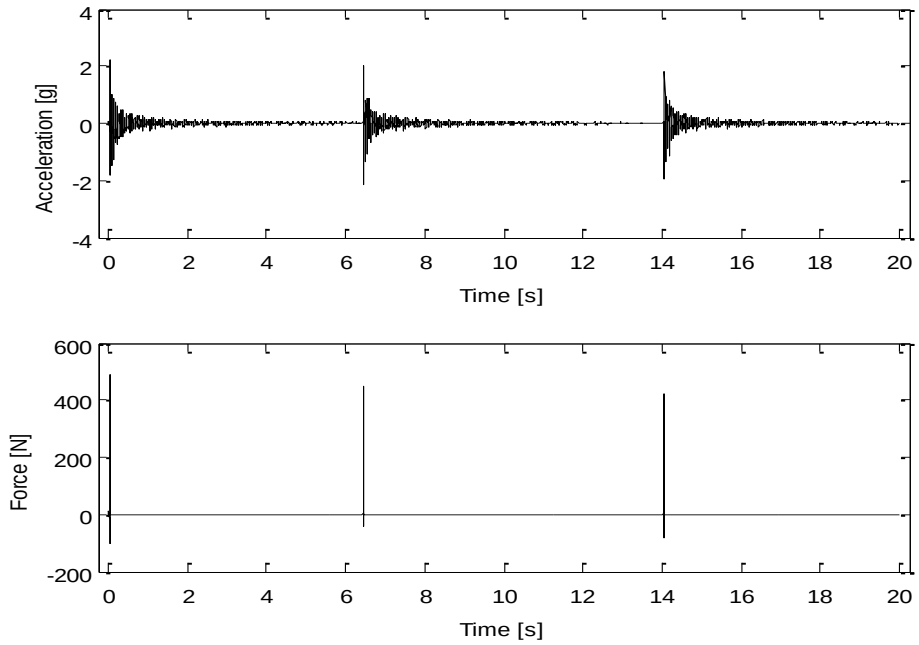

Figure 4.3. Typical time response from impact hammer testing
(Hammer impact at node 6, acceleration response from node 3)

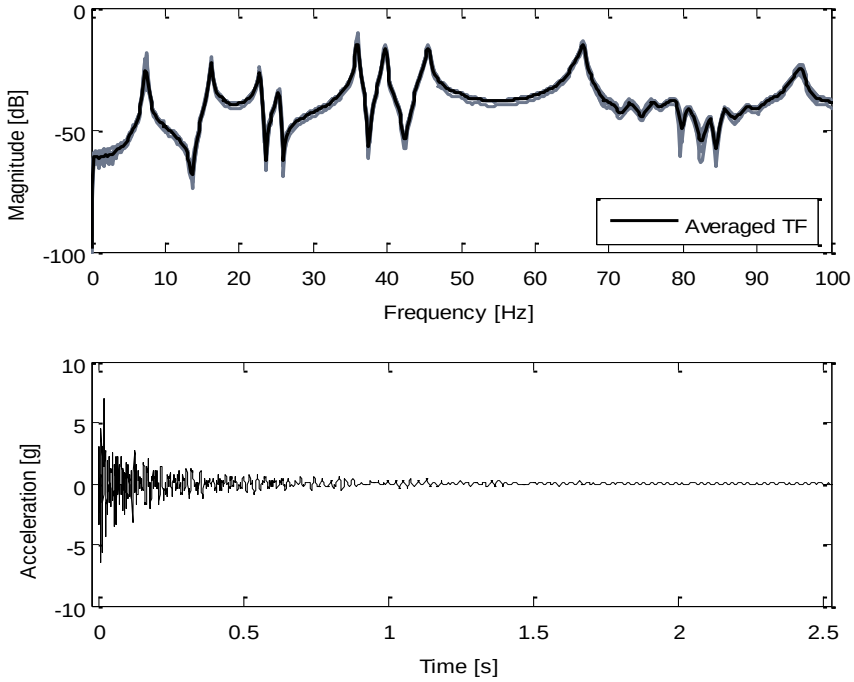

Figure 4.4. Averaged Transfer Function and IRF from node 3
(Test #1, impact at node 6, 10 acceleration records for averaging)

Natural frequencies, damping ratios and mode shapes are estimated using ERA. The size of the Hankel matrix is varied in order to develop a stabilization diagram and identify stable modes. A rule of thumb for the setup is to make the number of columns equal to 4 times the number of poles and the number of rows to be equal to 8 times the number of columns (Caicedo 2011). With this is mind, a stabilization diagram is calculated changing the number of poles from 6 to 66 (Figure A.10, Figure A.11 and Figure A.12). The identification is completed with a subroutine for the elimination of modes with unrealistic frequencies and/or damping ratios (i.e. negative damping).

Vibration modes identified by ERA and identified as stable poles in the stabilization diagram are grouped and averaged according to their similarity, measured by the Modal Assurance Criteria (MAC) (Allemang 2003) and their frequency. The MAC is required to be greater than 0.95 and the tolerance in natural frequencies is set to a maximum of 2%. Prior to averaging, mode shapes are normalized respect to the same modal coordinate, corresponding to the coordinate with highest value. The results are presented in Table 4.4. This generates duplicated modes in modes 6 and 7, modes 8 and 9, and modes 10 and 11.

Table 4.4. Identified natural frequencies and damping ratios

#	Count	fn [Hz]	σ_{fn} [Hz]	ζ %	σ_{ζ} [%]
1	63	7.37	0.02	1.45	0.43
2	60	16.19	0.10	1.04	0.61
3	86	22.79	0.07	0.86	0.25
4	68	25.31	0.06	0.67	0.24
5	90	36.02	0.08	0.38	0.08
6	60	39.69	0.08	0.44	0.16
7	24	39.76	0.14	0.57	0.32
8	95	45.51	0.22	0.80	0.37

#	Count	fn [Hz]	σ_{fn} [Hz]	ζ %	σ_{ζ} [%]
9	21	45.75	0.03	0.46	0.03
10	18	65.88	0.40	4.10	0.61
11	102	66.44	0.22	0.62	0.23
12	41	79.36	0.33	0.72	0.21
13	20	80.76	0.18	0.83	0.17
14	72	83.44	0.20	1.20	0.30
15	36	85.68	0.29	0.76	0.16
16	88	95.80	0.31	0.77	0.29

The mode shapes shown in Figure 4.5 and Figure 4.6, and the natural frequencies in Table 4.4 indicate that the identified modes 6 and 7 correspond to the same mode and therefore, the averaged natural frequencies and mode shapes are used for any subsequent analysis. The same applies for modes 8 and 9, and modes 10 and 11. Finally, it is unclear if modes 12 through 16 correspond to actual modes. Peaks for modes up to 67Hz are sharp in the transfer functions plots (Figure A.10, Figure A.11 and Figure A.12), while modes over 67Hz are not. This is unlikely due to a lack of excitation at these frequencies because the Fourier Transform of the hammer impact is almost constant in this frequency range, as shown in Figure A.1 through Figure A.6. In any case, modes above 67 Hz are considered not reliable and discarded from any subsequent analysis (Table 4.5, Table 4.6 and Table 4.7).

Table 4.5. Reported results from modal identification

#	fn [Hz]	σ_{fn} [Hz]	ζ %	σ_{ζ} [%]
1	7.37	0.02	1.45	0.43
2	16.19	0.10	1.04	0.61
3	22.79	0.07	0.86	0.25
4	25.31	0.06	0.67	0.24
5	36.02	0.08	0.38	0.08
6	39.71	0.10	0.47	0.22
7	45.55	0.20	0.74	0.33
8	66.44	0.22	0.62	0.23

Table 4.6. Identified Modal Coordinates

Node #	Mode							
	1	2	3	4	5	6	7	8
1	0.043	0.022	-0.139	0.121	-0.091	0.059	0.103	-0.070
2	0.840	0.925	-0.302	-0.384	0.837	0.738	0.677	-0.652
3	0.935	1.000	0.488	-0.369	-0.974	-0.865	1.000	0.905
4	0.047	0.039	0.232	0.185	0.131	-0.134	0.270	0.373
5	0.137	0.019	-0.863	0.804	-0.760	0.128	0.498	-0.200
6	0.911	0.325	-0.577	0.142	0.484	0.255	-0.638	0.675
7	1.000	0.372	0.675	0.205	-0.660	-0.316	-0.875	-0.847
8	0.164	-0.029	1.000	1.000	0.990	-0.150	0.664	0.411
9	0.139	-0.014	-0.849	0.797	-0.747	0.027	0.505	-0.284
10	0.886	-0.332	-0.566	0.124	0.409	-0.356	-0.533	0.455
11	0.999	-0.354	0.640	0.177	-0.554	0.416	-0.878	-0.922
12	0.158	-0.037	0.979	0.989	1.000	0.002	0.610	0.225
13	0.043	-0.012	-0.167	0.146	-0.126	-0.031	0.102	-0.087
14	0.821	-0.916	-0.313	-0.379	0.578	-0.844	0.606	-0.581
15	0.901	-0.998	0.445	-0.379	-0.707	1.000	0.965	1.000
16	0.039	-0.024	0.177	0.161	0.152	0.070	0.152	0.129

Table 4.7. Standard deviation for identified modal coordinates

Node #	Mode							
	1	2	3	4	5	6	7	8
1	0.019	0.016	0.040	0.033	0.038	0.021	0.048	0.035
2	0.283	0.156	0.113	0.084	0.337	0.200	0.293	0.260
3	0.052	0.000	0.069	0.035	0.044	0.032	0.000	0.039
4	0.027	0.058	0.037	0.026	0.042	0.034	0.089	0.087
5	0.105	0.089	0.205	0.199	0.285	0.057	0.221	0.097
6	0.301	0.104	0.167	0.066	0.197	0.088	0.242	0.280
7	0.084	0.080	0.081	0.054	0.061	0.045	0.084	0.052
8	0.032	0.061	0.000	0.000	0.029	0.029	0.051	0.027
9	0.128	0.078	0.205	0.175	0.294	0.040	0.212	0.121
10	0.293	0.082	0.139	0.061	0.165	0.108	0.225	0.190
11	0.000	0.069	0.054	0.048	0.040	0.031	0.051	0.025
12	0.038	0.046	0.030	0.025	0.000	0.031	0.066	0.051
13	0.036	0.033	0.039	0.037	0.049	0.017	0.048	0.038
14	0.261	0.168	0.087	0.083	0.242	0.245	0.215	0.249
15	0.064	0.047	0.082	0.042	0.044	0.000	0.094	0.000
16	0.012	0.016	0.010	0.009	0.006	0.010	0.021	0.020

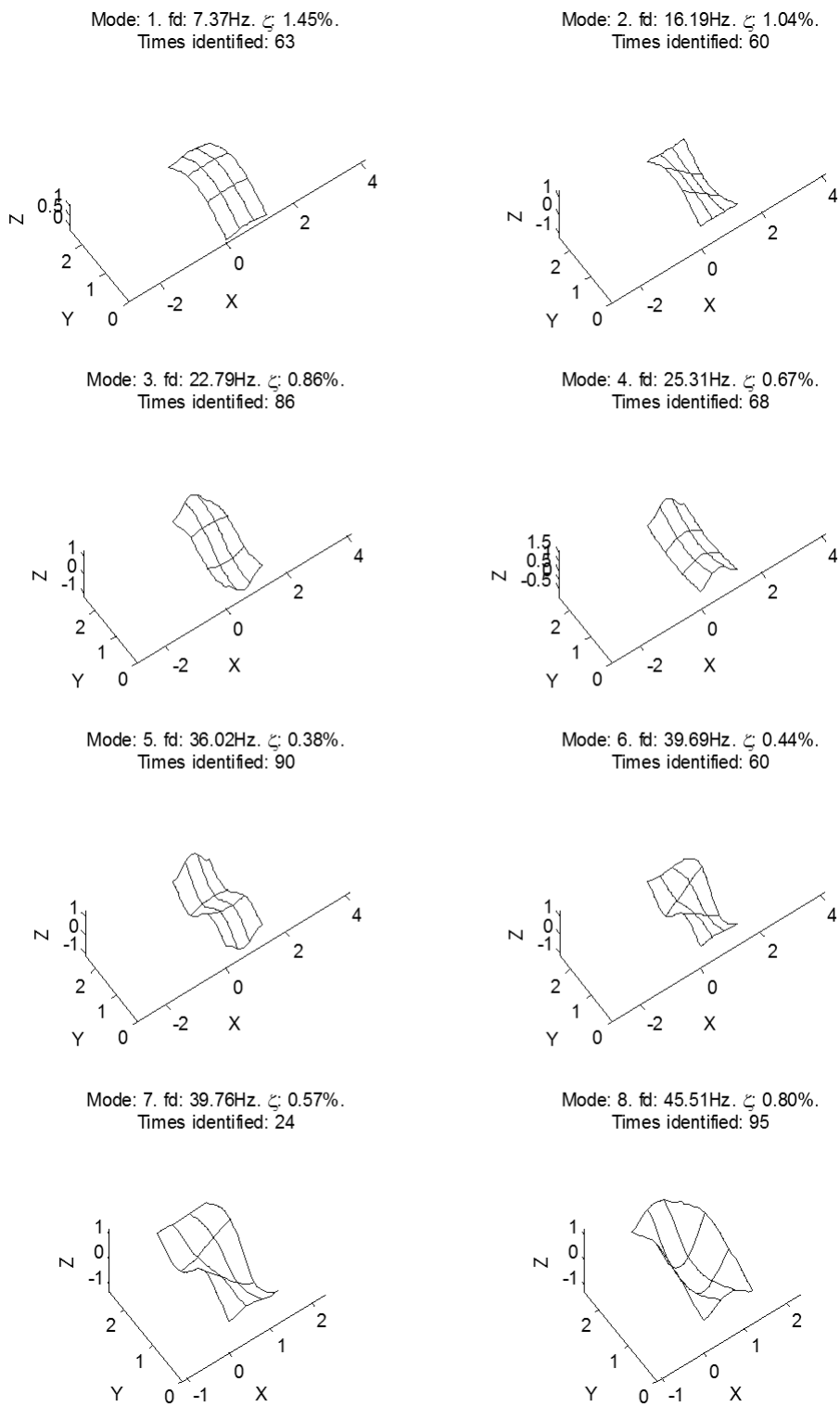

Figure 4.5. Identified modes (1st through 8th)

Mode: 9. fd: 45.75Hz. ζ 0.46%.
Times identified: 21

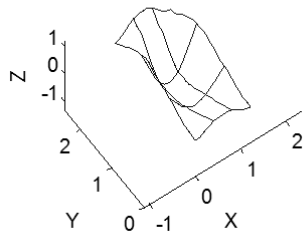

Mode: 10. fd: 65.88Hz. ζ 4.10%.
Times identified: 18

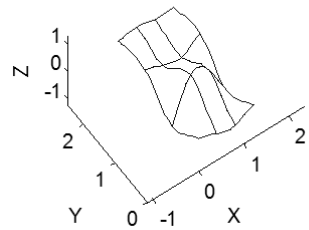

Mode: 11. fd: 66.44Hz. ζ 0.62%.
Times identified: 102

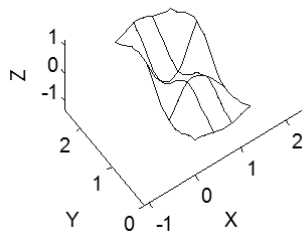

Mode: 12. fd: 79.36Hz. ζ 0.72%.
Times identified: 41

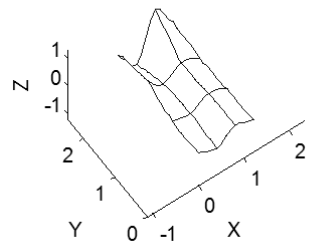

Mode: 13. fd: 80.76Hz. ζ 0.83%.
Times identified: 20

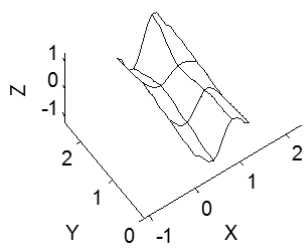

Mode: 14. fd: 83.44Hz. ζ 1.20%.
Times identified: 72

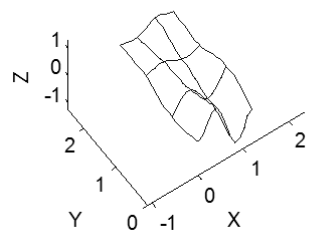

Mode: 15. fd: 85.68Hz. ζ 0.76%.
Times identified: 36

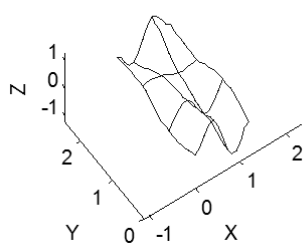

Mode: 16. fd: 95.80Hz. ζ 0.77%.
Times identified: 88

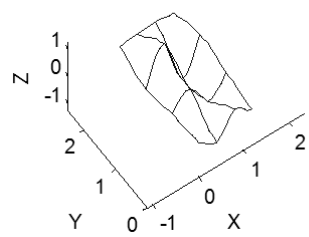

Figure 4.6. Identified modes (9th through 16th)

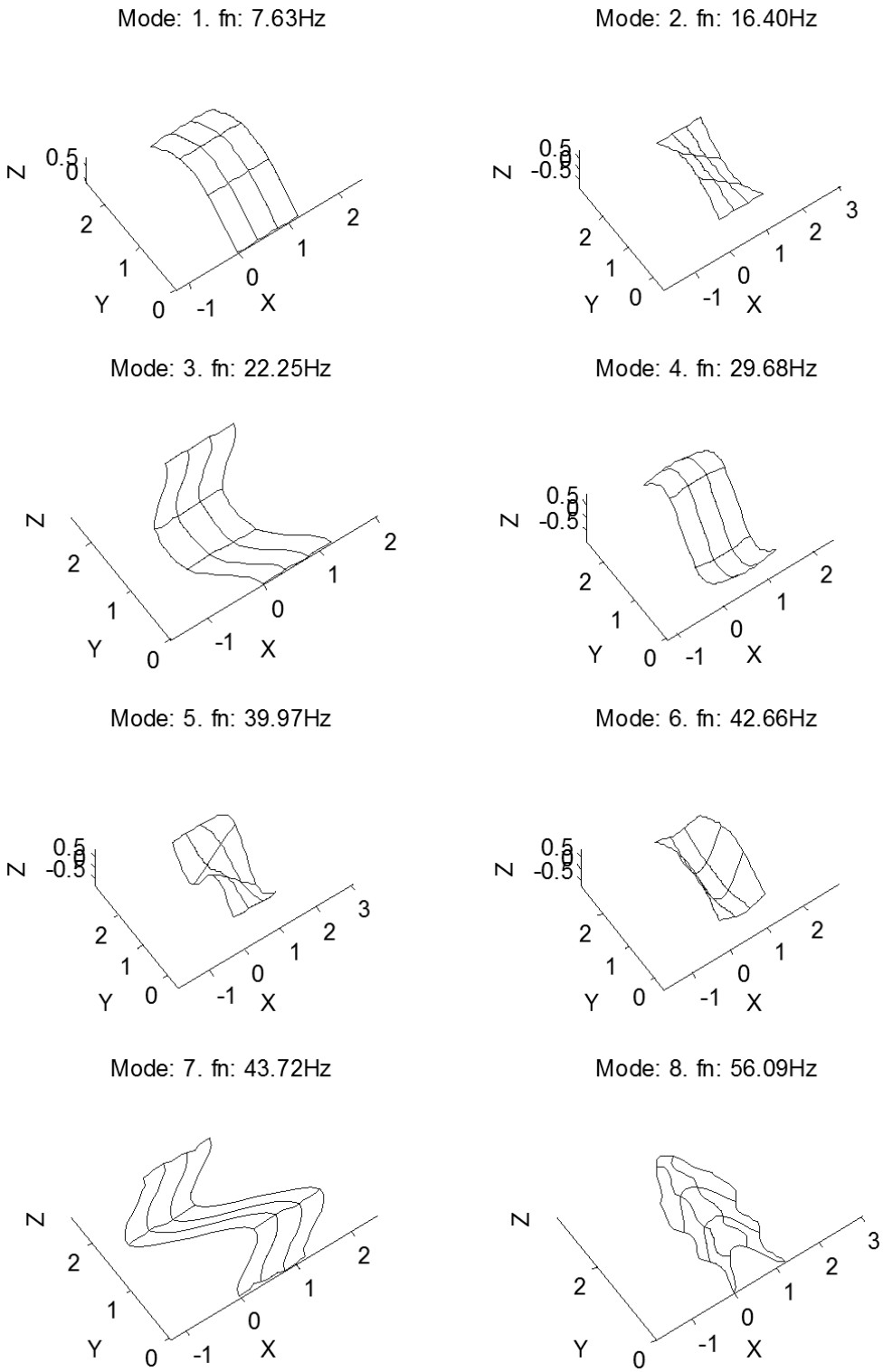

Figure 4.7. Numerical mode shapes (1st to 8th)

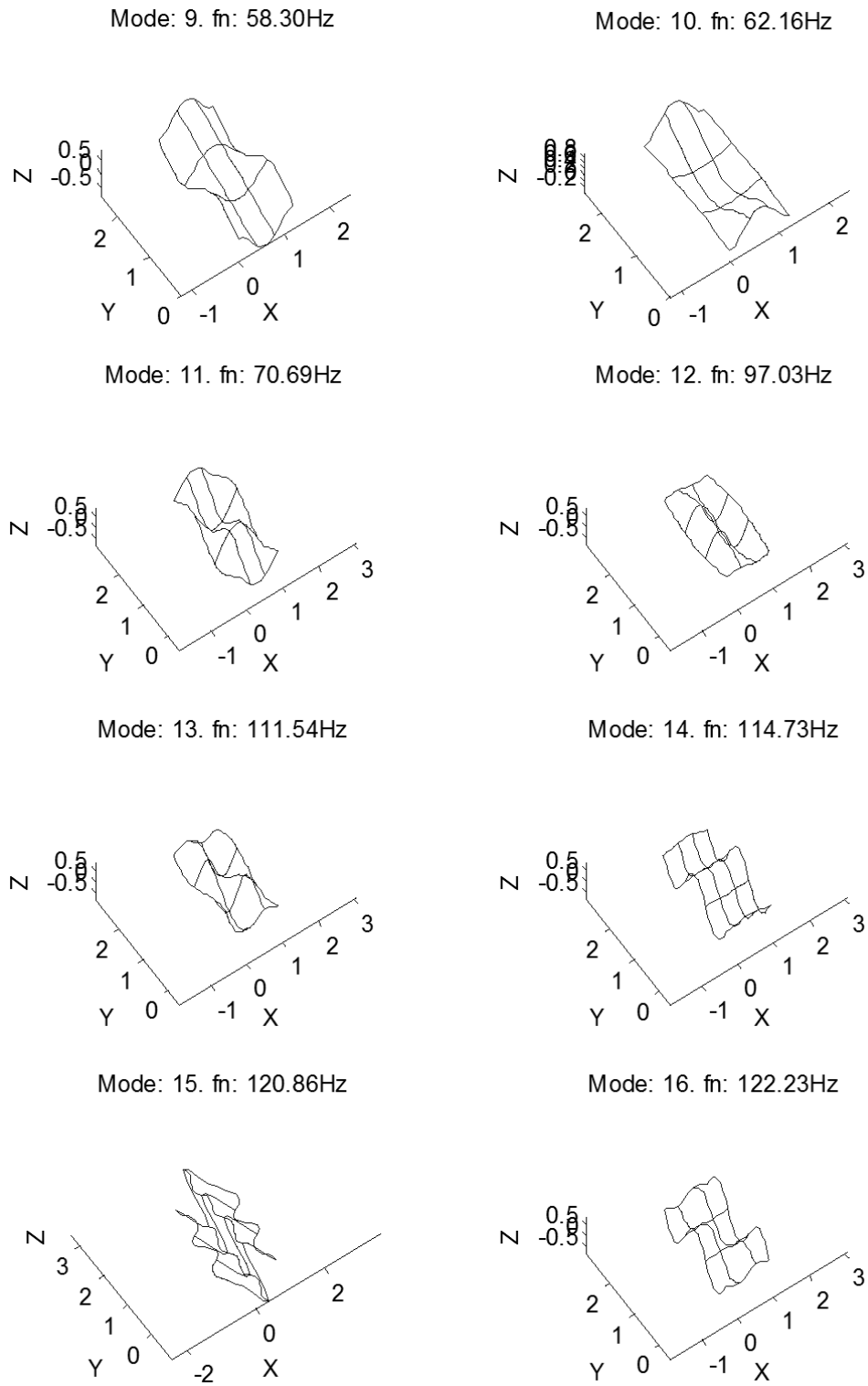

Figure 4.8. Numerical mode shapes (9th to 16th)

4.4. RAW MODEL COMPARISON

An initial numerical model using the information provided in 4.1 is created in Matlab. This model does a good job representing the experimental modes 1, 2, 6, and 8. The maximum error of the natural frequencies for these modes is 6.69% (4.44 Hz for mode 8) with a MAC value of 0.758 (lowest MAC value of the group). However, the numerical model does a poor job representing the other modes. This can be explained by modeling errors, for example in the supporting conditions (pinned in this case). Also, the values of the lumped masses at the nodes are uncertain. Table 4.8 shows a summary of the comparison between selected numerical modes and the reported identified modes.

Table 4.8. Error and MAC values between selected modes

Experimental		Numerical		Error in ω_n		MAC	Observation
ω_n (Hz)		ω_n (Hz)		Hz.	%		
1	7.370	1	7.634	0.264	3.58%	0.987	Exp. Mode reproduced
2	16.189	2	16.407	0.218	1.34%	0.998	Exp. Mode reproduced
3	22.794	3	22.272	-0.522	-2.29%	0.009	Horizontal Mode (Numerical)
3	22.794	4	29.726	6.932	30.41%	0.489	
4	25.314	4	29.726	4.411	17.43%	0.001	
5	36.019	5	40.066	4.047	11.24%	0.011	
6	39.714	5	40.066	0.352	0.89%	0.979	Exp. Mode reproduced
6	39.714	6	42.825	3.111	7.83%	0.001	
6	39.714	7	43.786	4.072	10.25%	0.001	Horizontal Mode (Numerical)
7	45.551	7	43.786	-1.766	-3.88%	0.614	Horizontal Mode (Numerical)
7	45.551	8	56.104	10.553	23.17%	0.103	Horizontal Mode (Numerical)
7	45.551	9	58.559	13.008	28.56%	0.004	
8	66.441	9	58.559	-7.882	-11.86%	0.126	
8	66.441	10	62.375	-4.067	-6.12%	0.006	
8	66.441	11	70.885	4.444	6.69%	0.758	Exp. Mode fairly reproduced
8	66.441	12	99.127	32.686	49.20%	0.006	

4.5. MODAL IDENTIFICATION WITH ADDED MASS

The performance of the updated model is investigated by changing the numerical model and the experimental structure and comparing their dynamic behavior. This

mimics the case of a retrofit analysis (for example). The test structure is changed by adding a lumped mass at one of its nodes. Three steel plates with dimensions 200mm x 200mm x 10mm weighting a total of 8.68±0.01 Kg are attached to node 6. The mass is securely attached such that it would not rattle on the structure and would not add any stiffness to the connection. The modal identification procedure described in the previous section is repeated in identical conditions.

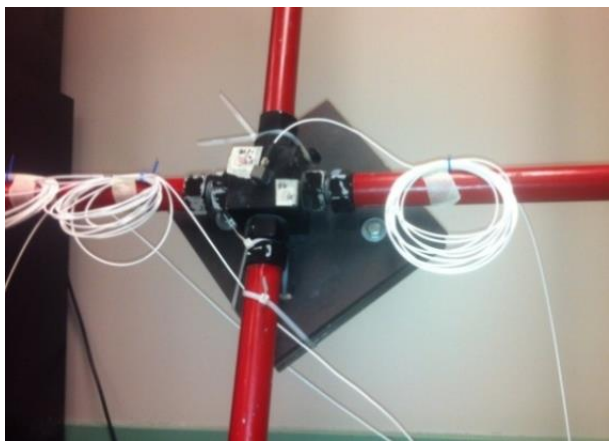

Figure 4.9. Attached mass of 8.68±0.01 Kg to node 6

Table 4.9. Natural frequencies and damping ratios of the modified system

#	fn [Hz]	σ_{fn} [Hz]	ζ %	σ_{ζ} [%]
1	6.78	0.03	1.23	0.55
2	16.11	0.19	1.16	0.48
3	21.63	0.09	0.58	0.22
4	25.16	0.10	0.52	0.11
5	34.66	0.08	0.33	0.23
6	39.22	0.08	0.39	0.13
7	42.92	0.12	0.49	0.42
8	61.15	0.14	0.58	0.17

Table 4.10. Experimental modal coordinates of modified system

Node #	Mode							
	1	2	3	4	5	6	7	8
1	0.038	-0.008	0.176	0.124	0.143	-0.043	0.100	0.048
2	1.085	-0.877	0.015	-0.512	-0.600	-0.365	1.000	1.000
3	0.970	-0.803	-0.709	-0.360	0.867	0.549	0.184	-0.705
4	0.044	0.002	-0.144	0.196	-0.086	0.112	0.103	-0.185
5	0.193	-0.041	1.000	0.787	0.971	-0.124	0.414	0.117
6	1.152	-0.336	0.583	0.108	-0.449	-0.197	-0.285	-0.472
7	1.000	-0.255	-0.653	0.205	0.460	0.091	-0.454	0.507
8	0.152	0.075	-0.621	0.996	-0.605	0.257	0.347	-0.256
9	0.223	-0.072	0.992	0.776	1.000	-0.011	0.406	0.281
10	1.115	0.389	0.607	0.056	-0.217	0.412	-0.319	-0.041
11	0.988	0.421	-0.523	0.197	0.259	-0.417	-0.312	0.608
12	0.145	0.060	-0.605	1.000	-0.639	0.160	0.347	-0.165
13	0.084	0.019	0.180	0.135	0.177	0.030	0.077	0.084
14	0.992	1.000	0.294	-0.477	-0.228	1.000	0.390	0.441
15	0.903	1.001	-0.348	-0.332	0.315	-0.729	0.464	-0.684
16	0.034	0.015	-0.114	0.165	-0.107	-0.017	0.081	-0.074

Table 4.11. Standard deviation of modal coordinates of the modified system

Node #	Mode							
	1	2	3	4	5	6	7	8
1	0.025	0.025	0.008	0.026	0.008	0.007	0.012	0.013
2	0.298	0.069	0.043	0.109	0.066	0.038	0.000	0.000
3	0.074	0.162	0.120	0.035	0.129	0.061	0.048	0.311
4	0.028	0.038	0.046	0.022	0.025	0.028	0.037	0.121
5	0.092	0.089	0.000	0.166	0.027	0.026	0.051	0.044
6	0.305	0.072	0.036	0.048	0.032	0.028	0.021	0.023
7	0.000	0.069	0.113	0.033	0.085	0.036	0.101	0.221
8	0.039	0.035	0.120	0.021	0.098	0.033	0.080	0.118
9	0.075	0.110	0.030	0.165	0.000	0.025	0.035	0.039
10	0.290	0.055	0.038	0.033	0.039	0.030	0.031	0.042
11	0.101	0.052	0.091	0.030	0.068	0.047	0.075	0.273
12	0.042	0.044	0.114	0.000	0.102	0.029	0.081	0.074
13	0.059	0.080	0.010	0.031	0.006	0.006	0.008	0.014
14	0.269	0.000	0.049	0.110	0.062	0.000	0.042	0.044
15	0.045	0.169	0.074	0.047	0.062	0.083	0.105	0.307
16	0.013	0.021	0.023	0.005	0.019	0.012	0.021	0.036

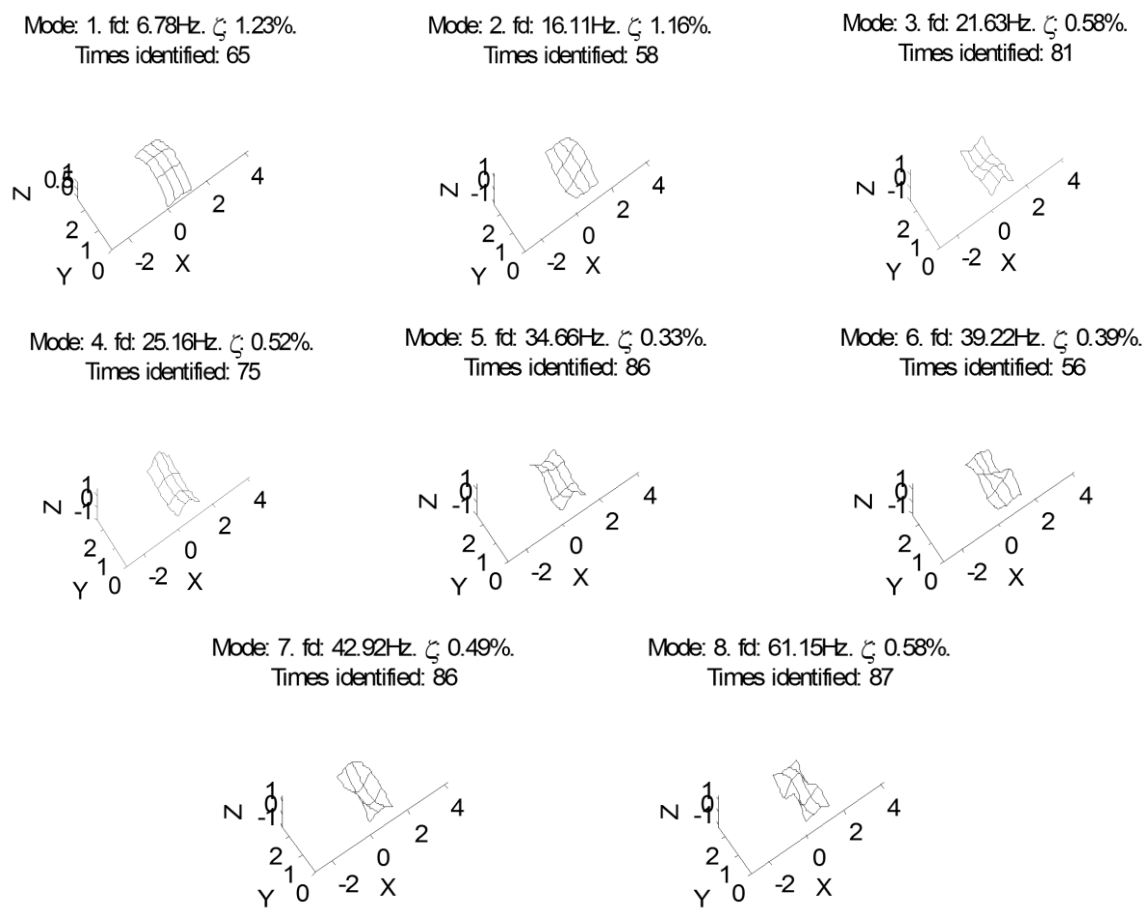

Figure 4.10. Identified modes for modified system

4.6. METRICS

Metrics are established to compare different model updating methodologies. The modal identification of the modified system performed in 4.5 reports 8 available natural frequencies and their modal shapes. The metrics proposed here intend to measure how well model updating solutions predict the 8 modal parameters of the modified system (modal parameters identified in 4.5) by measuring the error in natural frequencies, and the error of the mode shapes.

It is important to point here that regardless the methodology used for model updating, a criteria for matching experimental and numerical modes has to be defined. In this document, pairs of numerical/experimental modes are defined as those modes

matching with a maximum allowed error in natural frequencies (MaxErr) of 5Hz and minimum MAC values (MinMac) of at least 0.8. If the updating methodology disregards the modes outside these constrains, the metrics must be computed considering the values of MaxErr and MinMac for the unpaired modes. Under this definition, the error in natural frequencies and the error in mode shapes are measured as

$$err(fn)_k = \left| fn_i^{identified} - fn_j^{numerical} \right|$$

$$err(\phi)_k = 1 - MAC(\phi_i^{identified}, \phi_j^{numerical})_k$$

4.6.1. METRICS 1, 2 AND 3

Metrics 1, 2 and 3 will compare the computed error in natural frequencies. Metric #1 will measure the mean value, the metric #2 will measure the standard deviation, and the metric #3 will measure the skewness of such error. Mathematically, the metrics are expressed as:

$$M_1 = \mu(err(fn)_{1:8}) = \frac{1}{8}\sum_{k=1}^{8} err(fn)_k$$

$$M_2 = \sigma(err(fn)_{1:8}) = \sqrt{\frac{1}{8}\sum_{k=1}^{8} (err(fn)_k - M_1)^2}$$

$$M_3 = \gamma(err(fn)_{1:8}) = \frac{1}{8}\sum_{k=1}^{8} \left(\frac{err(fn)_k - M_1}{M_2}\right)^3$$

4.6.2. METRICS 4, 5 AND 6

Metrics 4, 5 and 6 will compare the computed error in mode shapes expressed in terms of MAC values. Similar with the previous, metric #4 will measure the mean value,

the metric #5 will measure the standard deviation, and the metric #6 will measure the skewness of such error. Mathematically, the metrics are expressed as:

$$M_4 = \mu(err(\phi)_{1:8}) = \frac{1}{8}\sum_{k=1}^{8} err(\phi)_k$$

$$M_5 = \sigma(err(\phi)_{1:8}) = \sqrt{\frac{1}{8}\sum_{k=1}^{8}(err(\phi)_k - M_4)^2}$$

$$M_6 = \gamma(err(\phi)_{1:8}) = \frac{1}{8}\sum_{k=1}^{8}\left(\frac{err(\phi)_k - M_4}{M_5}\right)^3$$

4.6.3. METRIC #7

The last proposed metric measures the number of unpaired modes (modes which do not fit within the constrains defined by MaxErr and MinMac). As closer to zero, this metrics expresses a better prediction of the modal parameters of the modified system:

$$M_7 = 8 - k, \;\; k \leq 8$$

In the previous, k expresses the number of modes matching the pairing constrains.

CHAPTER 5. APPLICATIONS

The proposed methodology in chapter 3 is verified in this chapter. Four numerical models are used to solve the benchmark problem described in chapter 4. The first case considers only 2 independent variables allowing visualization of the solution space. Cases 2, 3 and 4 use models with more variables. The family of models is considered to determine the probability of the models and each solution.

5.1. SOURCES OF UNCERTAINTY

The modal identification performed on the test structure (Chapter 4) shows dynamic characteristics that do not match those obtained with the raw numerical model. The differences between the model and the actual structure are due to assumptions made during the modeling of the structure. These assumptions can be modeling errors (e.g. assuming an Euler-Bernoulli model when a Timoshenko model is more appropriate) or incorrect value of parameters of the model. The numerical model described in chapter 4 considers a structure made of beam elements ideally connected at each node. The structure is shown in Figure 4.2 and is repeated in Figure 5.1 for convenience. In practice, these ideal connections do not exist, given that the tubular sections are connected by threaded bars, giving the connection finite stiffness. As a result, other modeling error are introduced: i) the underestimation of the effective length of elements, critical parameter given that this term is a common denominator in all terms of the stiffness matrix of beam elements, ii) underestimation of lumped mass at the nodes and iii) modeling of the

supports at nodes 1, 4, 13 and 16 which are modeled as pinned connections that allow rotation along the x-axis. In reality, the structure is connected to the supports with a 5/16" bolt to a ball bearing attached to a stiff plate. A stiff spring restraining the vertical and lateral deformations and a soft spring restraining rotations in the x-direction could be a better model.

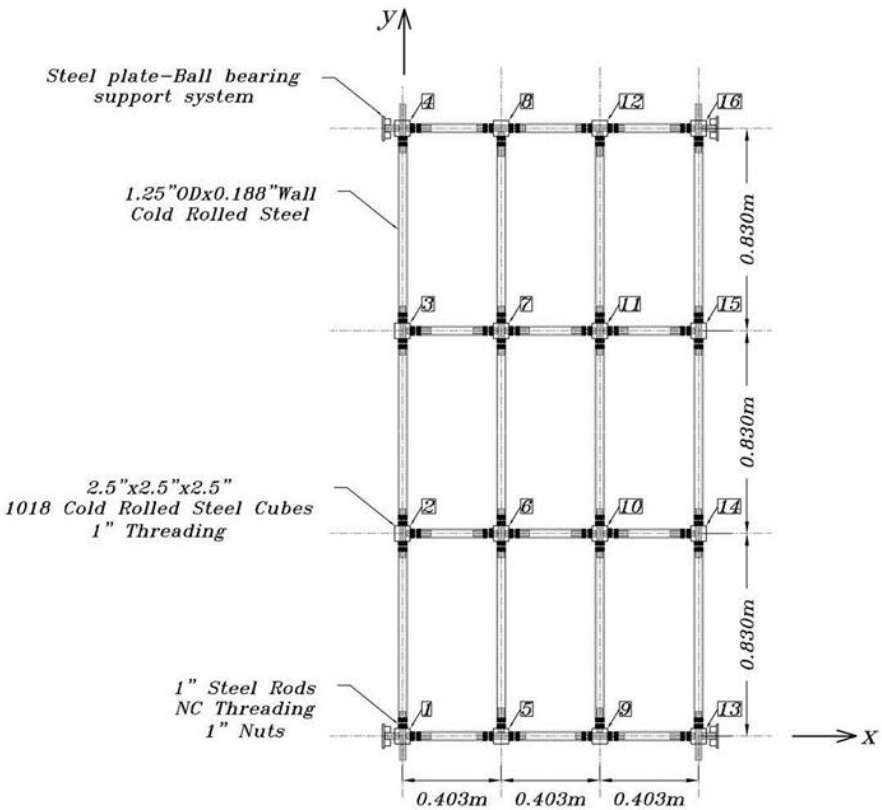

Figure 5.1. Test structure plan drawing

The physical dimension of the structure (Figure 5.1) can be used to estimate the initial values of the numerical model. The material is steel, whose Young Modulus is widely accepted in the literature as 29000ksi (199.9 MPa). Threaded bars with diameter 1" extend approximately 10cm beyond every node, and have an approximate moment of inertia $I_{xx} = I_{yy} = 20431\ mm^4$ ($EI=4084.3\ N*m^2$) and contribute an approximate mass of

3.13Kg to nodes with 3 connected elements and 3.59Kg to nodes with 4 connected elements (estimated threaded rod mass plus 2.5”x2.5”x2.5” steel cube connection). The effective length of the elements is taken as 0.403m and 0.830m for elements in the x-axis and y-axis respectively. The vertical and rotational stiffness of the supports is assumed to be 5% of the contributed stiffness at these degrees of freedom by the connected beam elements (78914 N/m and 2599 N/rad respectively). These estimations have a degree of uncertainty and their value is updated. Table 5.1 contains a summary of all the parameters considered and an original deterministic estimation. Not all parameters are considered in all models. For example, the model used for case #1 only uses parameters 3 and 4, while the model used in case #2 uses the parameters 2, 3, 4, 5, 7 and 8.

Table 5.1. Updating parameters for study cases

#	Parameter	Elements affected	Initial estimated value	Feasible Range
1	EI	24 beam elements	7724.1 N*m^2	[-50% +50%]
2	Lef, shorter elements	12 beam elements	0.403 m	[-50% +0%]
3	Lef, longer elements	12 beam elements	0.83 m	[-50% +0%]
4	kuz, supports vertical deformation stiffness	4 supporting nodes	78914 N/m	[-100% +5900%]
5	kθx, supports longitudinal rotation stiffness	4 supporting nodes	2599 N/rad	[-100% +900%]
6	kθy, supports transversal rotation stiffness	4 supporting nodes	4191 N/rad	[-100% +9900%]
7	lm3, lumped mass at 3-element connection	8 connections	3.13 kg	[-50% +50%]
8	lm4, lumped mass at 4-element connection	4 connections	3.59 kg	[-50% +50%]
9	EI, nodes crossed by threaded bar	16 nodes	7724.1 N*m^2	[-95% +50%]
10	EI, nodes not crossed by threaded bar, x-dir	16 nodes (16 th'd. bar-node connections)	7724.1 N*m^2	[-95% +50%]
11	EI, nodes not crossed by threaded bar, y-dir	16 nodes (4 th'd. bar-node connections)	7724.1 N*m^2	[-95% +50%]
12	EI, nodes not crossed by threaded bar, supports	4 nodes (Supporting nodes)	7724.1 N*m^2	[-95% +50%]

5.2. Finding Multiple Solutions

The posterior PDF, assuming that a feasible range of the parameters is known, is defined by the equation

$$P(\theta|D) = c * \exp\left(-\frac{1}{2}\sum_{j=1}^{n}\left|\frac{\omega_j^{id} - \omega_j^{fe}(\theta)}{\sigma_j^{\omega error}}\right|^2 - \frac{1}{2}\sum_{j=1}^{n}\sum_{i=1}^{m}\left|\frac{\phi_{j,i}^{id} - \phi_{j,i}^{fe}(\theta)}{\sigma_{j,i}^{\phi error}}\right|^2\right)$$

$$\theta_{lower} < \theta < \theta_{upper}$$

$$P(\theta|D) = 0 \quad \text{otherwise}$$

The calculation of P(θ|D) considers only vibration modes whose absolute difference with the experimental natural frequencies are not greater than 5Hz and whose MAC values are greater than 0.8. The output modal coordinates are mass normalized and reduced to a maximum number of 16 modal coordinates by using Guyan reduction, in order to be consistent with the available experimental data. The parameters θ are also normalized respect to their initial estimated value (Table 5.1) in such a way that parameters are unitless. The "raw" model state corresponds then to the position $\theta = \theta_o$ = [1 1 …. 1].

The search for solutions (as defined in section 3.3) is performed by using a modified Genetic Algorithm (HTMGA) specialized for the search of multiple solutions. HTMGA finds local and global maxima of P(θ|D). HTMGA is an optimization methodology modified and implemented as part of MUCogS by other members of the SDII research group (http://sdii.ce.sc.edu/htmga). This methodology is based on Genetic Algorithms, where random samples across the solution space simulate individuals whose chances for survival are determined by their fitness values.

5.3. CASE STUDY #1

Case study #1 considers a numerical model composed of 24 beam elements connected with 16 nodes, 16 lumped masses at the nodes and supports modeled as springs (rotation in x-direction and deformation in z-direction only). The two parameters to be updated are the stiffness of the modeled supports (k_{uz}, $k_{\theta x}$). This 2D case allows the visualization of $P(\theta|D)$ and $P(\theta|D,V_R)$. Figure 5.2 illustrates this numerical model.

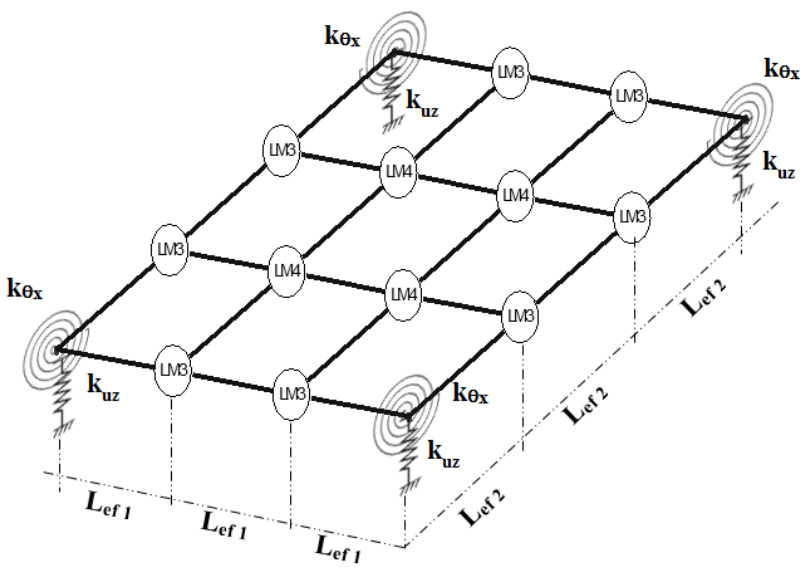

Figure 5.2. Numerical model for Case study #1

Table 5.2 shows the solutions found by HTMGA and the associated probabilities after integrating around each maxima:

Table 5.2. Model updating results for case study #1

#	$k_{uz}/(k_{uz})_o$	$k_{\theta x}$ / $(k_{\theta x})_o$	k_{uz} [N/m]	$k_{\theta x}$ [N/rad]	$P(S_i\|D,M_i)$
1	0.6	7.9	46148.4	20575.0	25.9%
2	20.0	19.9	1576878.8	51811.0	25.2%
3	0.6	4.7	49876.5	12180.6	12.8%
4	21.0	0.0	1658798.6	2.9	12.4%
5	4.1	0.2	321588.6	613.3	15.8%
6	9.0	20.0	709975.9	51901.9	4.9%
7	6.4	14.0	507625.1	36416.7	2.9%
8	57.9	13.7	4569782.8	35717.2	0.1%

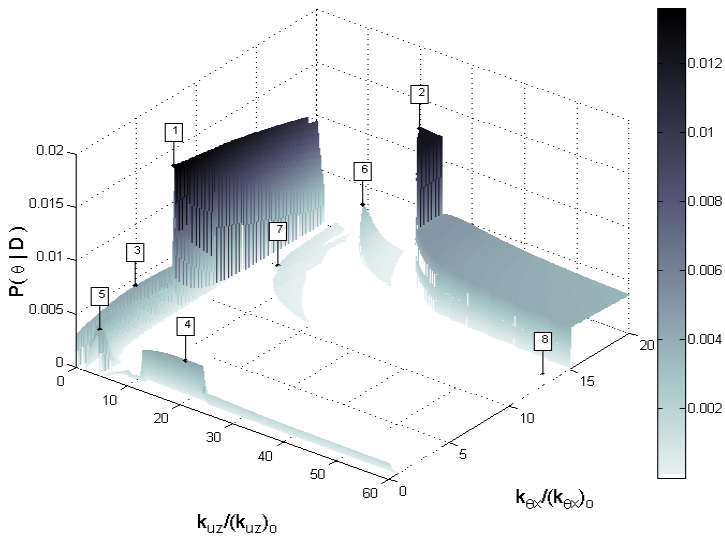

Figure 5.3. Posterior distribution for case study #1

Figure 5.3 presents the graphical representation of P(θ|D) and the location of the local maxima. The existence of multiple maxima indicates that different set of parameters can provide a numerical model that represents the structure. The top 2 solutions in Table 5.2 have very similar probability, being both physically different. Several solutions have low values of $k_{\theta x}$, some of them with the lower probability values, and some of those solutions make more physical sense given that the attached ball bearing to the support is expected to have little resistance to rotation. It is expected that the inclusion of the analyst's expertise using a prior PDF changes these probabilities associated with each solution. This is performed by the virtual response described in the following section.

5.3.1. VIRTUAL RESPONSE

The behavioral selection methodology presented in chapter 3 is used to help the analyst add additional information and better estimate the probability of each of the solutions found in Table 5.2. The numerical model for case study 1 considers springs to model the supported nodes and thus deformation on such nodes can be expected.

Therefore, the expected displacement and rotation due to a static force can be considered as a virtual experiment. The analyst believes that a 100N force applied at node 10 will cause a deformation of about 1mm based on prior experience with this structural system. Node 13 will deform approximately 5/100 mm. Therefore, the resulting rotation of node 13 is estimated as

$$\theta_{13} = \arctan((1-0.05)/830) = 0.066^{o} = 0.001 \text{ rad}$$

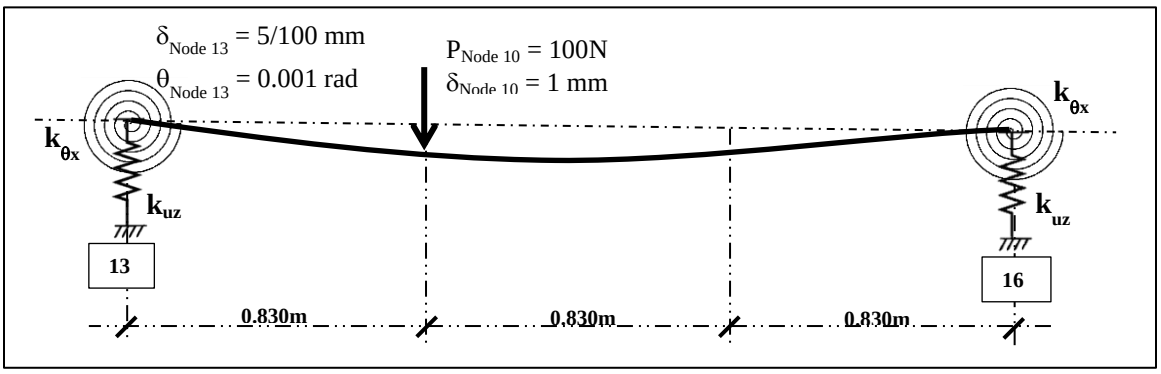

Figure 5.4. Virtual experiment: Expected deformation of node 13

Considering the estimated information as mean values of the virtual experiment, and assuming that the deformation of node 13 under the given load follows a normal distribution with standard deviations of 1/5000 of the mean values, a probability density distribution $P(z_{13},\theta_{13})$ expressing the analyst expertise can be obtained:

$$P(V_R) = \frac{1}{\sqrt{(2\pi)^2|\Sigma|}} \exp\left(-\frac{1}{2}(x-\mu)^T\Sigma^{-1}(x-\mu)\right)$$

The previous expression denotes the Multivariate Normal Distribution, where μ denotes the mean values for the deformations expected from the virtual experiment, and Σ denotes the covariance matrix of these deformations. In this case, the analyst dismisses any correlation between the variables, and expresses the covariance matrix in terms of the expected standard deviations mentioned in the previous paragraph.

The expression $P(V_R|\theta)$ is obtained as shown in chapter 3 and it is described by the equation

$$P(V_R|\theta) = \frac{1}{c_o} * \exp\left(-\frac{1}{2}\left|\frac{\delta_{10}^{VR} - \delta_{10}^{fem}(\theta)}{\sigma_{\delta 10}^{\omega error}}\right|^2 - \frac{1}{2}\left|\frac{\theta_{13}^{VR} - \theta_{13}^{fem}(\theta)}{\sigma_{\theta 13}^{\omega error}}\right|^2 \right)$$

$P(V_R|\theta)$ is shown in Figure 5.6, and the updated PDF $P(\theta|D,V_R)$ is shown in Figure 5.7:

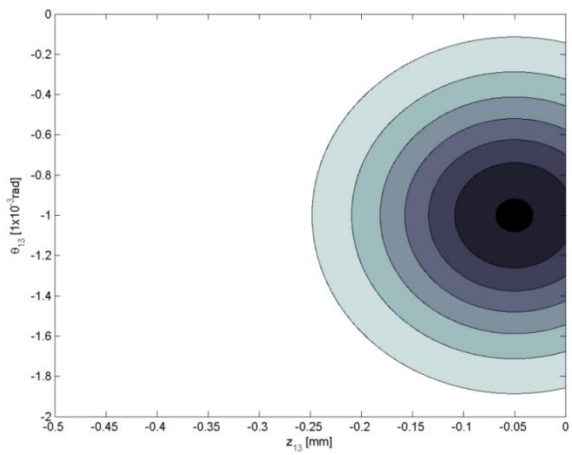

Figure 5.5. Analyst's virtual response, $P(V_R)$: expected nodal deformation at node 13, case study #1

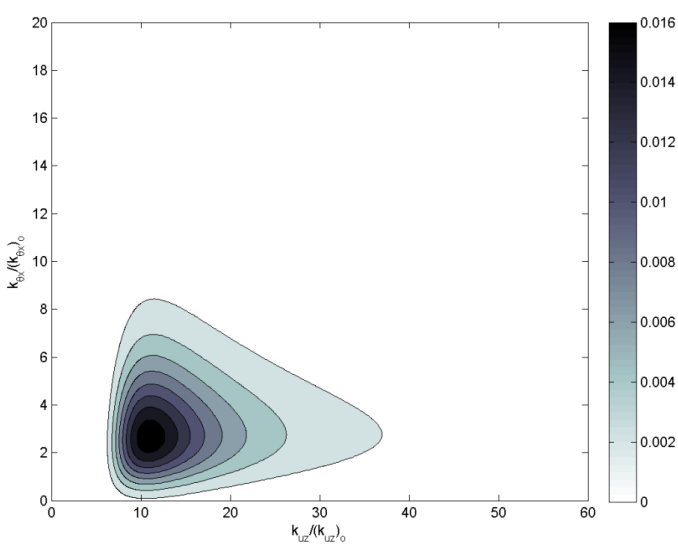

Figure 5.6. Analyst's virtual response $P(V_R|\theta{:}\{k_{uz},k_{\theta x}\})$ for case study #1

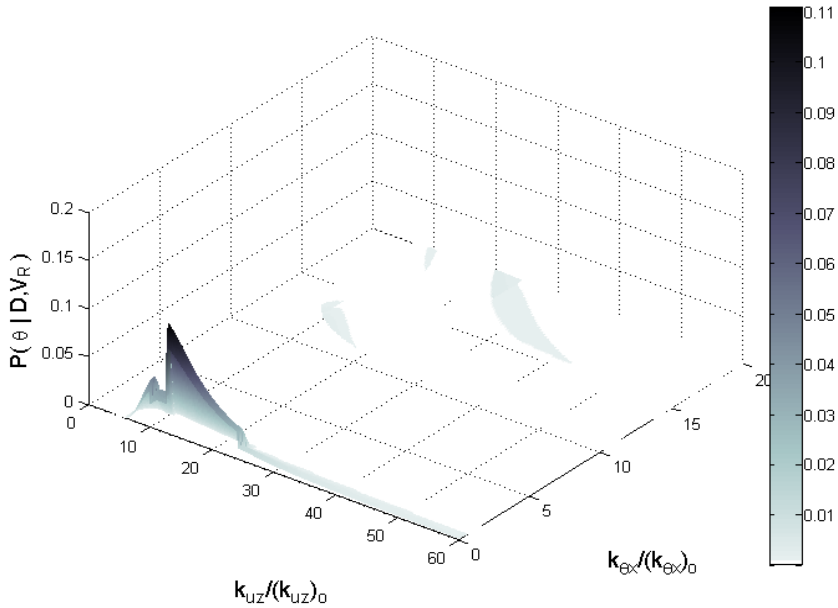

Figure 5.7. $P(\theta|D,V_R)$ for case study #1

Figure 5.7 shows that all 8 possible alternatives for the model updating problem have substantially changed their probability, all in favor of solution #4, as can be seen in Table 5.3:

Table 5.3. Updated probability for model updating solutions in 2D problem

#	$k_{uz}/(k_{uz})_o$	$k_{\theta x}$ / $(k_{\theta x})_o$	$P(S_i\|D,M_i)$	$P(S_i\|D,V_R,Mi)$
1	0.6	7.9	25.9%	0.0%
2	20.0	19.9	25.2%	3.2%
3	0.6	4.7	12.8%	0.0%
4	21.0	0.0	12.4%	94.7%
5	4.1	0.2	15.8%	0.1%
6	9.0	20.0	4.9%	1.0%
7	6.4	14.0	2.9%	0.9%
8	57.9	13.7	0.1%	0.0%

Case study #1 illustrates that including a virtual response can significantly change the probability of all possible solutions for the model updating problem. Solution #4 has the biggest probability change from $P(S_4|D,M_i)$ = 12.4% to $P(S_4|D,V_R,M_i)$ = 94.7% . Physically this might be the most meaningful solution, indicating a small (or no) stiffness

in the rotation about the x-axis, and a large stiffness in the displacement in the z-direction. This corresponds to having a pin-join at the supports. Also, it can be noticed that the solutions can be biased if the analyst does not pay particular attention to the estimation of the virtual response.

Table 5.4. Case study #1 metrics

S_i	m1	m2	m3	m4	m5	m6	m7
1	4.287	1.748	-2.184	0.188	0.023	-1.547	6
2	5.000	N/A	N/A	0.200	N/A	N/A	8
3	3.774	1.933	-1.018	0.183	0.030	-1.360	5
4	2.668	2.506	-0.029	0.135	0.086	-0.671	4
5	3.596	2.117	-0.904	0.147	0.084	-1.015	5
6	4.964	0.101	-2.268	0.179	0.060	-2.268	7
7	4.720	0.660	-2.126	0.156	0.082	-1.172	6
8	4.827	0.320	-1.171	0.157	0.080	-1.237	6

Table 5.3 shows that solutions 1 and 2 have the highest probability prior the inclusion of the analyst's expertise, but the metrics for this study case in Table 5.4 indicate that these solutions have a low performance predicting the changes of the modified system. Solution 1 can only match 2 modes with MAC values greater than 0.8 and average error in natural frequencies less than 5Hz (M_7 = 6). Solution 2 can't even pair one mode, making not available the computation of the metrics (M_7 = 8). Solution 4, having the highest probability after the inclusion of the analyst's expertise, has the best performance within the group of solutions with 4 modes matching within error constrains (M_7 = 4). Also, this solution has the lowest average errors in this group of solutions (M_1 = 2.668, M_4 = 0.135) agreeing with the analyst's expected behavior.

5.4. CASE STUDY #2

The previous case is extended to consider 6 parameters: one variable describing the effective length of the 12 beams in the x-direction (L_{ef1}), one variable describing the

effective length of the 12 beams in the y-direction (L_{ef2}), one variable for the lumped masses at the connections with 3 elements LM_3, one variable for the lumped masses of connections with 4 elements LM_4; and two variables describing the stiffness of the springs representing the supports of the structure (k_{uz}, $k_{\theta x}$), as shown in Figure 5.2 (Parameters 2, 3, 4, 5, 7 and 8 from Table 5.1) and repeated here for convenience.

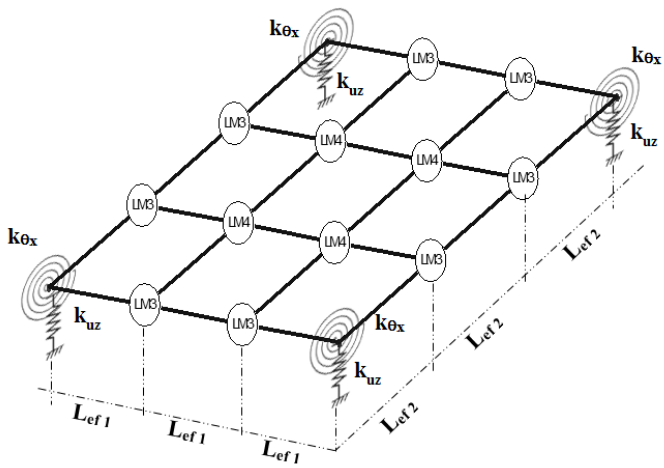

Figure 5.8. Numerical model for Case study #2

The probability distributions $P(\theta|D)$, $P(V_R|\theta)$ and $P(\theta|D,V_R)$ are recalculated using these 6 parameters and the virtual response described in section 5.3.1. HTMGA is used for the search of points of maximum probability density in $P(\theta|D)$. The solutions obtained from HTMGA and their respective probabilities are shown in Table 5.5.

Table 5.5. Case study #2 solutions

S_i	$P(S_i\|D)$	$P(S_i\|D,V_R)$	$L_{ef1}/(L_{ef1})_o$	$L_{ef2}/(L_{ef2})_o$	$k_{uz}/(k_{uz})_o$	$k_{\theta x}/(k_{\theta x})_o$	$LM_3/(LM_3)_o$	$LM_4/(LM_4)_o$
1	3.2%	0.0%	0.895	1.000	0.380	0.191	1.497	0.720
2	2.3%	0.0%	0.895	0.998	0.327	0.020	1.479	0.889
3	14.4%	0.8%	0.810	0.941	3.389	0.087	1.484	1.156
4	41.7%	80.2%	0.675	0.951	3.308	0.169	1.429	1.091
5	31.7%	3.0%	0.992	0.753	11.561	8.068	1.405	1.409
6	3.8%	14.7%	0.996	0.983	37.308	9.463	0.673	0.971
7	0.7%	1.3%	0.994	0.868	8.071	7.897	1.468	0.550
8	2.3%	0.0%	0.911	0.975	1.465	6.642	1.317	1.494
9	0.0%	0.0%	0.937	0.981	0.652	5.198	1.319	1.252

Table 5.5 shows the probability associated with every solution, and Table 5.6 shows the actual values for the updating parameters. Prior to the inclusion of the analyst's expertise, solutions 4 and 5 had the biggest probabilities within the family of solutions, with 41.7% and 31.7% respectively. The probability of solution 4 increases to 80.2% after including the virtual response. The probability of solution 5 decreased to 3.0%. Clearly, the inclusion of the analyst's expertise in terms of a probability distribution $P(\theta|V_R)$ has substantially changed the probability of the solutions.

Table 5.6. Parameters' actual values for case study #2 solutions

S_i	L_{ef1} [m]	L_{ef2} [m]	k_{uz} [N/m]	$k_{\theta x}$ [N/rad]	LM_3 [Kg]	LM_4 [Kg]
1	0.361	0.830	29952.6	496.7	4.693	2.588
2	0.361	0.829	25798.1	52.2	4.636	3.196
3	0.326	0.781	267427.8	225.4	4.651	4.154
4	0.272	0.789	261031.4	438.5	4.477	3.919
5	0.400	0.625	912362.1	20963.9	4.404	5.064
6	0.401	0.816	2944107.8	24590.3	2.111	3.487
7	0.401	0.721	636902.5	20519.5	4.600	1.976
8	0.367	0.810	115619.7	17258.5	4.129	5.368
9	0.378	0.814	51440.0	13506.8	4.134	4.499

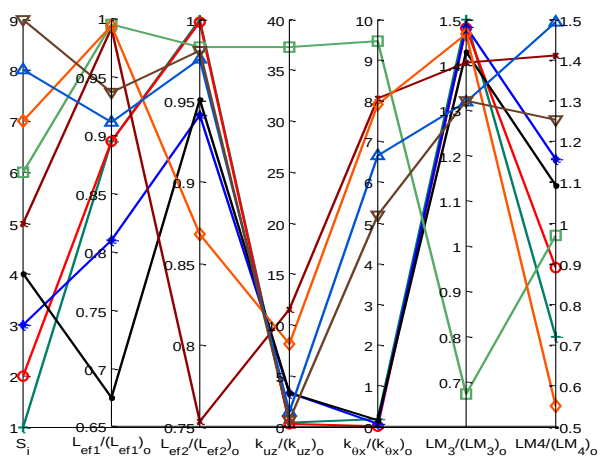

Figure 5.9. Case study #2 - Parallel plot

Arguably, solution 4 is more physically meaningful than the other solutions. The rotational stiffness at the supports is low, which is expected due to the bearings used at

the support plates. Also, the vertical stiffness at the supports is higher than other solutions (solutions 1, 2 and 9), which is expected because of the plates used for the supports. In addition, the effective length of the elements changes according to the length of the elements. The rods on the connections are expected to have a greater effect on the short elements since a greater portion of the element is used for the connection. Therefore the effective length is expected to change more in the short elements. This is exactly what solution 4 indicates.

Table 5.7. Case study #2 metrics

S_i	m1	m2	m3	m4	m5	m6	m7
1	4.059	1.852	-1.522	0.182	0.046	-2.238	6
2	4.386	1.736	-2.268	0.183	0.047	-2.268	7
3	4.393	1.718	-2.268	0.176	0.067	-2.268	7
4	4.392	1.721	-2.268	0.176	0.067	-2.268	7
5*	5.000	N/A	N/A	0.200	N/A	N/A	8
6	4.946	0.101	-1.311	0.152	0.088	-1.156	6
7	4.626	0.949	-2.220	0.154	0.084	-1.168	6
8	3.935	1.942	-1.185	0.170	0.047	-0.976	5
9	3.727	1.990	-1.032	0.183	0.032	-1.378	5

The metrics in Table 5.7 show how each solution tracks the case when additional mass has been added to the structure. This is a significant example because models that have been updated and have physically meaningful parameters are expected to perform better in the prediction of the behavior of the structure with the additional mass. Solution 8 has the best prediction of the model with an average error of M_1 = 3.93 for the natural frequencies and M_4 = 0.17 for the mode shapes. Solution 4 ($P(\Theta|D, V_R)$ = 80.2%) can be considered the second solution with best performance with a good balance between the error of the natural frequencies (M_1 = 4.39) and mode shapes (M_4 = 0.176) compared with the other solutions. Solution #5 ($P(\Theta|D)$ = 31.7%) shows an incapability of

predicting the modal parameters of the modified system (M_7 = 8). After the inclusion of the virtual response the probability of solution 5 drops to 3%, as expected by the analyst.

5.5. CASE STUDY #3

The third numerical model considers bar elements of length 10cm interconnecting the cylindrical sections and the nodes (Figure 5.10). The model consists of 76 beam elements, 52 of which represent the connecting threaded bars and 24 beam elements representing the cylindrical sections. The supports are no longer modeled as springs but as pinned nodes. The values of the lumped masses at the nodes are considered deterministic and no updating is performed on these parameters. Three updating parameters are selected for updating: i) contributed flexural stiffness EI from bars connected at supporting nodes (elements 1 through 12), ii) contributed flexural stiffness EI from bars connected at 3-element intersections (elements 13 through 36) and iii) contributed flexural stiffness EI from bars connected at 4-element intersections (elements 37 through 52). The probability distributions $P(\theta|D)$, $P(V_R|\theta)$ and $P(\theta|D,V_R)$ are setup in terms of the selected 3 updating parameters. The HTMGA optimization technique is used to search for model updating to the study case #3 model updating problem.

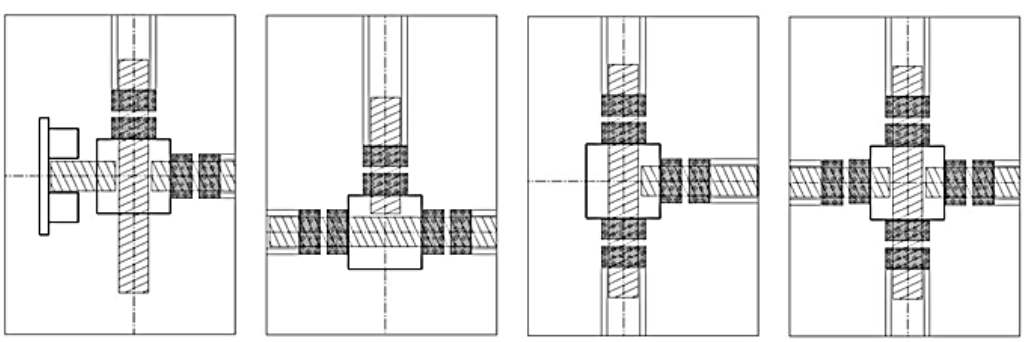

a. Connection at corner | b. 3-Element connection (x-dir) | c. 3-Element connection (y-dir) | d. 4-Element connection

Figure 5.10. Types of connections considered in case study #3

Table 5.8. Solutions for case study #3

#	$P(S_i\|D)$	$P(S_i\|D,V_R)$	$EI_2/(EI_2)_o$	$EI_3/(EI_3)_o$	$EI_4/(EI_4)_o$
1	81.4%	84.2%	0.465	0.179	0.825
2	10.4%	6.7%	0.804	0.420	0.449
3	2.2%	3.8%	1.480	0.980	0.142
4	4.6%	4.0%	0.354	0.424	0.484
5	1.3%	1.1%	1.267	0.295	0.618
6	0.1%	0.0%	1.477	0.429	0.354
7	0.1%	0.3%	0.078	0.090	1.464

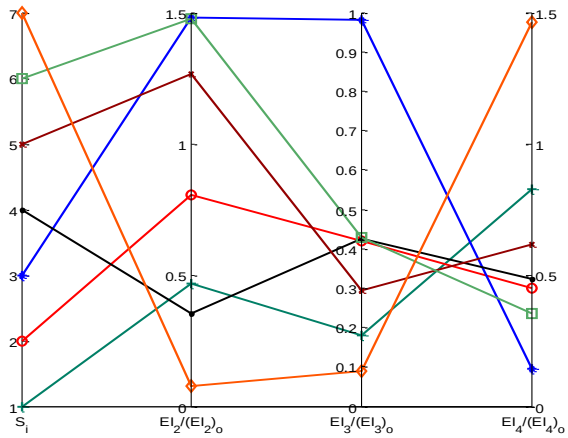

Figure 5.11. Case study #3 solutions - Parallel plot

Table 5.8 shows the solutions to the case study #3 and the associated probabilities, and Table 5.9 shows the actual values for the updating parameters. Table 5.8 shows that solution #1 has a probability of 81% and the inclusion of the analyst's expertise increased the probability to 84.2%. The solution shows that the estimated flexural stiffness of the nodes is higher than the actual values (all parameters are smaller than 1 in Table 5.8). This can be expected given that in all nodes only one bar can cross the node while the other connecting bars are interrupted (Figure 5.10). This condition lets the node to rotate more than it would do it the connection were continuous and thus, makes sense to expect less contributed stiffness from the interrupted bars.

Table 5.9. Parameters' actual values for case study #3 solutions

#	EI_2 [N*m^2]	EI_3 [N*m^2]	EI_4 [N*m^2]
1	3593.4	1386.2	6370.8
2	6206.8	3242.6	3466.2
3	11429.3	7569.3	1099.1
4	2731.4	3277.5	3738.3
5	9788.6	2278.3	4773.7
6	11409.4	3311.6	2735.0
7	603.3	695.8	11306.4

Table 5.10. Metrics for case study #3

S_i	m1	m2	m3	m4	m5	m6	m7
1	3.759	2.298	-1.155	0.155	0.083	-1.173	6
2	3.981	1.931	-1.303	0.155	0.083	-1.163	6
3	4.379	1.626	-2.245	0.161	0.074	-1.292	6
4	2.642	2.133	0.140	0.141	0.078	-0.978	3
5	4.005	1.917	-1.405	0.155	0.083	-1.162	6
6	4.122	1.734	-1.539	0.156	0.082	-1.164	6
7	3.240	2.250	-0.514	0.136	0.076	-0.497	4

The metrics presented in Table 5.10 show how study case #3 performs predicting the behavior of the modified system. For this case, solutions 4 and 7 have the best performance showing an average error in natural frequencies M_1=2.642 and 3.240 respectively, an average error in mode shapes M_4 = 0.141 and 0.136 respectively, and a number of unmatched modes M_7 = 3 and 4 respectively. The solution with highest probability shows M_1 = 3.759 and M_4 = 0.155. This shows that, although these solutions performs very well, the virtual response introduced by the analyst filtered proposed that solution #1 had a better physical sense that the other ones. Solution 7 shows parameters values close to zero, while solution 4 shows that stiffness at the nodes with 3 and 4 connections have a similar stiffness, which might not be true, as shown in the histograms in the annexed chapter (Figure A.19 through Figure A.24) where the histograms for solution #1 show to make better distribution around the experimental values.

5.6. CASE STUDY #4

Case study #4 is derived from case study #3. Here, 4 different types of connections (Figure 5.10) are considered: parameter 1 considers the stiffness EI contributed for the elements to the nodes at the supports, parameters 2 and 3 consider the stiffness EI contributed to the nodes connecting 3 elements in the x-direction and y-direction respectively, and parameter 4 considers the contributed stiffness EI to the nodes connecting 4 elements (parameters 9 through 12 from Table 5.1). This selection of parameters attempts to correct errors by unknown parameters as shown in case study #3. $P(\theta|D)$, $P(V_R|\theta)$ and $P(\theta|D,V_R)$ are recalculated in terms of the selected 4 updating parameters, and the updating solutions found with HTMGA are shown in Table 5.11:

Table 5.11. Solutions for case study #4

#	$P(\theta\|D)$	$P(\theta\|D,V_R)$	$EI_1/(EI_1)_o$	$EI_2/(EI_2)_o$	$EI_3/(EI_3)_o$	$EI_4/(EI_4)_o$
1	44.1%	45.0%	1.499	0.108	0.055	0.464
2	17.2%	16.5%	0.839	0.624	0.136	0.447
3	20.0%	19.4%	1.098	0.610	0.207	0.453
4	17.3%	15.7%	1.009	0.577	0.819	0.441
5	1.0%	2.3%	1.312	1.498	1.442	0.535
6	0.3%	0.9%	0.501	1.492	1.488	0.553
7	0.1%	0.1%	0.219	0.054	0.465	0.455

The solutions to case study #4 in Table 5.11 show solution 1 with probability of 45% and solutions 2, 3 and 4 with probability values of 16.5%, 19.4% and 15.7%. By considering again that in all nodes only one bar can cross the node while the other connecting bars are interrupted (Figure 5.10) letting the nodes to rotate more than it would do it with a connection in both directions, the contributed stiffness to the nodes should be smaller than the estimated values in all parameters. Solution 1 shows 3 parameters with values smaller to 1, while the remaining parameter is higher than 1. This

might show that this solution is not making a good physical meaning, opposite to what solution #2 shows, where all parameter values are smaller to 1 and consistent with the observed in case study #3.

Table 5.12. Parameters' actual values for case study #3 solutions

#	EI_1 [N*m^2]	EI_2 [N*m^2]	EI_3 [N*m^2]	EI_4 [N*m^2]
1	11578.1	832.3	422.5	3581.1
2	6482.0	4820.2	1048.1	3451.8
3	8484.9	4709.8	1599.3	3496.5
4	7797.3	4455.3	6329.2	3407.5
5	10136.5	11572.1	11139.4	4133.7
6	3867.5	11526.8	11492.3	4273.6
7	1692.4	415.9	3595.3	3516.1

Table 5.13. Metrics for case study #4

S_i	m1	m2	m3	m4	m5	m6	m7
1	3.756	2.303	-1.155	0.156	0.081	-1.178	6
2	3.973	1.949	-1.314	0.155	0.083	-1.163	6
3	3.975	1.951	-1.333	0.155	0.083	-1.163	6
4	3.983	1.933	-1.324	0.155	0.083	-1.163	6
5	4.419	1.615	-2.267	0.155	0.083	-1.160	6
6	4.426	1.596	-2.267	0.155	0.083	-1.162	6
7	3.826	2.173	-1.156	0.157	0.080	-1.218	6

Metrics 1 through 7 shown in Table 5.13 show that although all solutions have a similar performance, solution #1 having the highest probability (45%) has the metrics with better values among all solutions. It can be noticed that in this problem solutions 1 to 4 have significant values of probability (45%, 16.5%, 19.4% and 15.7%), and the metrics 1 to 4 have also significant values when compared with all solutions. The virtual response has improved the probability of the solution #1 which makes the best physical sense as noticed in the annexed figures (Figure A.25 through Figure A.30).

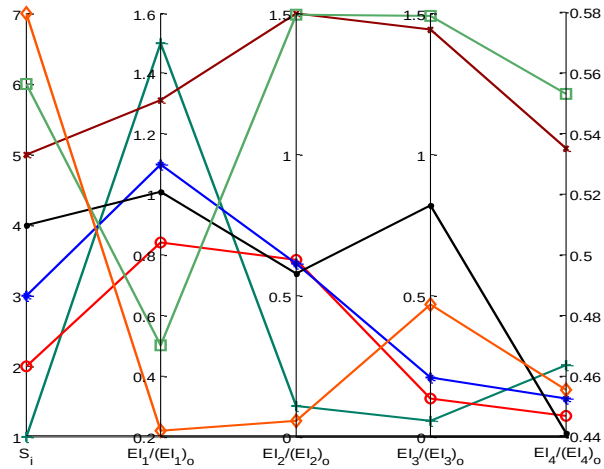

Figure 5.12. Case study #4 solutions - Parallel plot

5.7. Solution Selection Using a Family of Models

Cases #2, #3 and #4 considered different parameters. Therefore, it is possible to compare each of the solutions found considering the complete family of models. According to the expression presented in 0, a family of models can be compared using the expression

$$\frac{P(M_i|D,V_R,\boldsymbol{M})}{P(M_j|D,V_R,\boldsymbol{M})}=\frac{P(V_R|\,M_i,\boldsymbol{M})P(D|\,M_i,\boldsymbol{M})P(M_i|\boldsymbol{M})}{P(V_R|\,M_j,\boldsymbol{M})P(D|\,M_j,\boldsymbol{M})P(M_j|\boldsymbol{M})}$$

The normalization constants for $P(\theta|D)$ and $P(\theta|D,V_R)$ are required for every case study as discussed in section 3.4. A numerical integration is required to estimate each of these constants. Monte-Carlo integration (Robert, Casella et al. 1999) is used for the estimation of such constants. The technique computes integral of the function $f(\theta)$ as

$$I=\int_{\Omega} f(\bar{\theta})d\bar{\theta}$$

Given that I is a definite integral, the volume enclosing $f(\bar{\theta})$ can be mathematically written as

$$V = \int_{\Omega} d\bar{\theta}$$

where $[\bar{\theta}_1, \bar{\theta}_2, \bar{\theta}_3, \ldots, \bar{\theta}_N] \in \Omega$ represent uniform samples taken from the known volume V. The integral I can be approximated as

$$I \approx Q_N = V \frac{1}{N} \sum_{i=1}^{N} f(\bar{\theta}_i)$$

The previous expression is true based on the law of large numbers. This means that as bigger the sample size N chosen, the closest to the actual value of the integral:

$$\lim_{N \to \infty} Q_N = I$$

The error in the computation of I can be measured in terms of the standard deviation of Q_N as

$$\sigma(Q_N) = \frac{V}{\sqrt{N}} \sigma(f(\bar{\theta}))$$

$\sigma(Q_N)$ shows that the standard deviation of the approximation of the integral is bounded by number of samples used, and tends to be zero as N tends to infinity. Given that obtaining a value for $\sigma(Q_N)$ close to zero is computationally expensive, the integral values for $P(\theta|D)$ and $P(\theta|D,V_R)$ are calculated by taking enough uniform samples to obtain a ratio $\sigma(Q_N)/Q_N$ less than 2%.

Table 5.14 shows how the inclusion of the virtual response has significant effect on the probability of the models. Case study 6D has the highest probability and therefore seems to be the most "correct" of all of them prior to the inclusion of the virtual response. After the inclusion of the analyst's expertise, the probability of all models substantially changes making the cases 3D and 4D the models with the highest chances to be the correct model, being case study #3 the one with highest probability (52.0%).

Table 5.14. Normalization constants

		Study Case		
		#2	**#3**	**#4**
	# Samples	18757494	22901043	7242500
$P(\theta\|D)$	**Q_N**	0.0577	0.0024	0.0025
	$\sigma(f(\theta))$	0.9463	0.0196	0.0212
	$\sigma(Q_N)$	0.0002	0.0000	0.0000
	$\sigma(Q_N)/Q_N$	0.0038	0.0017	0.0031
	Q_N Ratios	0.9214	0.0381	0.0405
$P(\theta\|D,V_R)$	**Q_N**	0.0244	0.1437	0.1084
	$\sigma(Q_N)$	0.0003	0.0002	0.0003
	$\sigma(Q_N)/Q_N$	0.012	0.002	0.003
	Q_N Ratios	0.0882	0.5198	0.3919

It's important to notice the different type of modeling errors addressed by each model. Case #2 considers errors in lumped masses, effective length of elements and stiffness of supports, while cases #3 and #4 address uncertainty in flexural stiffness EI at the connections. The inclusion of the virtual response tells that cases #3 and #4 make a better reduction of uncertainty, reflected in the higher probability for these models.

Table 5.15. Family of models comparison

Study Case #2		
S_i	**$P(S_i\|D,M)$**	**$P(S_i\|D,V_R,M)$**
1	2.9%	0.0%
2	2.1%	0.0%
3	13.3%	0.1%
4	38.5%	7.1%
5	29.2%	0.3%
6	3.5%	1.3%
7	0.6%	0.1%
8	2.1%	0.0%
9	0.0%	0.0%

Study Case #3		
S_i	**$P(S_i\|D,M)$**	**$P(S_i\|D,V_R,M)$**
1	3.1%	43.8%
2	0.4%	3.5%
3	0.1%	2.0%
4	0.2%	2.1%
5	0.0%	0.6%
6	0.0%	0.0%
7	0.0%	0.1%

Study Case #4		
S_i	**$P(S_i\|D,M)$**	**$P(S_i\|D,V_R,M)$**
1	1.8%	17.6%
2	0.7%	6.5%
3	0.8%	7.6%
4	0.7%	6.2%
5	0.0%	0.9%
6	0.0%	0.4%
7	0.0%	0.1%

Table 5.15 compares how the probabilities of all solutions changes prior and after the inclusion of the virtual response. If the analyst has equal degree of belief on each model, i.e., $P(M_i) = 1/3$ for each model M_i, the solution #1 from study case #3 (3D

problem) has the highest probability (43.8%) among all available solutions. This was not the case prior to the inclusion of the virtual response, where the solution with highest probability is solution #3 from study case #2 (6D problem). The probability associated to each solution reflects their physical meaning and solutions can be selected based on this criterion.

The performance of the updated models is evaluated by taking the solutions with highest probability from each study case. The solutions are sampled using the Gibbs Sampling methodology and the samples are used to simulate the behavior of the modified system (Test structure with added mass of 8.68kg). Histograms of natural frequencies and MAC values for vibration modes 1, 2 and 3 evaluate the prediction capabilities of each solution.

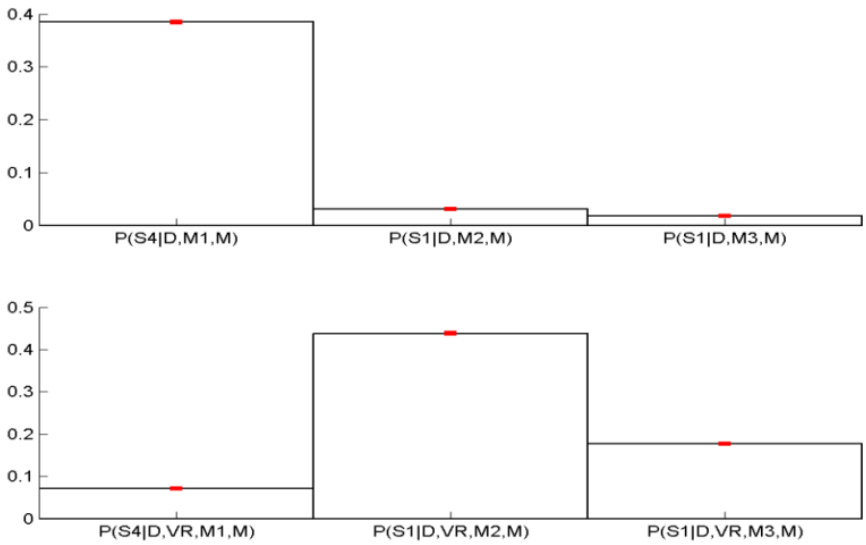

Figure 5.13. Probabilities for solutions with highest probabilities

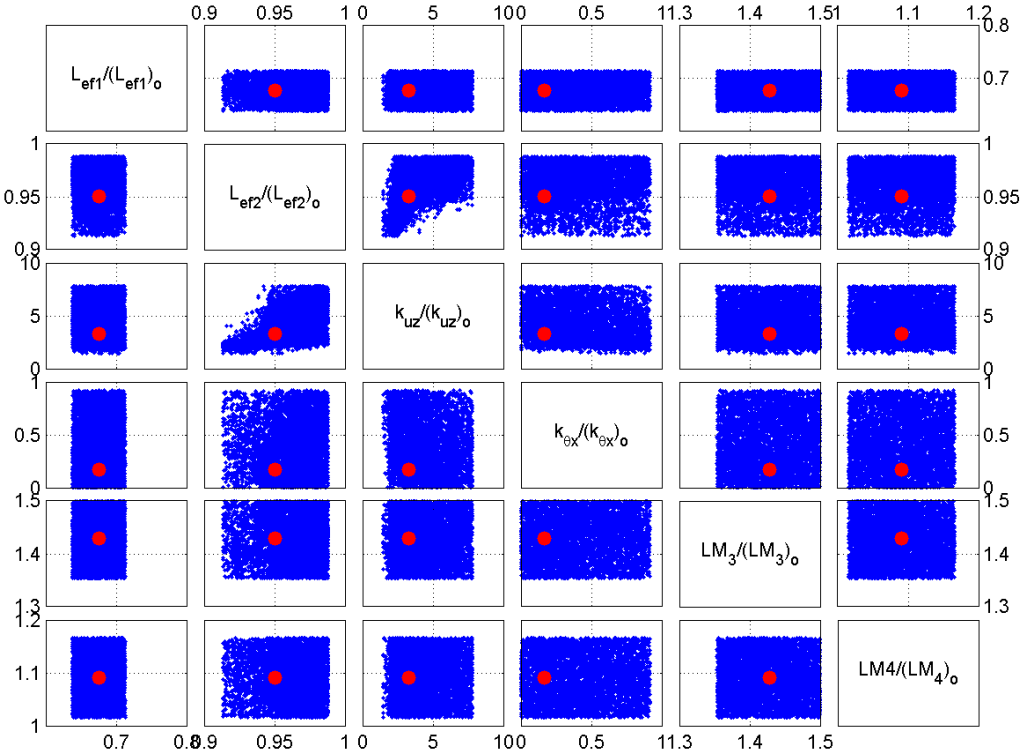

Figure 5.14. Gibbs' sampling for solution #4, study case #1
(Red dot indicates starting sample)

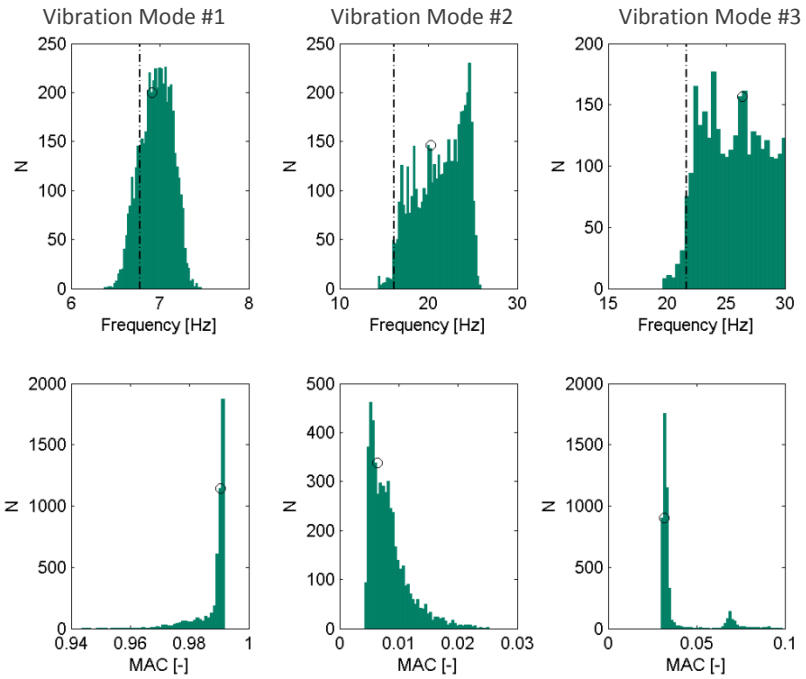

Figure 5.15. Histograms for modes 1, 2 and 3 from Gibbs' sampling
(Solution #4, study case #1. Dashed line: Experimental Value. Circle: starting sample)

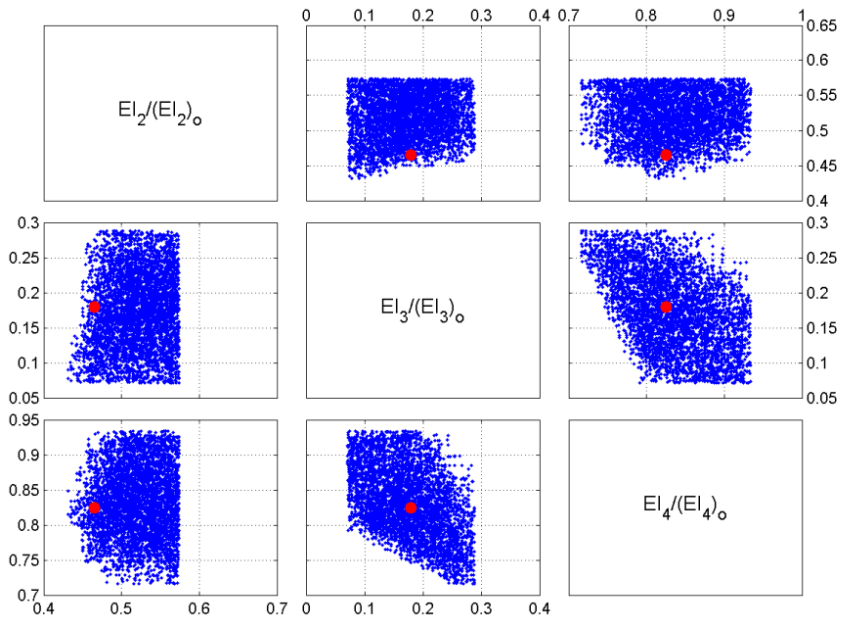

Figure 5.16. Gibbs' sampling for solution #1, study case #3
(Red dot indicates starting sample)

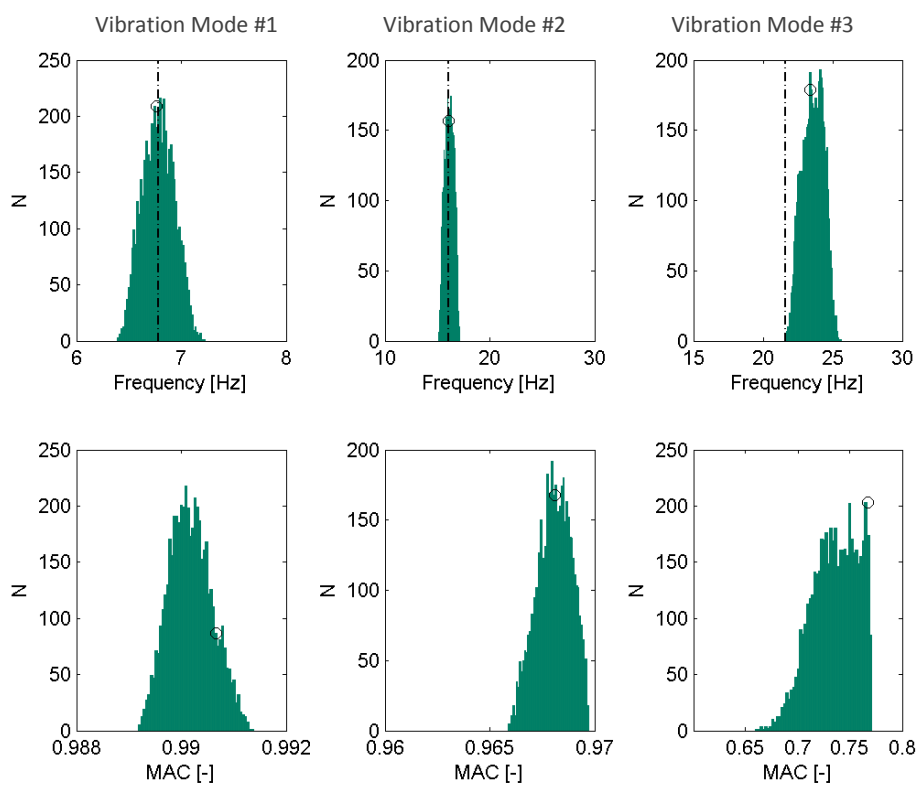

Figure 5.17. Histograms for modes 1, 2 and 3 from Gibbs' sampling
(Solution #1, study case #3. Dashed line: Experimental Value. Circle: starting sample)

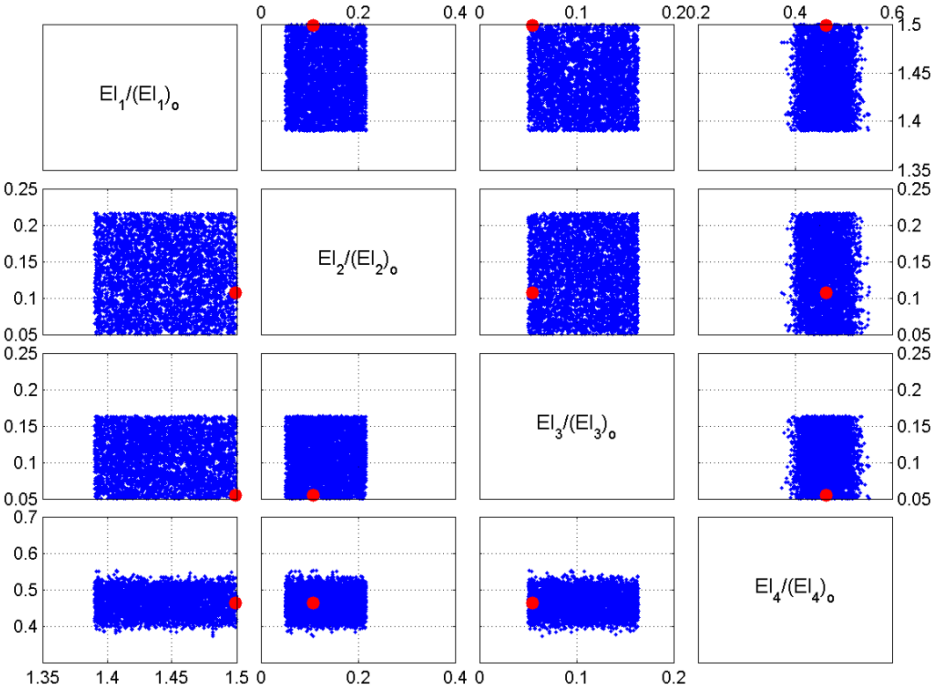

Figure 5.18. Gibbs' sampling for solution #1, study case #4
(Red dot indicates starting sample)

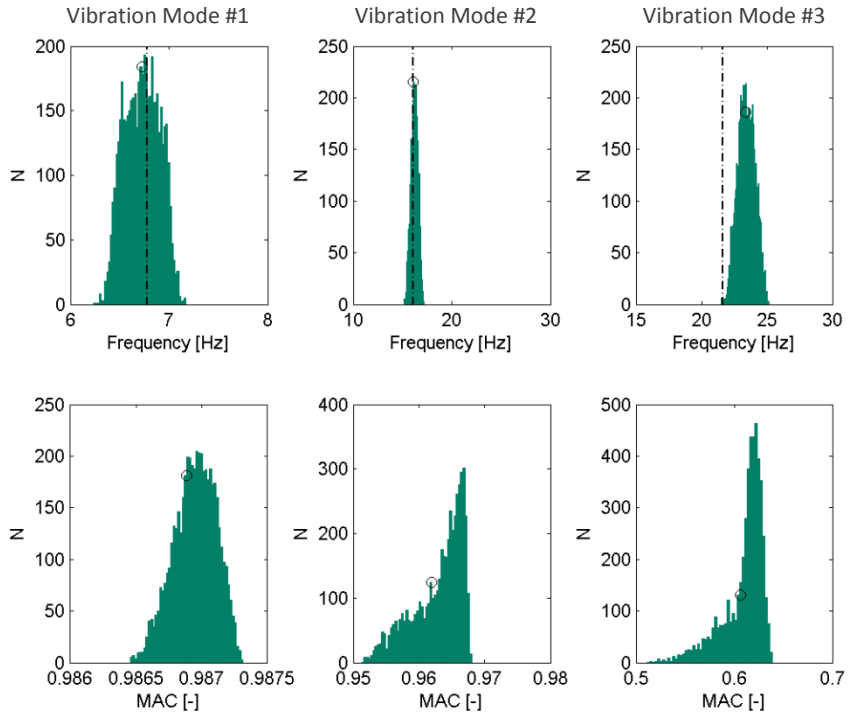

Figure 5.19. Histograms for modes 1, 2 and 3 from Gibbs' sampling
(Solution #1, study case #4. Dashed line: Experimental Value. Circle: starting sample)

From Figure 5.15, Figure 5.17 and Figure 5.19 it can be said that the selected solutions from study cases #3 and #4 with probabilities 43.8% and 17.6% have better performance predicting the changes in modal parameters of the system, showing good prediction of modes 1, 2 and 3. The solution from study case #2 with probability 7.1% can only make a good prediction of the first vibration mode, while modes 2 and 3 are not well predicted.

CHAPTER 6. CONCLUSIONS

The research proposed here introduces a methodology for the selection of solutions in probabilistic model updating problems that facilitates the use of engineering judgment. As described by (Udwadia and Sharma 1978; Udwadia 1985; Franco, Betti et al. 2006), model updating problems are commonly multivariate and ill-conditioned problems. These characteristics usually lead to several solutions, some of which might not be physically meaningful.

An expert is defined as a person who can make a judgment based on an extensive prior knowledge (Chi, Glaser et al. 1981). The expert must be understood here as somebody who has extensive knowledge about structural systems and can perform a reasonable estimation of the behavior of a structure in a hypothetical situation.

Bayes inference allows the addition of prior knowledge in the prior PDF ($P(\theta)$). Theoretically, this PDF can include the expert judgment about the parameters θ. Arguably, in most situations, prior information about the parameters (θ) is difficult to define because the expert has not had direct interaction with the parameter itself. For example, it would be difficult for the expert to define a PDF for the stiffness of rubber bearings on a bridge that has been in service for a number of years. However, it is easier for the engineer to estimate the behavior of the system. For example, estimate the deflection of the same bridge under static loading. Therefore, the analyst's expertise can be expressed through a virtual response of the structure. Such virtual response could be expressed in terms of a non-deterministic variable (or variables) with an associated

uncertainty. Although both cases are valid, the proposed methodology in this research focuses on the probabilistic approach. The degree of belief on this virtual response (i.e. assumed uncertainty) is then expressed by an estimated PDF.

The inclusion of the analyst's expertise into the model updating problem using virtual responses has demonstrated to be effective for the selection of solutions. The experimental validation (Chapter 5) uses a laboratory structure to explore the capabilities of the technique. Results show that the points of high probability in posterior PDF without the virtual response ($P(\theta|D)$) includes values that are not physically meaningful. The use of the virtual response ($P(\theta|D,V_R)$) helps the analyst to select parameters and models that are physically meaningful and provide a reasonable estimation of the behavior of the structure if the system changes.

The concept of virtual response can be extended to the case where multiple models are available, which is a common situation in several fields where numerical modeling is required. Uncertainty in the model can be due to modeling errors (i.e. using an approximation of the physics of the structure) and uncertainty in the parameters. It makes sense then that several models can be required to describe one physical system if the source of uncertainty is not clearly identified, which can be the case for most of modeling problems in structural engineering. The implementation of a virtual response helps the analyst in the selection of appropriate models.

The formulation of a benchmark problem contributes to disseminate the philosophy of MUCogS. This framework intends to encourage researches in the evaluation of multiple solutions in non-deterministic problems. Given the non-uniqueness of this type of problems, it can be said that few has been done in this area, mostly due to

the complexity and high computational cost required from simple model updating problems. However, new computational resources such as High Performance Computing machines and an enhanced cyber-infrastructure enabled by programs like XSEED enable this type of research.

CHAPTER 7. FUTURE WORK

The proposed methodology is successful for the identification of numerical models with parameters that are physically meaningful. However, several considerations can be taken in future work:

a. Expected behavior can also be expressed in terms of a non-probabilistic interval. For instance, an interval can be used to indicate what parts of the solution space are appropriate based on the expected behavior of the system. Arguably, intervals are easier to define than PDFs. The proposed technique could also be extended to use intervals to express the analyst's expertise.

b. Depending on the type of structural system (shear buildings, frame buildings, bridges, etc.), some virtual responses would yield better results than others. A methodology to select the appropriate virtual test can be developed.

c. The number of solutions to a model updating problem obtained with an optimization technique depends on the sensor density available for system identification. In this document, the sensor density was high, since all 16 degrees of freedom of interest were instrumented. However, bigger systems will have low sensor density, increasing the number of solutions. This research can be extended to consider the effect of variable sensor density on the selection of model updating solutions. In this document, $P(\theta|D)$ considered vibration modes whose error in natural frequency was not greater that 5Hz, and whose MAC values were

at least 0.8. Under a consideration of higher tolerance in these constrains, the probability space defined by $P(\theta|D)$ becomes smaller, affecting the number of identified solutions in the model updating problem. Future work can take this into account and investigate the behavior of the selected solutions based on relaxed constrains.

d. This research defined a "solution" as a hyper-cube around a point with maximum $P(\theta|D)$. A methodology to better define the shape and size of the areas of high probability is needed.

REFERENCES

Adhikari, S. and M. Friswell (2004). Random eigenvalue problems in structural dynamics. Proceedings of the 45th AIAA/ASME/ASCE/AHS/ASC Structures, Structural Dynamics & Materials Conference, Palm Springs, California.[Links].

Allemang, R. J. (2003). "The modal assurance criterion - Twenty years of use and abuse." Journal of Sound and Vibration **37**(8): 14-23.

Ang, A. H.-S., W. H. Tang, et al. (2007). Probability concepts in engineering : emphasis on applications in civil & environmental engineering. New York, Wiley.

Baeza, L. and H. Ouyang (2011). "A railway track dynamics model based on modal substructuring and a cyclic boundary condition." Journal of Sound and Vibration **330**(1): 75-86.

Baranyi, J., C. Pin, et al. (1999). "Validating and comparing predictive models." International Journal of Food Microbiology **48**(3): 159-166.

Beck, J. L. and S. K. Au (2002). "Bayesian updating of structural models and reliability using Markov chain Monte Carlo simulation." Journal of Engineering Mechanics-Asce **128**(4): 380-391.

Beck, J. L. and L. S. Katafygiotis (1998). "Updating Models and Their Uncertainties. I: Bayesian Statistical Framework." Journal of Engineering Mechanics **124**(4): 455-461.

Bendat, J. S. and A. G. Piersol (2000). Random data : analysis and measurement procedures. New York, Wiley.

Box, G. E. and G. C. Tiao (2011). Bayesian inference in statistical analysis, John Wiley & Sons.

Bradford, M. and P. Cuk (1988). "Elastic Buckling of Tapered Monosymmetric I-Beams." Journal of Structural Engineering **114**(5): 977-996.

Brill, E. D., S.-Y. Chang, et al. (1982). "Modeling to generate alternatives: The HSJ approach and an illustration using a problem in land use planning." Management Science **28**(3): 221-235.

Brownjohn, J. and P. Xia (2000). "Dynamic Assessment of Curved Cable-Stayed Bridge by Model Updating." Journal of Structural Engineering **126**(2): 252-260.

Brownjohn, J. M. W. and P.-Q. Xia (2000). "Dynamic Assessment of Curved Cable-Stayed Bridge by Model Updating." Journal of Structural Engineering **126**(2): 252-260.

Burnham, K. P. and D. R. Anderson (2002). Model selection and multi-model inference: a practical information-theoretic approach, Springer.

Caicedo, J. (2011). "Practical guidelines for the natural excitation technique (NexT) and the eigensystem realization algorithm (ERA) for modal identification using ambient vibration." Experimental Techniques **35**(4): 52-58.

Caicedo, J. M. and G. Yun (2010). "A novel evolutionary algorithm for identifying multiple alternative solutions in model updating." Structural Health Monitoring **1**(11).

Caicedo, J. M. and B. A. Zarate (2011). "Reducing Epistemic Uncertainty using a Model Updating Cognitive System." Advances in Structural Engineering **14**(1): 55-65.

Cheung, S. H. and J. L. Beck (2009). "Bayesian Model Updating Using Hybrid Monte Carlo Simulation with Application to Structural Dynamic Models with Many Uncertain Parameters." Journal of Engineering Mechanics-Asce **135**(4): 243-255.

Chi, M. T., R. Glaser, et al. (1981). Expertise in problem solving. Pittsburgh, University of Pittsburgh.

Eberhart, R. and J. Kennedy (1995). A new optimizer using particle swarm theory. Micro Machine and Human Science, 1995. MHS'95., Proceedings of the Sixth International Symposium on, IEEE.

Estrada, M. A. R. (2011). "Multi-Dimensional coordinate spaces." International Journal of the Physical Sciences **6**(3): 340-357.

Fonseca, J. M. R. (2005). Uncertainty in Structural Dynamic Models, University of Wales Swansea. **Ph.D.**

Fox, D. G. (1981). "Judging Air Quality Model Performance." Bulletin of the American Meteorological Society **62**(5): 599-609.

Franco, G., R. Betti, et al. (2006). "On the uniqueness of solutions for the identification of linear structural systems." Journal of Applied Mechanics-Transactions of the Asme **73**(1): 153-162.

Goldberg, D. E. (1989). "Genetic algorithms in search, optimization, and machine learning."

Goller, B., H. J. Pradlwarter, et al. (2009). "Robust model updating with insufficient data." Computer Methods in Applied Mechanics and Engineering **198**(37–40): 3096-3104.

Helton, J. C., J. D. Johnson, et al. (2006). "Survey of sampling-based methods for uncertainty and sensitivity analysis." Reliability Engineering & System Safety **91**(10): 1175-1209.

Inselberg, A. and B. Dimsdale (1991). Parallel coordinates. Human-Machine Interactive Systems, Springer**:** 199-233.

Jaynes, E. T. (2003). Probability theory: the logic of science, Cambridge university press.

Juang, J.-N. and R. S. Pappa (1985). "An Eigensystem Realization Algorithm for Modal Parameter Identification and Model Reduction." Journal of Guidance **8**(5): 620-627.

Karimi, K., M. J. Tait, et al. (2011). "Testing and modeling of a novel FRP-encased steel–concrete composite column." Composite Structures **93**(5): 1463-1473.

Kass, R. E. and L. Wasserman (1996). "The selection of prior distributions by formal rules." Journal of the American Statistical Association **91**(435): 1343-1370.

Lam, H.-F. (1998). Structural Model Updating And Health Monitoring In The PresenceOf Modeling Uncertainties, Hong Kong University of Science and Technology**:** 263.

Link, M. and M. Weiland (2009). "Damage identification by multi-model updating in the modal and in the time domain." Mechanical Systems and Signal Processing **23**(6): 1734-1746.

Madarshahian, R., J. M. Caicedo, et al. (2013). Using P-Box and PiFE to Express Uncertainty in Model Updating. Topics in Model Validation and Uncertainty Quantification, Volume 5, Springer**:** 81-88.

Marwala, T. and S. Sibisi (2005). "Finite Element Model Updating Using Bayesian Framework and Modal Properties." Journal of Aircraft **42**(1): 275-278.

Matott, L. S., J. E. Babendreier, et al. (2009). "Evaluating uncertainty in integrated environmental models: A review of concepts and tools." Water Resources Research **45**(6): W06421.

Moriasi, D. N., J. G. Arnold, et al. (2007). "Model evaluation guidelines for systematic quantification of accuracy in watershed simulations." Transactions of the Asabe **50**(3): 885-900.

Muhanna, R. L., H. Zhang, et al. (2007). "Interval finite elements as a basis for generalized models of uncertainty in engineering mechanics." Reliable Computing **13**(2): 173-194.

Papadimitriou, C., J. L. Beck, et al. (2001). "Updating robust reliability using structural test data." Probabilistic Engineering Mechanics **16**(2): 103-113.

Parrott, D. and L. Xiaodong (2006). "Locating and tracking multiple dynamic optima by a particle swarm model using speciation." Evolutionary Computation, IEEE Transactions on **10**(4): 440-458.

Ren, W.-X., Y.-Q. Lin, et al. (2007). "Field load tests and numerical analysis of Qingzhou Cable-Stayed Bridge." Journal of Bridge Engineering **12**(2): 261-270.

Robert, C. P., G. Casella, et al. (1999). Monte Carlo statistical methods, Springer New York.

Sanayei, M., S. Wadia-Fascetti, et al. (2001). "Significance of modeling error in structural parameter estimation." Computer-Aided Civil and Infrastructure Engineering **16**(1): 12-27.

Sharko, J., G. Grinstein, et al. (2008). "Vectorized Radviz and Its Application to Multiple Cluster Datasets." IEEE Transactions on Visualization and Computer Graphics **14**(6): 1444 - 1427

Tarantola, A. (2002). Inverse problem theory: Methods for data fitting and model parameter estimation, Elsevier Science.

Tsai, C. W. and S. Franceschini (2005). "Evaluation of probabilistic point estimate methods in uncertainty analysis for environmental engineering applications." Journal of environmental engineering **131**(3): 387-395.

Tsai, R. Y. (1987). "A Versatile Camera Calibration Technique for High-Accuracy 3d Machine Vision Metrology Using Off-the-Shelf Tv Cameras and Lenses." Ieee Journal of Robotics and Automation **3**(4): 323-344.

Udwadia, F. E. (1985). "Some Uniqueness Results Related to Soil and Building Structural Identification." Siam Journal on Applied Mathematics **45**(4): 674-685.

Udwadia, F. E. and D. K. Sharma (1978). "Some Uniqueness Results Related to Building Structural Identification." Siam Journal on Applied Mathematics **34**(1): 104-118.

Vanik, M. W., J. L. Beck, et al. (2000). "Bayesian probabilistic approach to structural health monitoring." Journal of Engineering Mechanics-Asce **126**(7): 738-745.

Venter, G. and J. Sobieszczanski-Sobieski (2003). "Particle swarm optimization." Aiaa Journal **41**(8): 1583-1589.

Willmott, C. J. (1982). "Some Comments on the Evaluation of Model Performance." Bulletin of the American Meteorological Society **63**(11): 1309-1313.

Wong, K.-Y. (2007). "Design of a structural health monitoring system for long-span bridges." Structure and Infrastructure Engineering **3**(2): 169-185.

Wong, P. C. and R. D. Bergeron (1997). "30 Years of Multidimensional Multivariate Visualization." IEEE Computer Society Press: 3--33.

Yuen, K.-V. (2010). "Recent developments of Bayesian model class selection and applications in civil engineering." Structural Safety **32**(5): 338-346.

Zarate, B. A. (2009). Alternative solutions and their probabilities for the model updating of structural systems. Civil Engineering Columbia, SC, University of South Carolina. **Doctor of Phylosophy:** 122.

Zarate, B. A. and J. M. Caicedo (2008). "Finite element model updating: Multiple alternatives." Engineering Structures **30**(12): 3724-3730.

Zarate, B. A., J. M. Caicedo, et al. (2007). Model updating of cable-stayed bridges using MGA. International Modal Analysis Conference (IMAC). Orlando, Florida, SEM.

Zechman, E. M. and S. R. Ranjithan (2004). "An evolutionary algorithm to generate alternatives (EAGA) for engineering optimization problems." Engineering Optimization **36**(5): 539-553.

Zhang, Q., T. Chang, et al. (2001). "Finite-Element Model Updating for the Kap Shui Mun Cable-Stayed Bridge." Journal of Bridge Engineering **6**(4): 285-293.

APPENDIX A. EXPERIMENTAL FIGURES

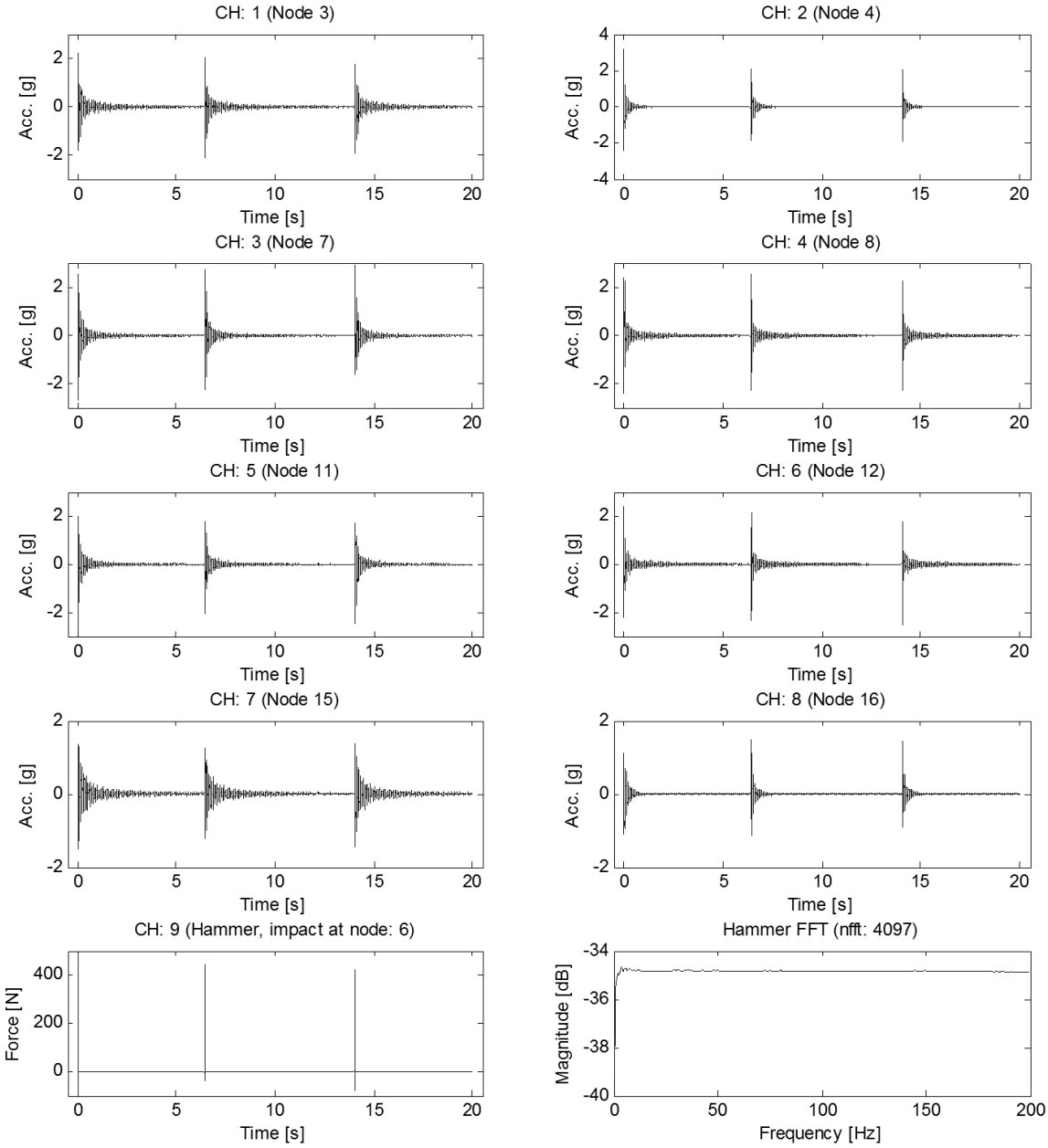

Figure A.1. Time responses from test 1 (Hammer impact at node 6)

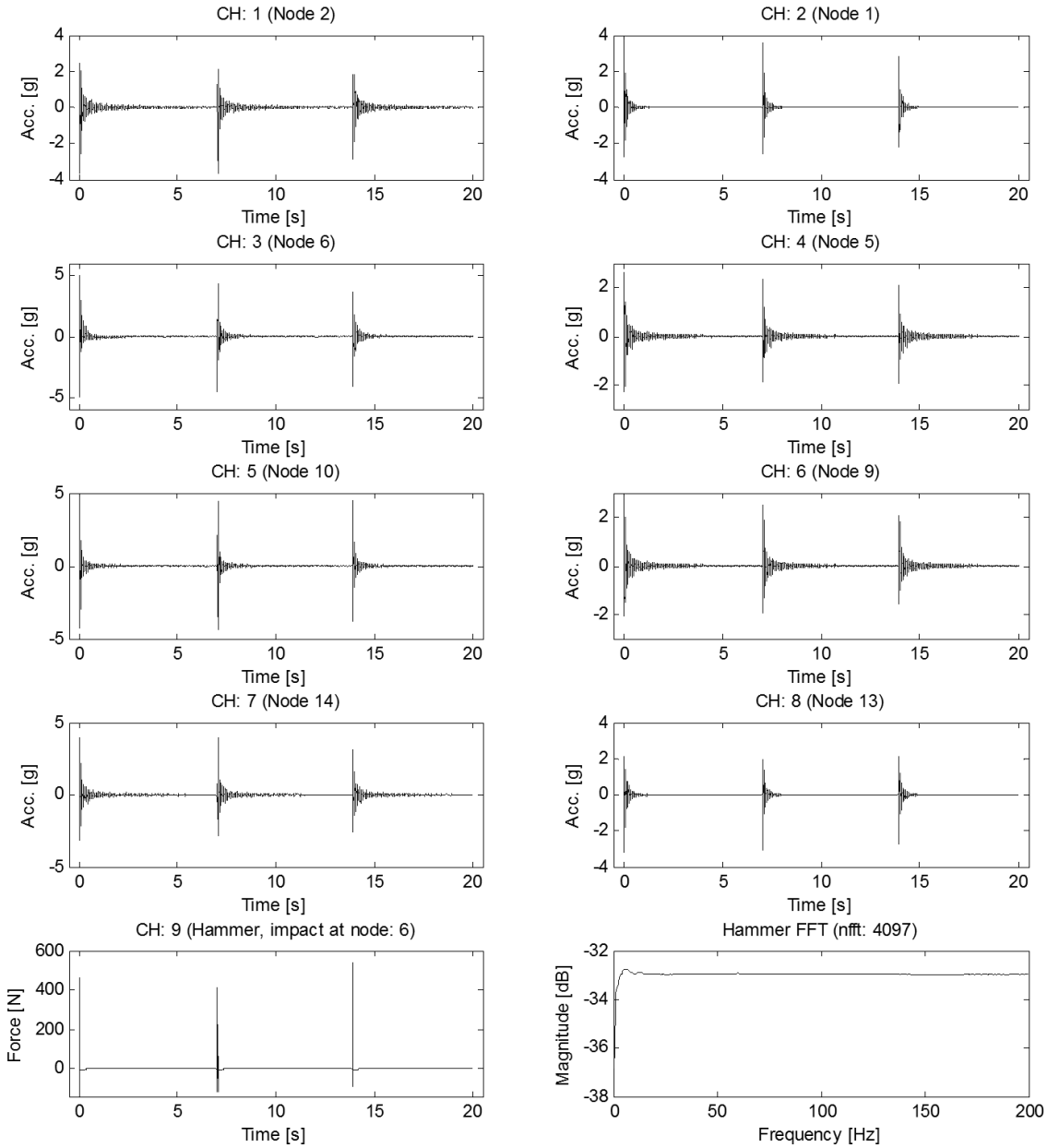

Figure A.2. Time responses from test 2 (Hammer impact at node 6)

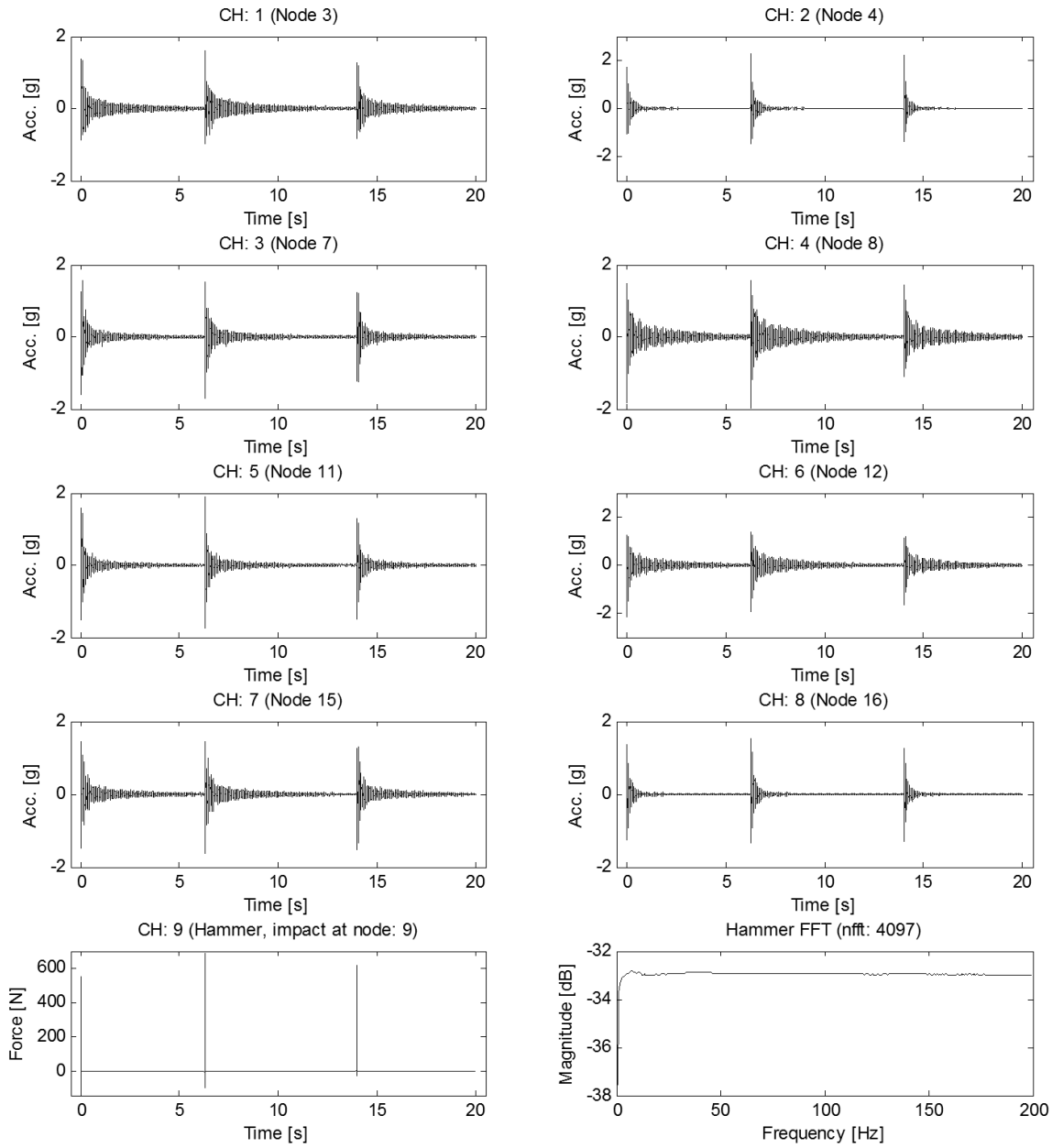

Figure A.3. Time responses from test 1 (Hammer impact at node 9)

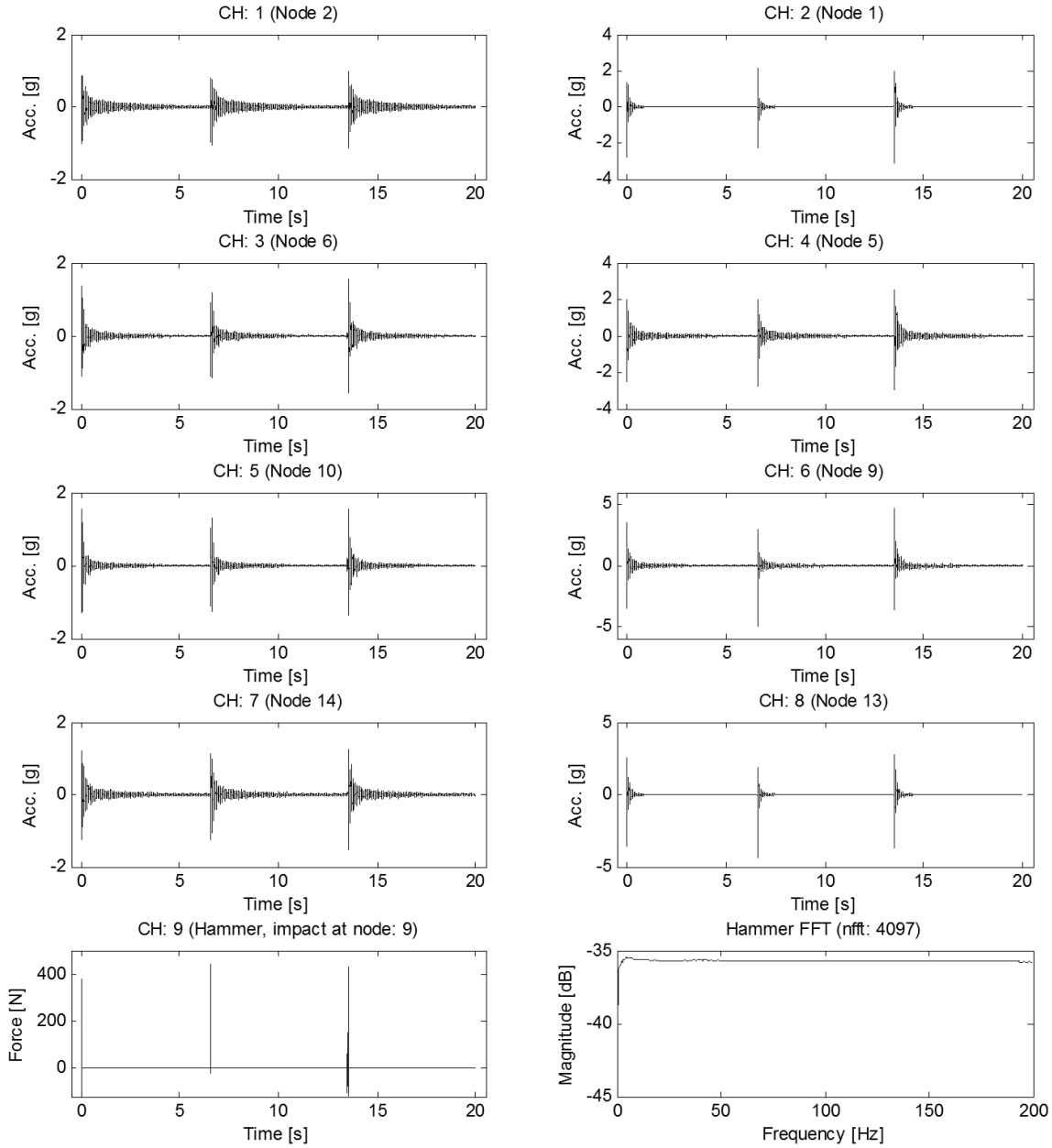

Figure A.4. Time responses from test 2 (Hammer impact at node 9)

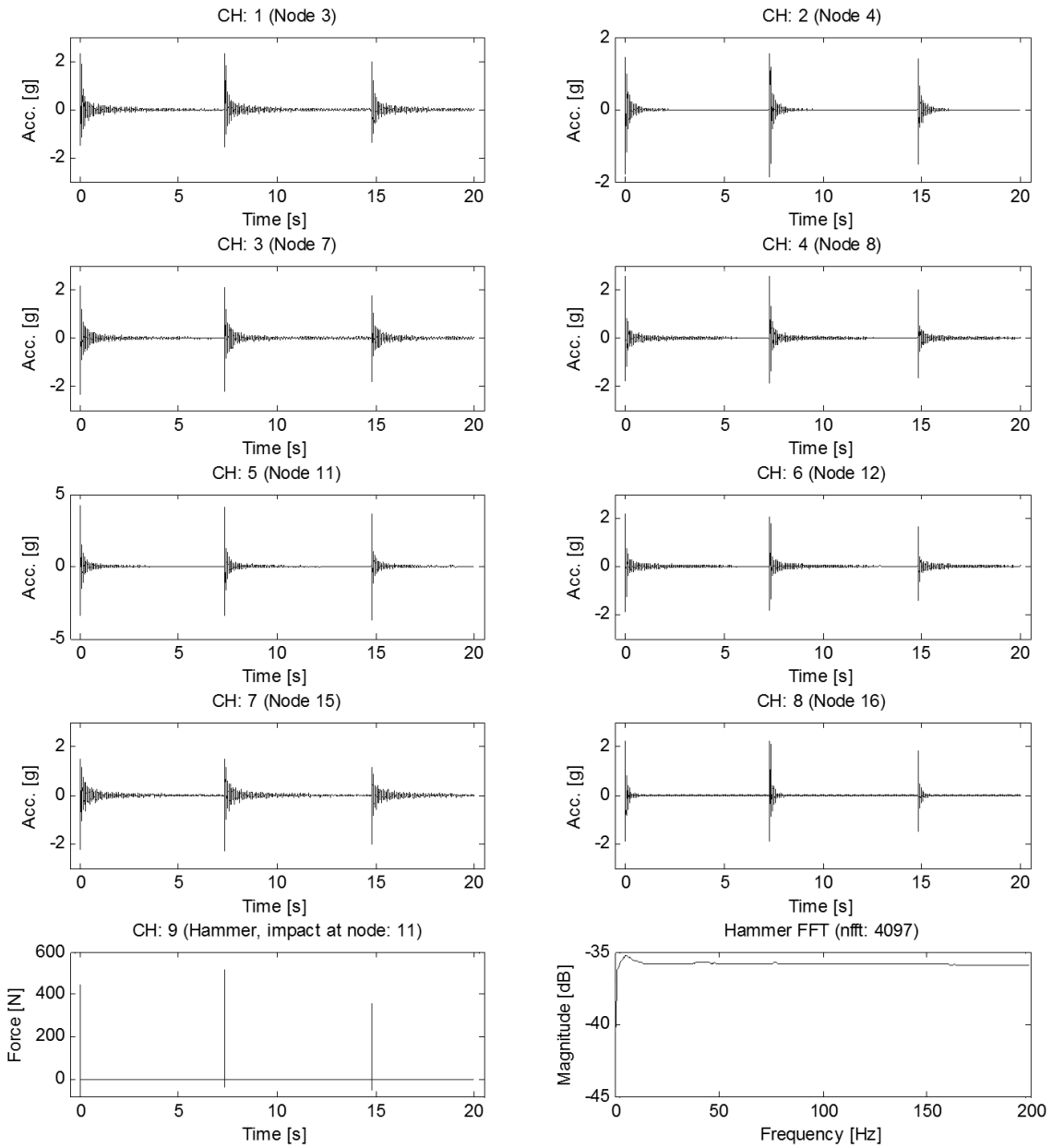

Figure A.5. Time responses from test 1 (Hammer impact at node 11)

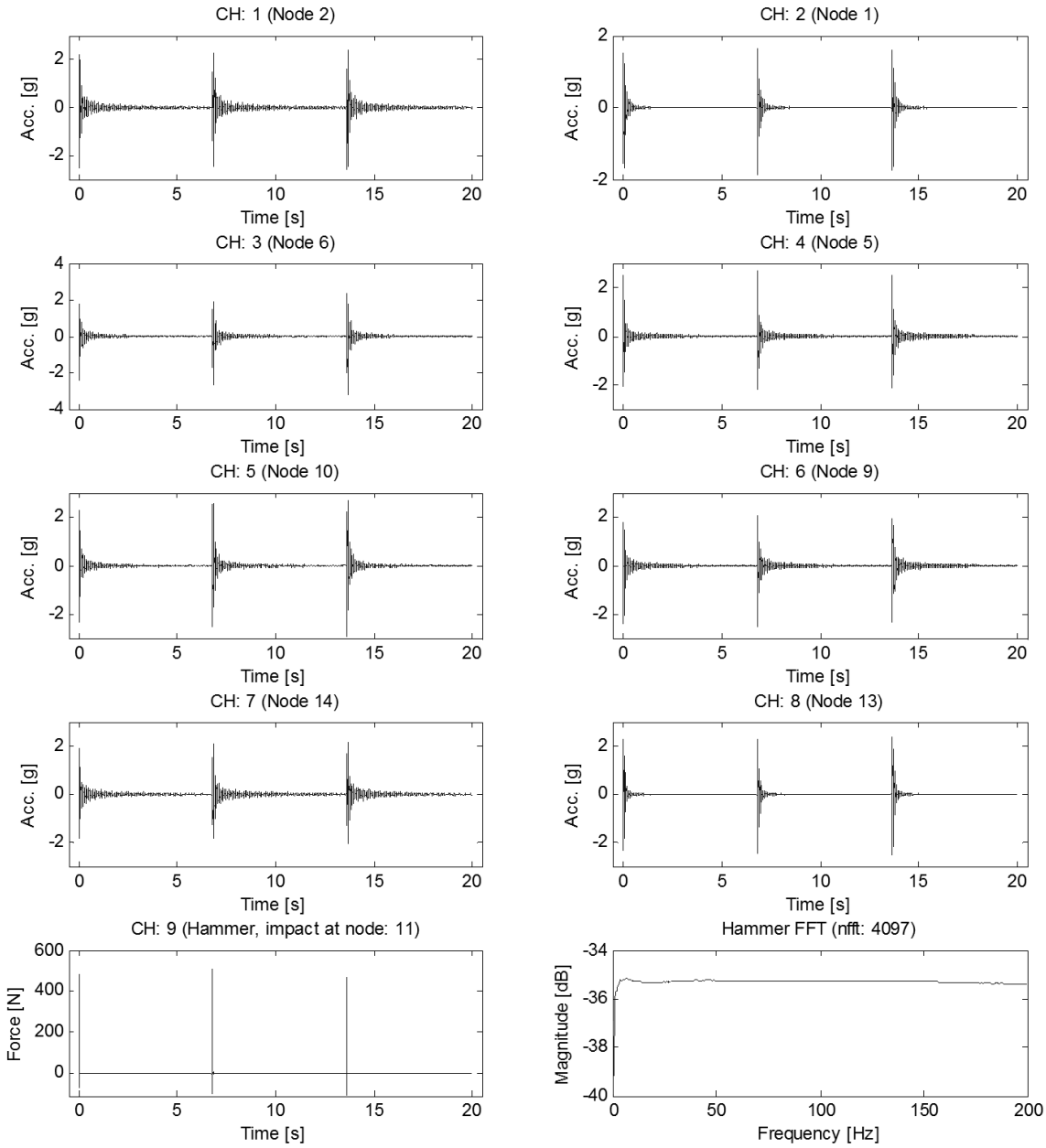

Figure A.6. Time responses from test 2 (Hammer impact at node 11)

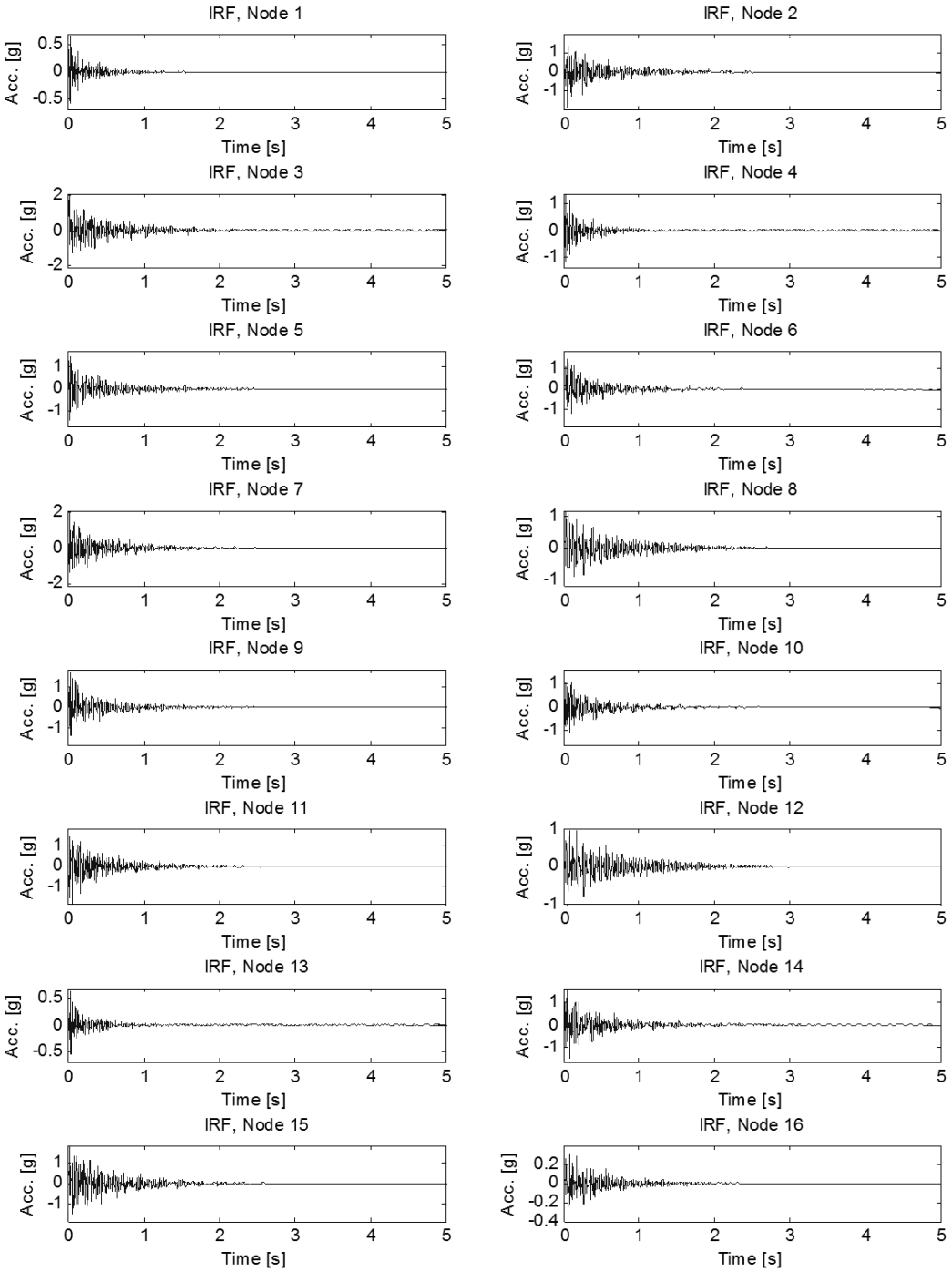

Figure A.7. Impulse response functions (IRF) from hammer impact at node 6

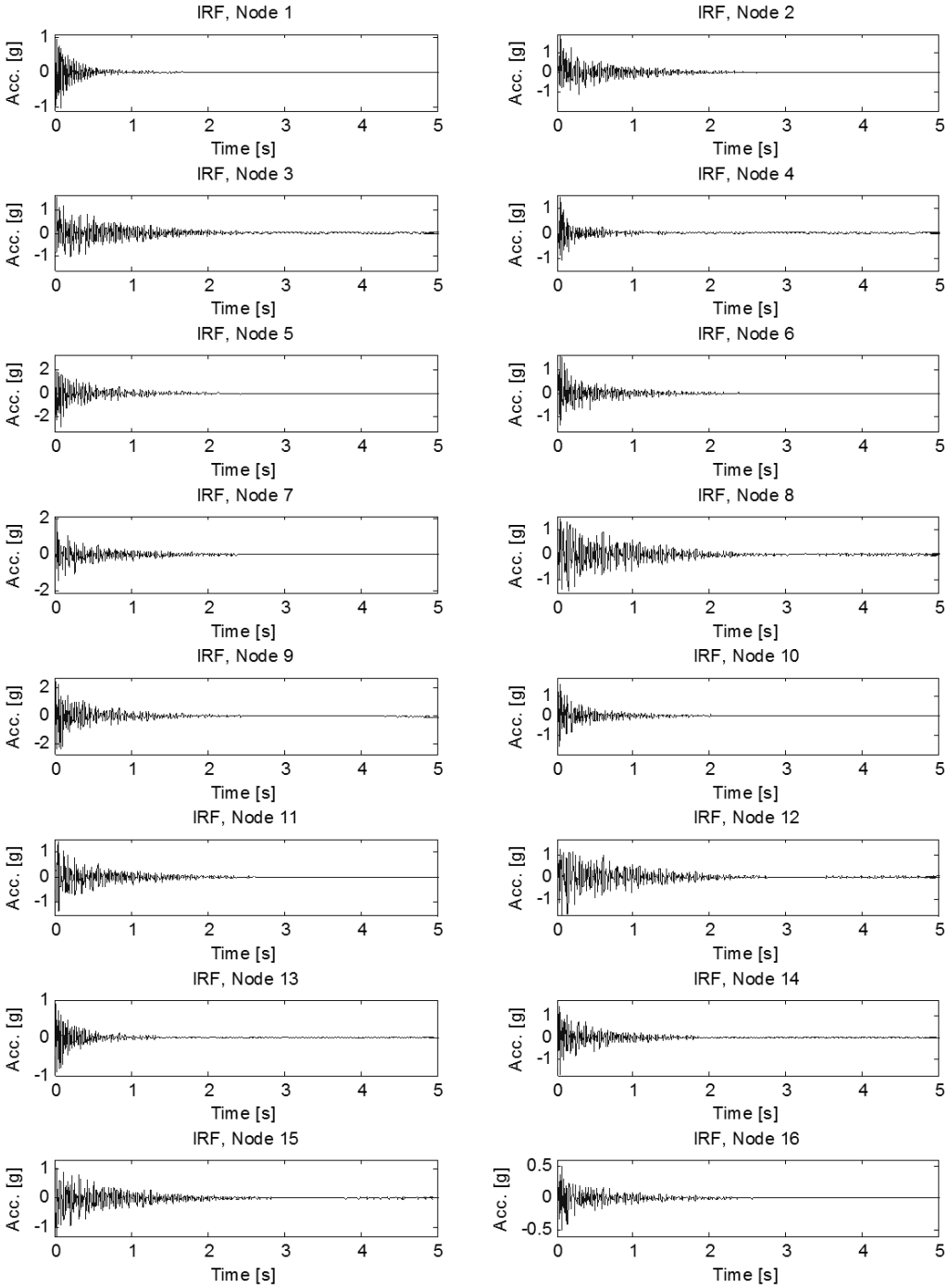

Figure A.8. Impulse response functions (IRF) from hammer impact at node 9

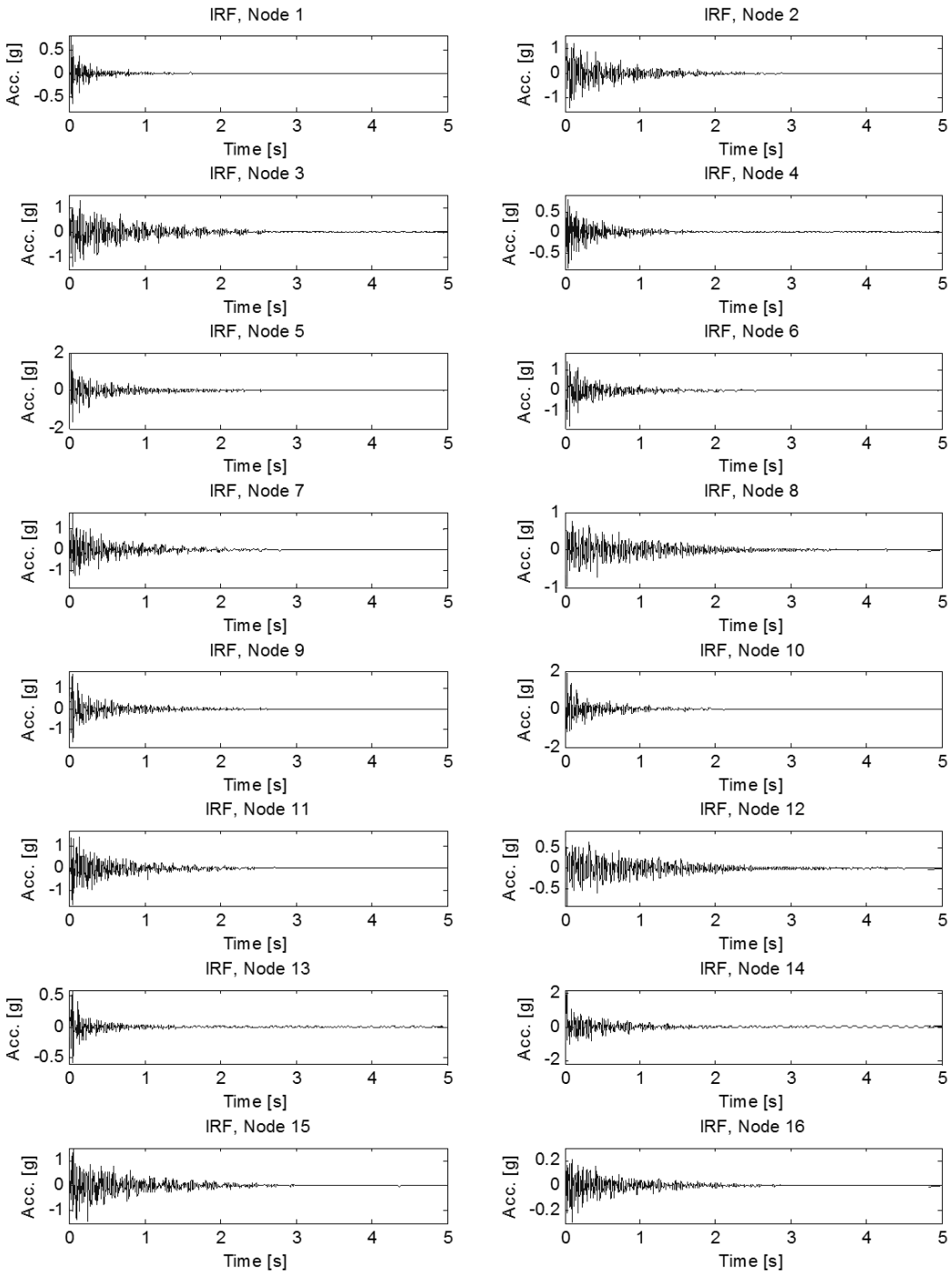

Figure A.9. Impulse response functions (IRF) from hammer impact at node 11

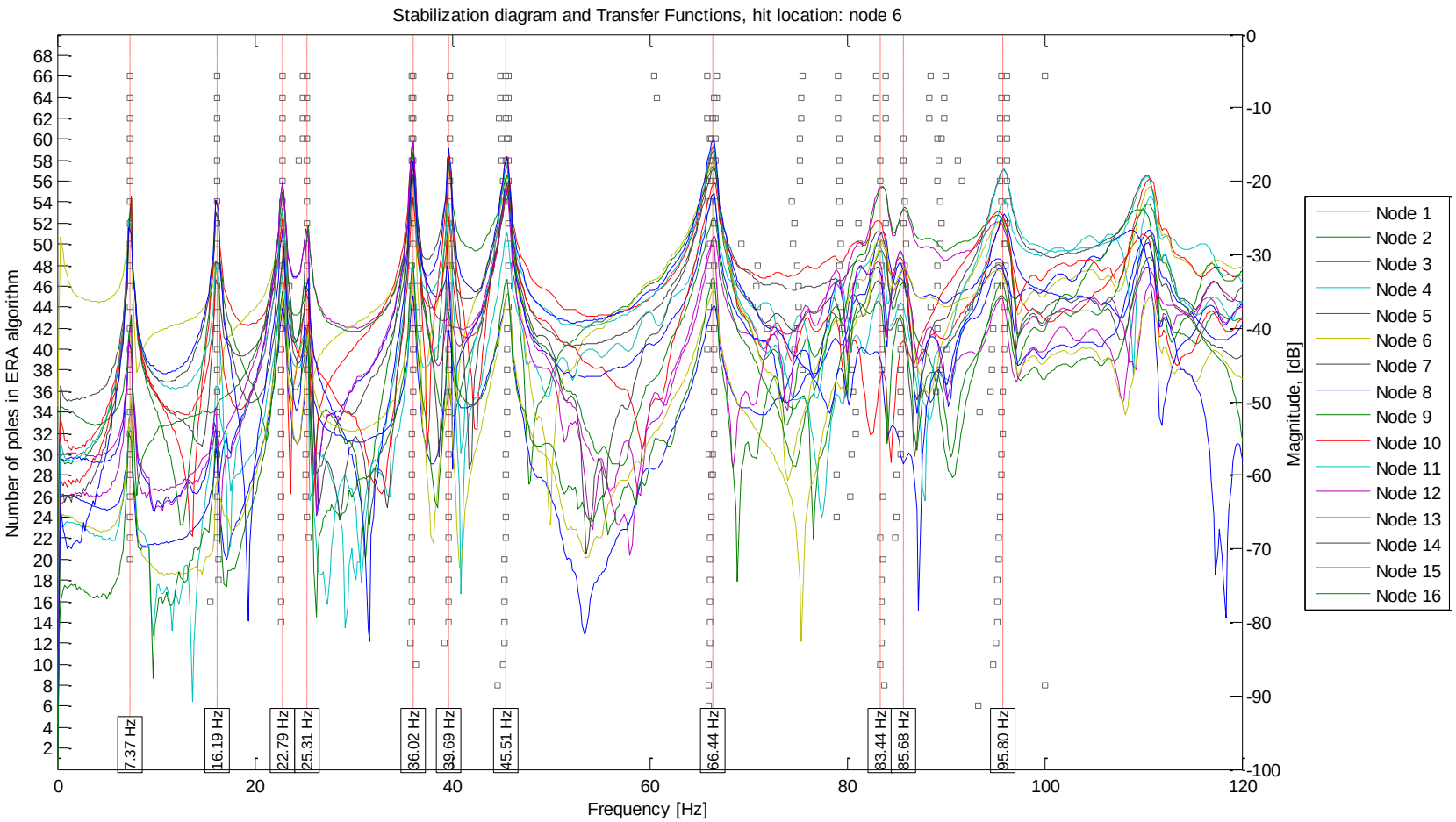

Figure A.10. Stabilization diagram and Transfer Function plots (Impact at node 6)

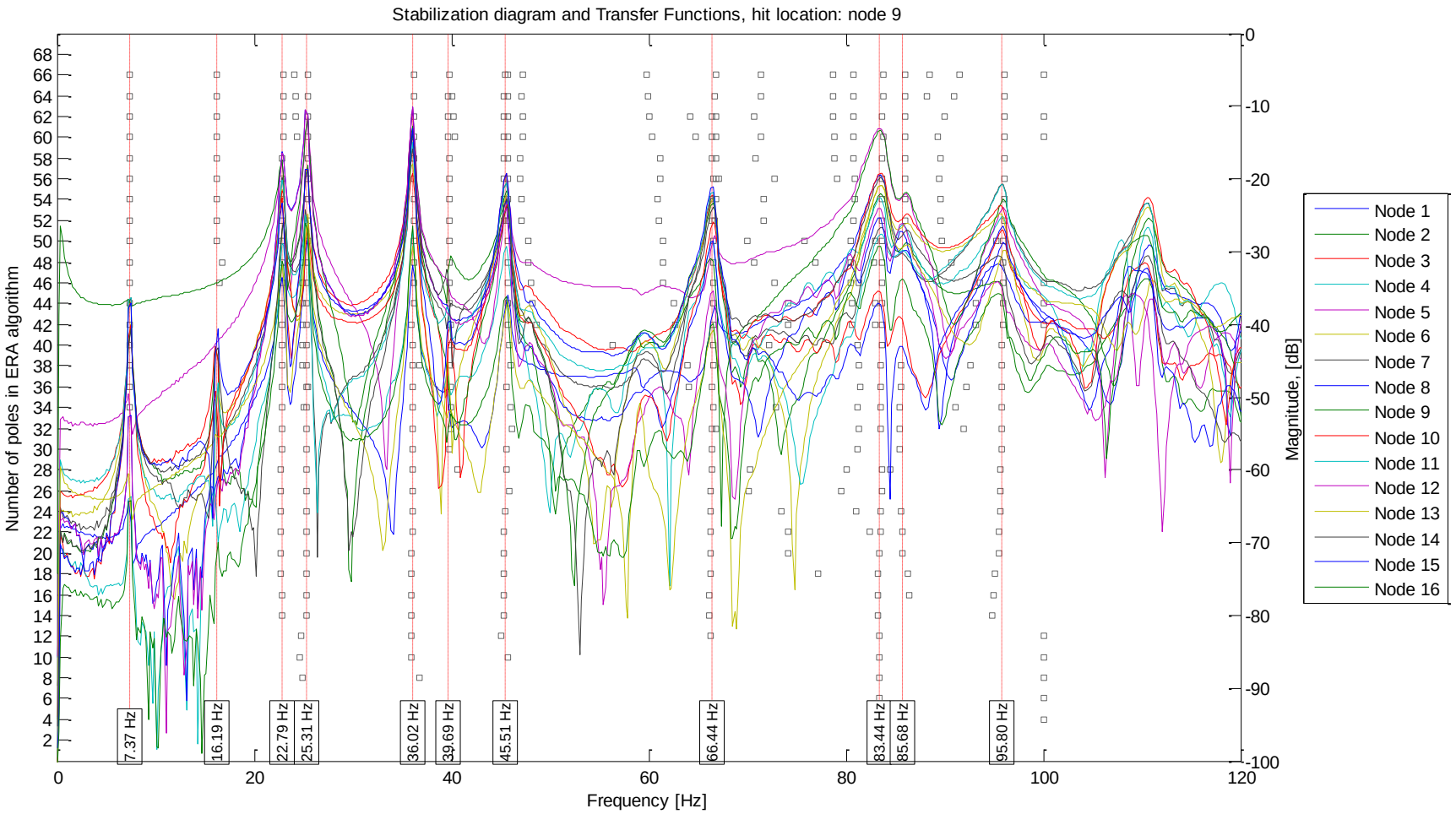

Figure A.11. Stabilization diagram and Transfer Function plots (Impact at node 9)

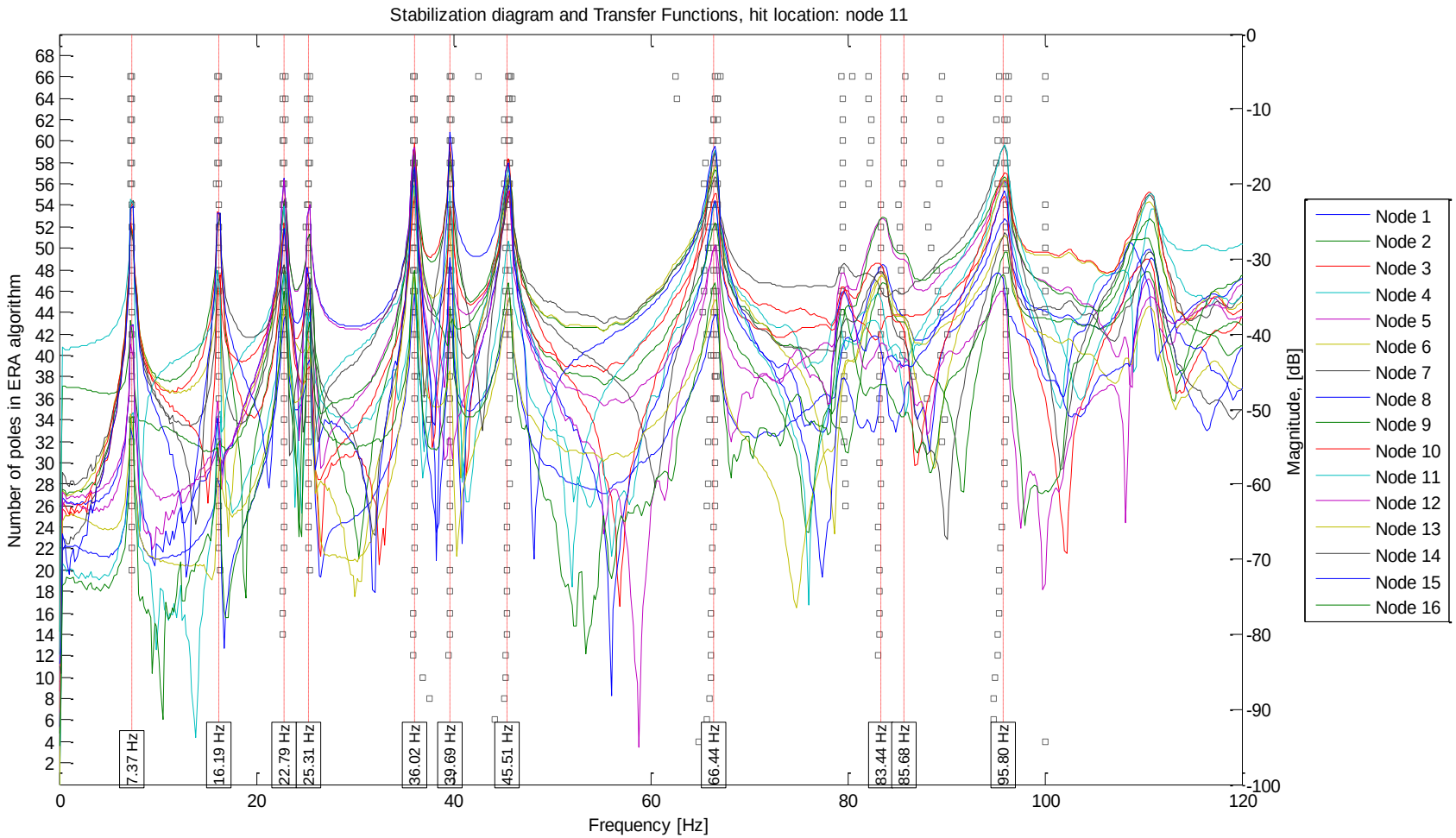

Figure A.12. Stabilization diagram and Transfer Function plots (Impact at node 11)

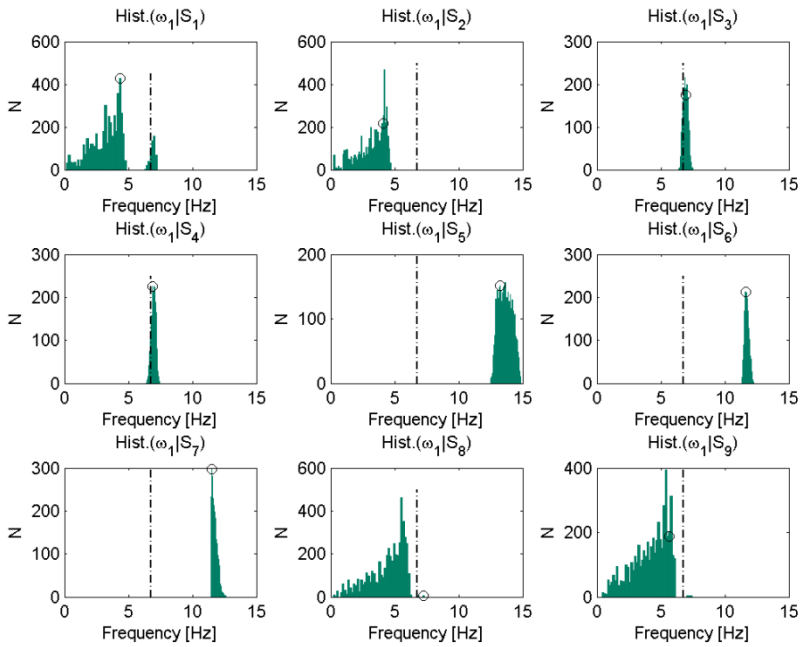

Figure A.13. Histograms for natural frequencies (Mode 1), study case #2
(Dashed line: Experimental Value. Circle: starting sample)

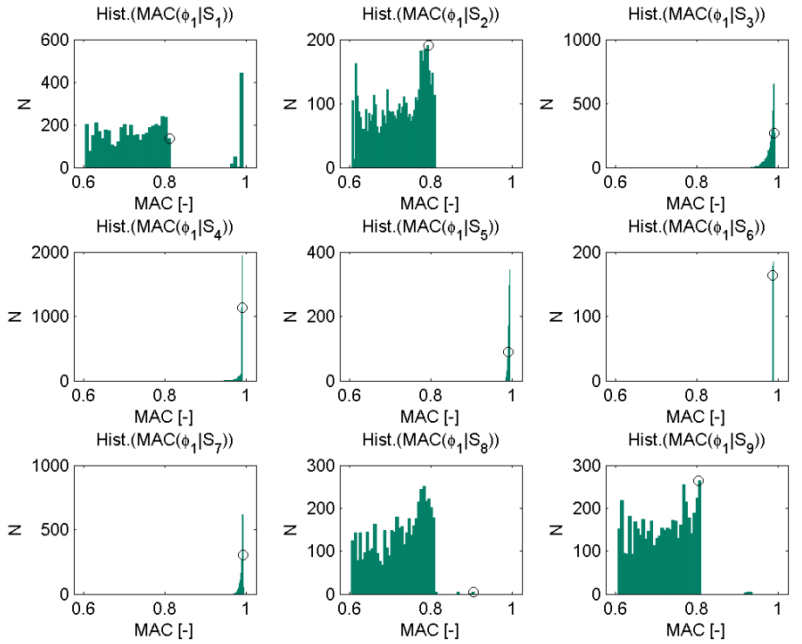

Figure A.14. Histograms for mode shapes (Mode 1), study case #2
(Dashed line: Experimental Value. Circle: starting sample)

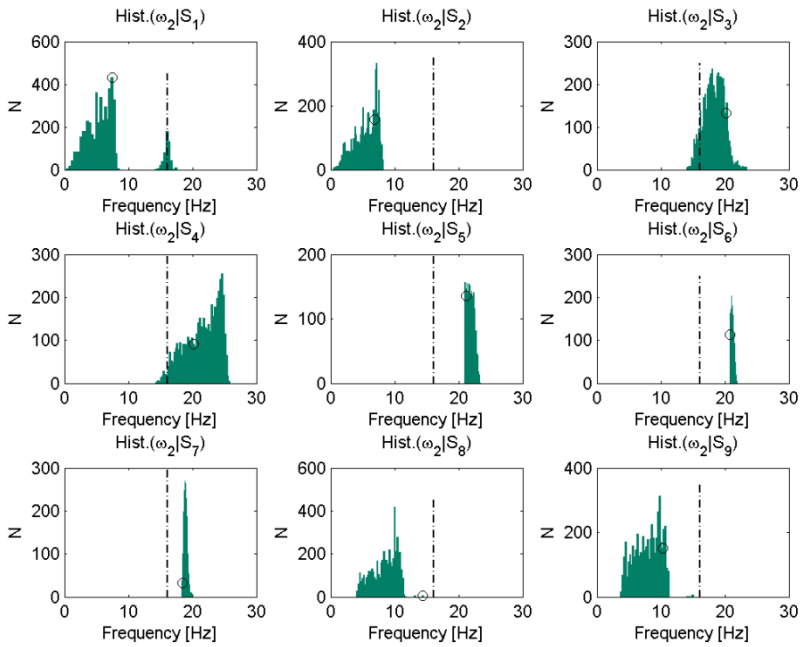

Figure A.15. Histograms for natural frequencies (Mode 2), study case #2
(Dashed line: Experimental Value. Circle: starting sample)

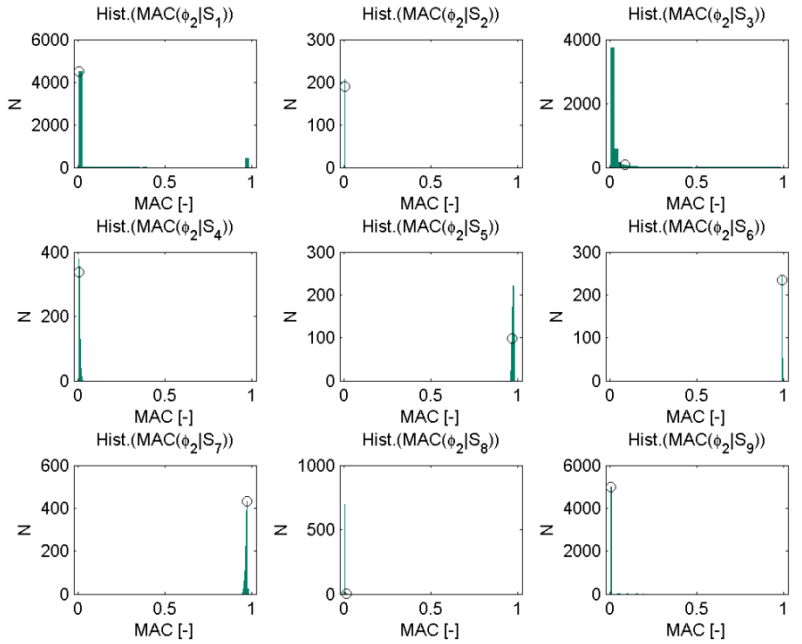

Figure A.16. Histograms for mode shapes (Mode 2), study case #2
(Dashed line: Experimental Value. Circle: starting sample)

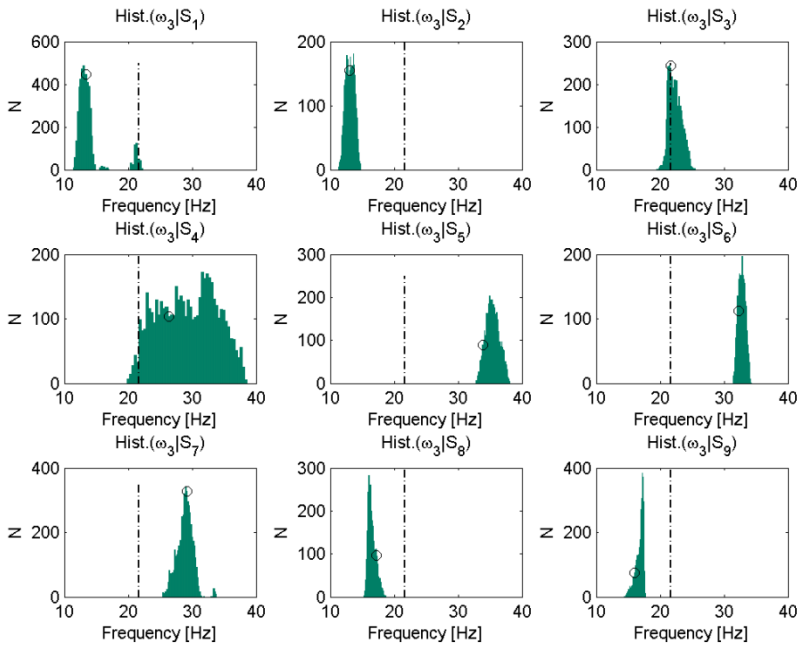

Figure A.17. Histograms for natural frequencies (Mode 3), study case #2
(Dashed line: Experimental Value. Circle: starting sample)

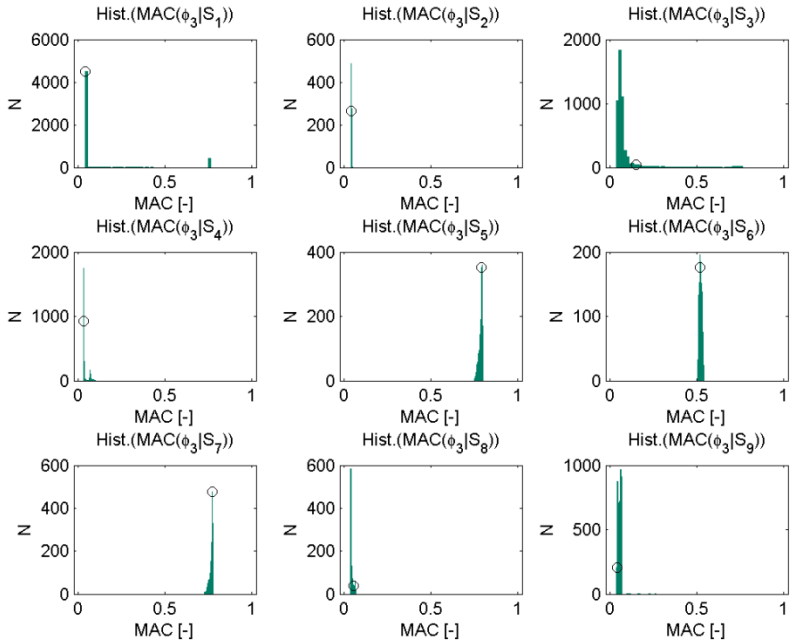

Figure A.18. Histograms for mode shapes (Mode 3), study case #2
(Dashed line: Experimental Value. Circle: starting sample)

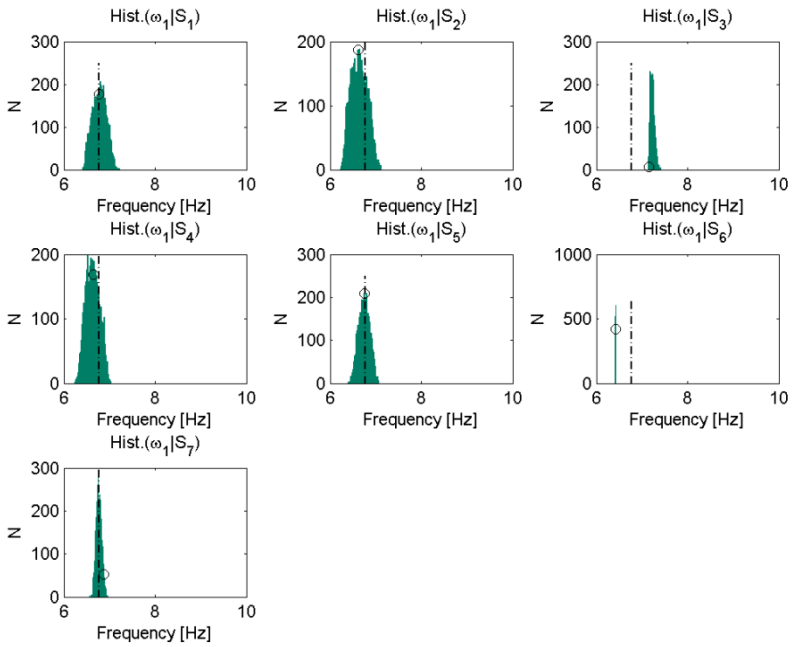

Figure A.19. Histograms for natural frequencies (Mode 1), study case #3
(Dashed line: Experimental Value. Circle: starting sample)

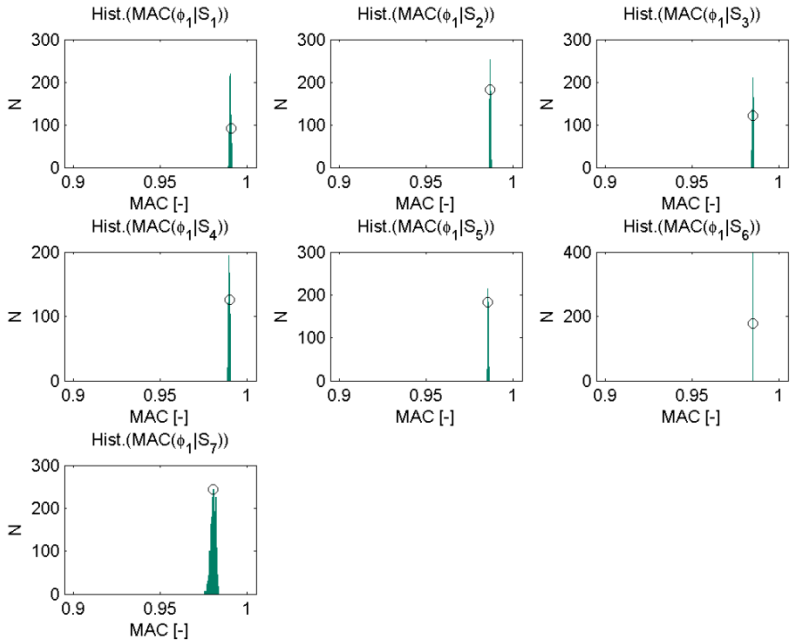

Figure A.20. Histograms for mode shapes (Mode 1), study case #3
(Dashed line: Experimental Value. Circle: starting sample)

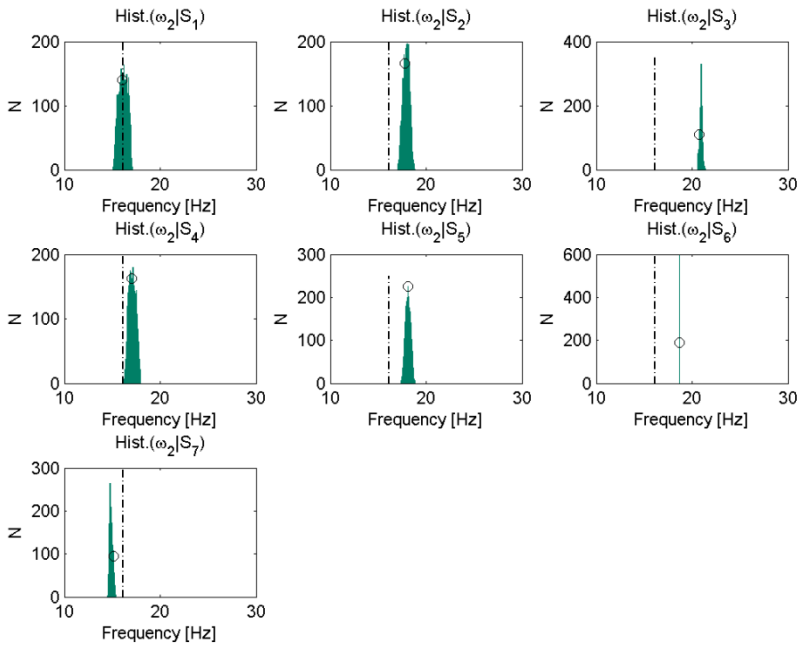

Figure A.21. Histograms for natural frequencies (Mode 2), study case #3
(Dashed line: Experimental Value. Circle: starting sample)

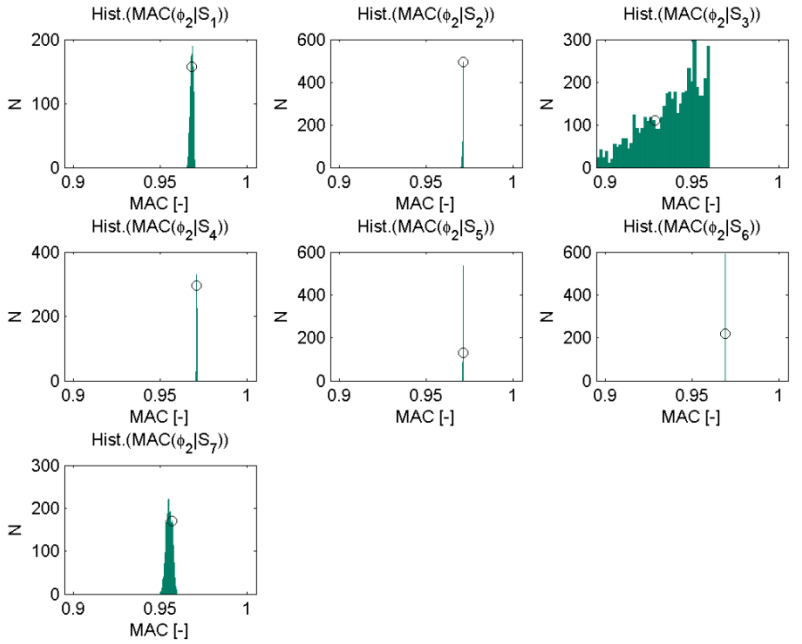

Figure A.22. Histograms for mode shapes (Mode 2), study case #3
(Dashed line: Experimental Value. Circle: starting sample)

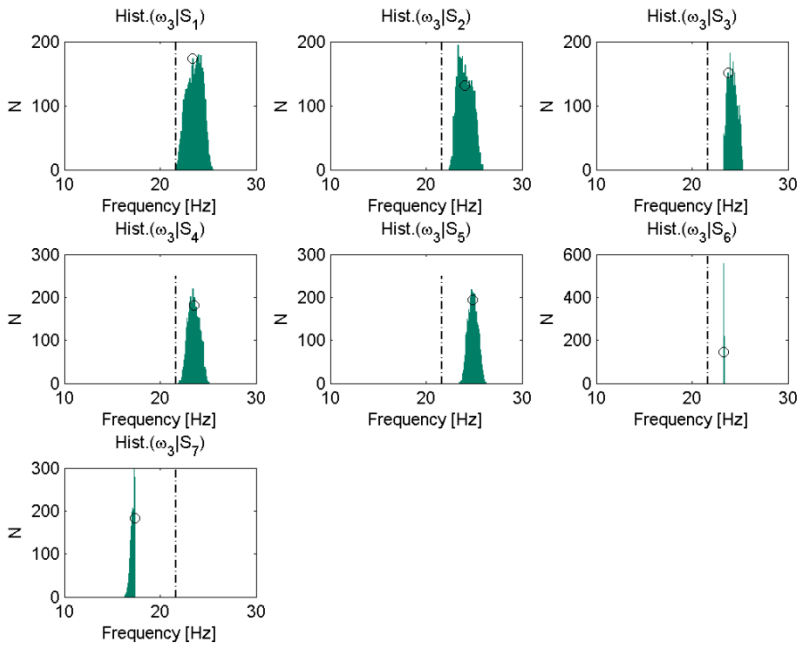

Figure A.23. Histograms for natural frequencies (Mode 3), study case #3
(Dashed line: Experimental Value. Circle: starting sample)

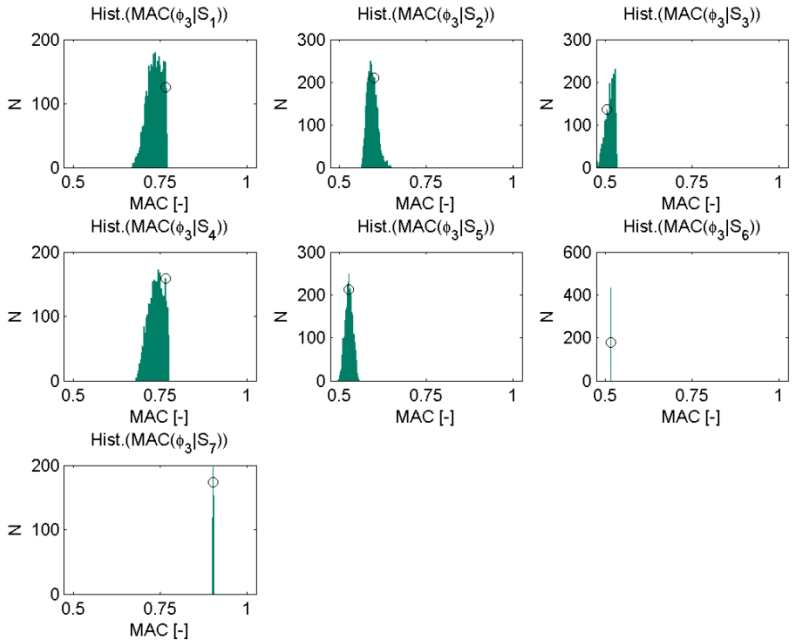

Figure A.24. Histograms for mode shapes (Mode 3), study case #3
(Dashed line: Experimental Value. Circle: starting sample)

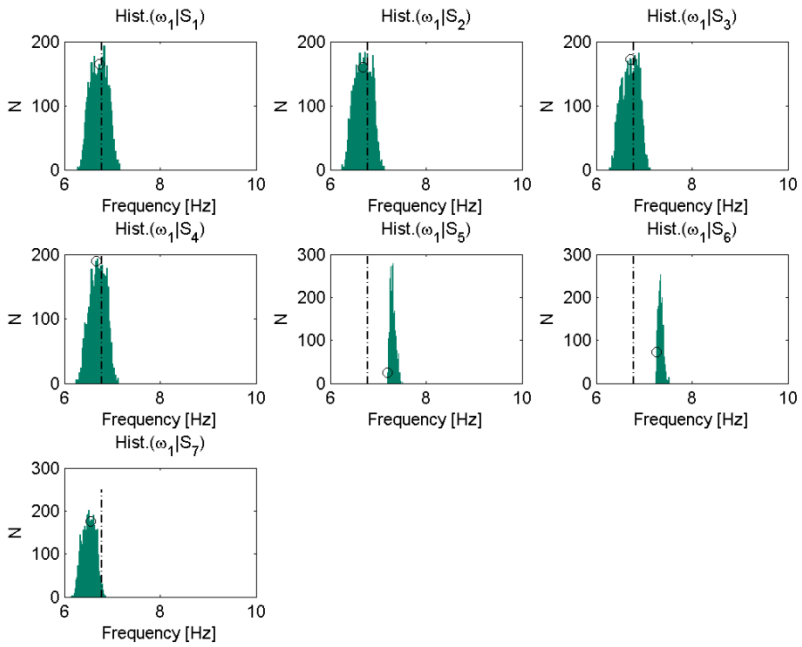

Figure A.25. Histograms for natural frequencies (Mode 1), study case #4
(Dashed line: Experimental Value. Circle: starting sample)

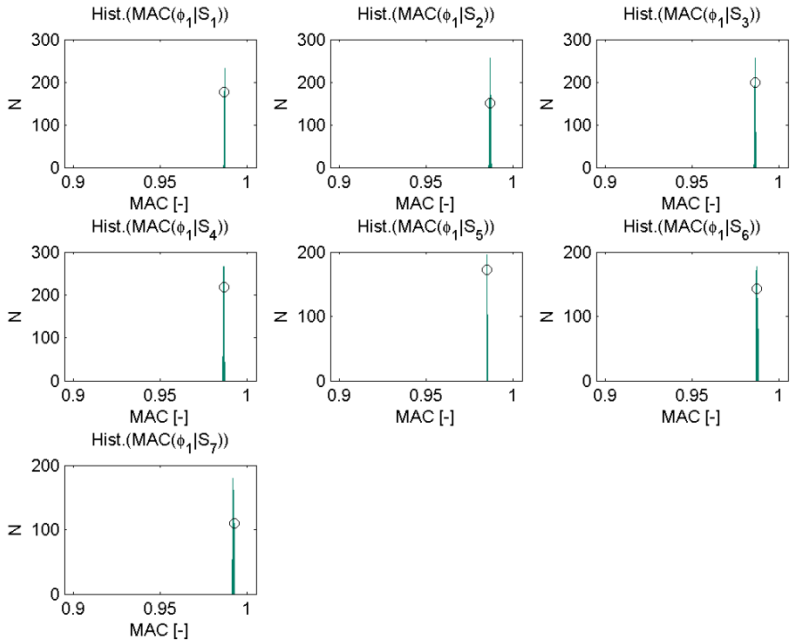

Figure A.26. Histograms for mode shapes (Mode 1), study case #4
(Dashed line: Experimental Value. Circle: starting sample)

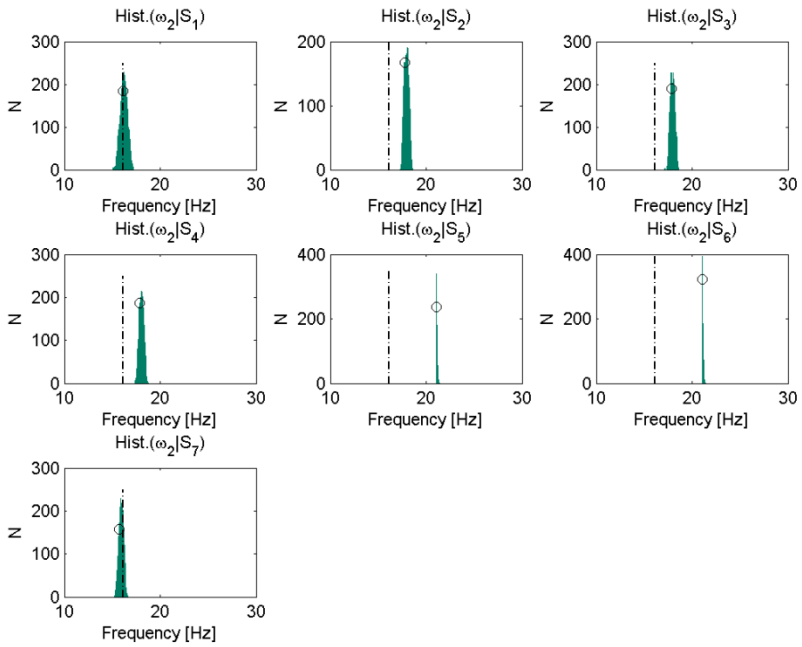

Figure A.27. Histograms for natural frequencies (Mode 2), study case #4
(Dashed line: Experimental Value. Circle: starting sample)

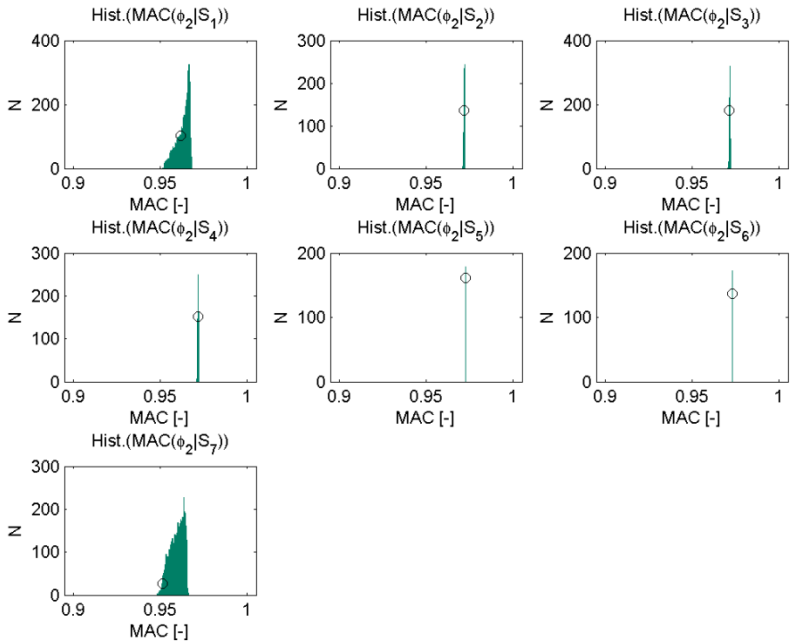

Figure A.28. Histograms for mode shapes (Mode 2), study case #4
(Dashed line: Experimental Value. Circle: starting sample)

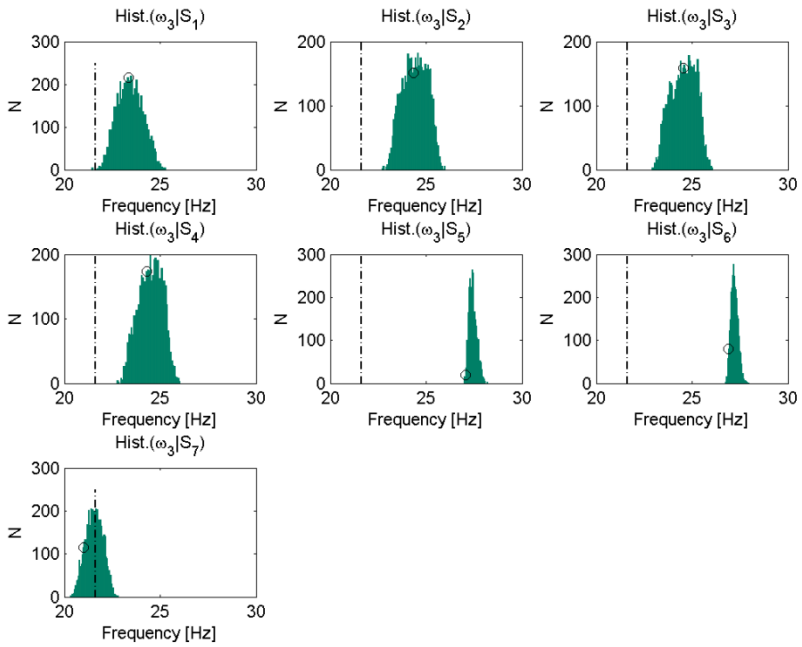

Figure A.29. Histograms for natural frequencies (Mode 3), study case #4
(Dashed line: Experimental Value. Circle: starting sample)

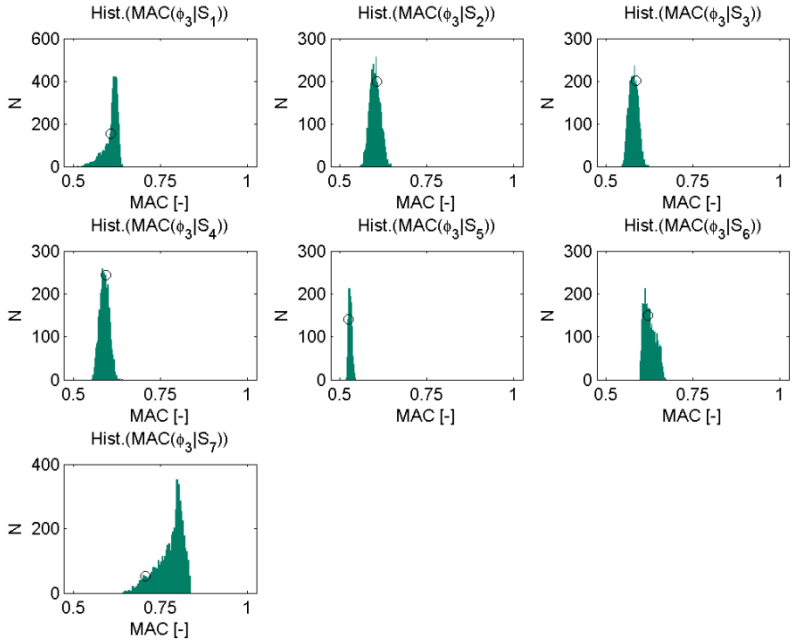

Figure A.30. Histograms for mode shapes (Mode 3), study case #4
(Dashed line: Experimental Value. Circle: starting sample)